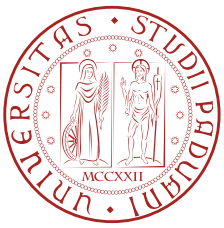

UNIVERSITÀ DEGLI STUDI DI PADOVA

UNIVERSITA' DEGLI STUDI DI PADOVA

Dipartimento di Ingegneria Industriale DII
Dipartimento di Tecnica e Gestione dei Sistemi Industriali DTG
Corso di Laurea Magistrale in Ingegneria Meccanica

MIXED-MODE FRACTURE EVALUATION ON A WIDE RANGE OF MATERIALS

Supervisors:
Paolo Ferro
Seyed Mohammad Javad Razavi
Filippo Berto

Candidate:
Saveria Spiller
1210563

Academic Year 2019/2020

Abstract

The present work aims to evaluate the mixed-mode fracture behavior of a wide range of materials. The topic belongs to the field of Fracture Mechanics and pre-cracked specimens are studied. A crack, even if small, is a defect that can strongly affect the integrity of a component and his behavior, if stressed. For this reason, a crack can not be ignored and cracked components need a specific evaluation. The analyses presented in this study are characterized by mixed-mode loading configurations, which are a combination of mode I and mode II. They are respectively the opening mode and the in-plane shear mode. Only static configurations are considered, therefore no fatigue problems are faced. The analyses are based on simulations made with the F.E. software Abaqus. The main purpose is to predict the failure load of a specimen and the stress intensity factors when the fracture occurs. The ASED criterion is applied to obtain these results. This is an energetic criterion recently found, and $ASED$ stands for Average Strain Energy Density. To validate the criterion it was necessary to compare predictions with experimental results. In order to have a proper comparison, the data used come from literature and the simulations are designed to be adherent to the real tests. A large range of materials is taken into account, to explore the field of application of the ASED criterion, with the fundamental hypothesis of linear elastic behavior. The materials studied belong to the class of Rocks, Polymers, Ceramics, and Steels.

Furthermore, other theoretical criteria are used to study the fracture. In order: Maximum Tangential Stress criterion (MTS), Generalized Maximum Tangential Stress criterion (GMTS), Minimum Strain Energy Density criterion (SED), and Maximum Energy Release Rate criterion (G).

For what concerns the ASED criterion, the precision of this method is in some cases astonishing. About the other criteria, it is not possible to establish which one is the best because for each class of materials they show different performances.

Sommario

L'obiettivo principale dello studio qui presentato è valutare il comportamento a frattura di diversi materiali sottoposti ad una configurazione di carico di tipo misto. L'argomento si inserisce nell'ambito della Meccanica della Frattura ed i componenti studiati presentano una cricca.
Una cricca, anche se piccola, influisce pesantemente sull'integrità di un pezzo. Per questo motivo non può essere ignorata e un componente criccato deve essere studiato con un approccio dedicato.
Le analisi esposte in questo studio presentano una configurazione di carico mista, una combinazione di modo I (apertura per trazione) e modo II (scorrimento nel piano dei lembi della cricca). Sono state considerate solo configurazioni statiche. L'analisi si basa su simulazioni ottenute tramite il software Abaqus. L'obiettivo principale è predire il carico di rottura e i fattori di intensificazione di tensione su provini criccati al momento della rottura. Per ottenere questi risultati è stato usato il criterio chiamato ASED, *Averaged Strain Energy Density*. Per validare il criterio è necessario un confronto con la realtà: i dati utilizzati sono stati trovati in letteratura e le simulazioni sono state pensate in modo da replicare perfettamente gli esperimenti reali. Se così non fosse, non sarebbe possibile un veritiero confronto.
Al fine di esplorare al meglio il campo di applicabilità del criterio, sono stati testati materiali appartenenti a diverse categorie, ipotizzando che presentassero un campo di deformazione lineare elastico. Le classi studiate sono rocce, polimeri, ceramici e acciai.
Inoltre, sono stati usati altri criteri teorici per predire l'angolo di iniziazione della cricca. Questi criteri sono nell'ordine: il criterio *Maximum Tangential Stress* (MTS), *Generalized Maximum Tangential Stress*(GMTS), *Minimum Strain Energy Density*(SED), e infine il criterio *Maximum Energy Release Rate*(G).
Per quanto riguarda il criterio ASED, i risultati sono sorprendenti: il criterio è estremamente preciso. Riguardo agli altri criteri invece non è stato possibile definire il migliore, in quanto, a seconda del materiale considerato, si comportano diversamente.

Acknowledgement

A page in a thesis is not enough to show gratitude for the people who went along with me in the last five years or more.
I am grateful to my mother, my father, my sister, and my aunts. I am a lucky person. I know it. Heartfelt thanks to my friends and fellows for being extraordinary.
To Andriy, words are unnecessary.

Sincere thanks also to my supervisors for bringing me through the pandemic.
There is a piece of Norway in this work.

Contents

List of Figures

List of Tables

Introduction

Fracture Mechanics is one of the most recent fields of Mechanics. It is the science that studies the structural integrity of components weakened by defects like cracks or other types of flaws. Fracture Mechanics is applied both to static and fatigue problems.
Specimens that are not ideally perfect need to be studied with a dedicated approach. This is a necessity arisen after too many tragedies occurred: when fundamental components of structures or machines broke down without expectation, the consequences can be the worst.
According to classic mechanics, speaking of structural resistance, the components are usually considered in perfect conditions, without any defects or discontinuity at both micro and macro-level. This assumption, in the majority of cases, is wrong. There are several ways in which a crack or a flaw can arise in a component: the main reason is related to the wrong use of the component or the wrong design of it. The result is the same, the component is not appropriate for his task and, therefore, the use will damage it. Eventually, cracks can origin also during the production process. With some traditional processes, like casting, if the process parameters are not properly controlled, it is likely to detect cracks in the pieces, mostly originated during the cooling phase. Also, modern techniques, like additive manufacturing, are well known for the difficulty to guarantee the quality of the component: to superpose layers of material means to introduce material discontinuities and flaws. Recently, a new approach of design has become common: Damage Tolerant approach, this is how it is called, imposes to consider since the beginning a component damaged, even if, inspecting it, no cracks are detected. This is precautional because if no cracks are detected it could be a matter of sensibility of the instrument used for the investigation. In this way, it is possible to predict when the component needs structural maintenance, to avoid rupture. This short overview shows how it is frequent to deal with cracks, that is the first reason why it is relevant to study Fracture Mechanics.

Furthermore, there are situations that it is not possible to handle without Fracture Mechanics. This is the case of components with a shape that presents notches of considerable dimensions, like holes, edges, or buttonholes. With a classical approach, it is possible to predict the structural limit of these specimens through a parameter called

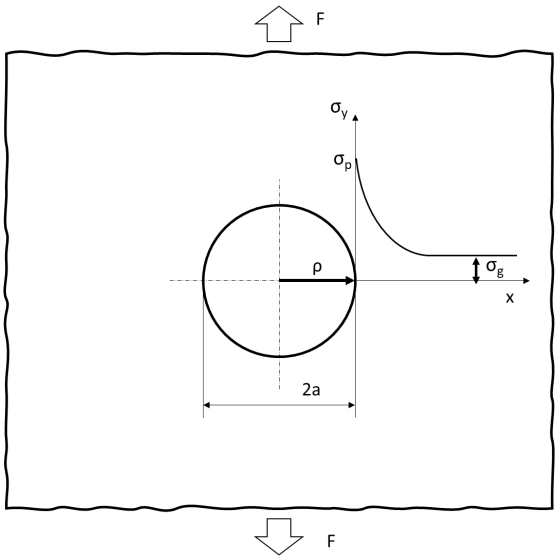

Figure 1: Infinite plate with a hole

elastic stress concentration factor, K_t. The factor is the ratio between the peak stress registered at the tip of the notch and the gross stress, the uniform tension registered in a generic section of the component far from the defect: $K_t = \sigma_p/\sigma_g$. There are several handbooks, the most famous is the Paterson one, where to find K_t according to the notch type and the loading scheme. K_t is an indicator of how much the notch affects the stress field. A typical example is a hole in an infinite plate. In fig 1, it is shown the trend of the stress (the component σ_y is considered). Along a direction perpendicular to the load, the stress increases while approaching the hole, until it reaches a maximum value, called the peak stress. It is demonstrated that if the hole becomes an ellipse, the peak stress is larger. Thanks to the following correlation (eq.(1)) found by Inglis in 1815, it is known the relation between the ratio a/ρ and the K_t factor, where ρ is the radius at the edge of the ellipse, and a is the semi-longitudinal length of the notch. With a circular hole $a/\rho = 1$.

$$K_t = 1 + 2\sqrt{\frac{a}{\rho}} \tag{1}$$

With this knowledge, it is possible to forecast that the sharper is the ellipse, the larger is K_t. When the ellipse is enough thin to be considered as a crack, with $\rho \to 0$, K_t tends to ∞.

Here the classic mechanics fails. With $K_t = \infty$ it is impossible to do any static check, nor for brittle neither for ductile materials. A static structural check is based on the comparison between the stress level in the component and the so-called *limit stress* of it, σ_L. This is the ideal structural limit of the component, calculated with one of the several criteria available in the literature. One of the most used is the Von Mises criterion. For brittle materials, if $K_t \to \infty$ the peak stress is ∞. And, therefore, the basic condition

$\sigma_p \leq \sigma_L$ is never verified. When dealing with ductile materials, the theory is different: the failure occurs when the process zone around a notch tip is completely invested with a uniform stress field, equal to the yielding stress. This phenomenon is called 'redistribution of stress', and it entails that a ductile material never undergoes brittle fracture. But in the reality, a ductile material can break in a brittle way, with apparently no explanation unless referring to Fracture Mechanics.

Even for fatigue problems, classic mechanics fails. When studying the fatigue life of a component it is necessary to define some parameters that give information on the shape, the loading configuration, the material surface, and some other aspects regarding the component, to characterize it properly. One of these parameters is the shape factor K_f. The shape factor depends on the parameter q according to eq. (2). But when the notch tip radius tends to zero, q tends to zero, as shown in fig. 2, and K_t tends to ∞, as already explained. This means that eq. (2) has no solutions and K_f is not determined. The consequence is that it is not even possible to determine the fatigue life of the component. In conclusion, with a cracked component, a specific approach is needed also for fatigue problems. This is another confirmation that Fracture Mechanics is important, even if in this study only static configurations are considered.

$$K_f = 1 + q(K_t - 1) \tag{2}$$

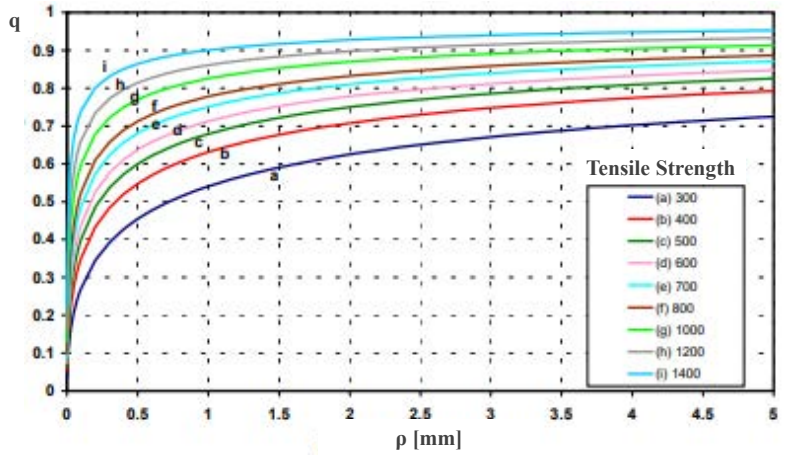

Figure 2: Notch sensibility

The present work is a study of the mixed-mode fracture behavior of pre-cracked specimens. The specimens are singular edge notch specimens (SEN), with a crack. As showed in fig. 3, the most common types of notches are the U-notches, the V-notches, and the so-called ideal cracks. The last ones present an opening angle $2\alpha = 0$, differently from

the V-notches, and a tip radius ρ that tends to zero.

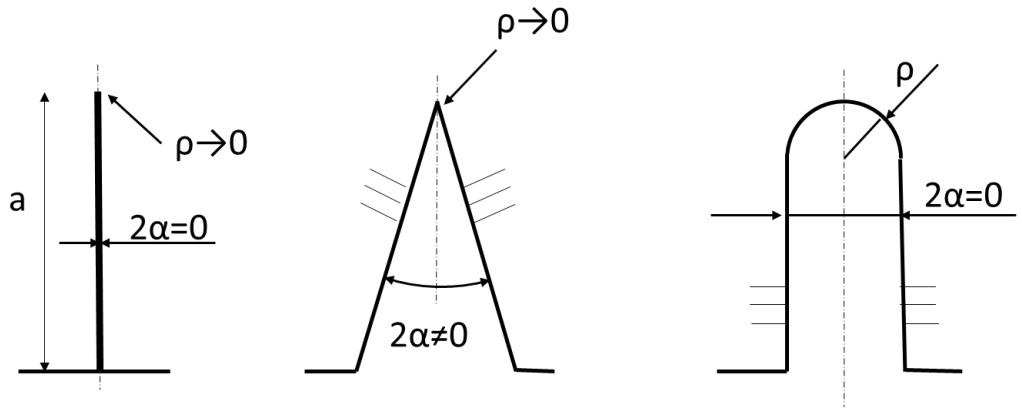

Figure 3: Different types of notches: an ideal crack, a V-notch and a U-notch

The specimens are subjected to the Asymmetric Four-Point Bending Test, (AFPB), which is a particular configuration that enables to obtained combined mode I and mode II fractures. There are three ways in which a crack deforms (fig. 4): the first one is the opening mode, called mode I. In these situations, the load is perpendicular to the crack plane and the crack is subjected to traction. The second mode is the in-plane shear mode, where the forces are parallel to the crack. The last one, mode III is the out-of-plane shear mode, where forces are transversal to the crack. In this study mode III is not considered.

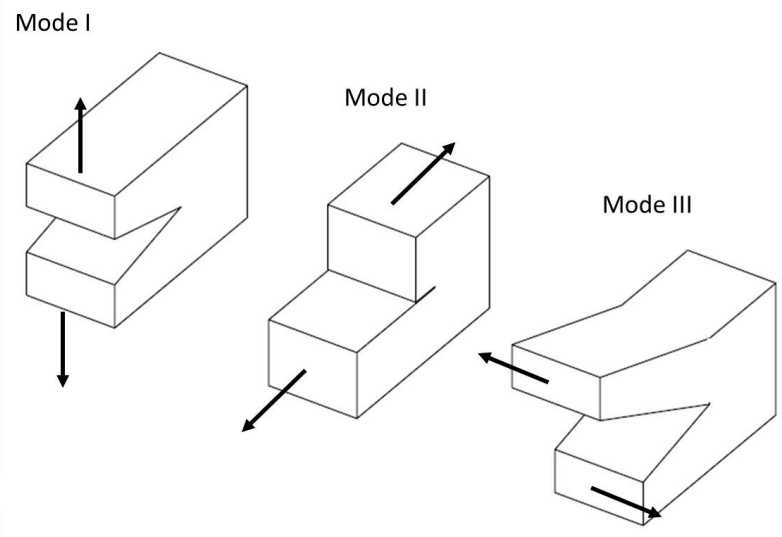

Figure 4: Crack deformation ways: opening, in-plane shear, out-of-plane shear

In the present work, the fracture is studied with different theoretical criteria able to predict the fracture behavior of cracked specimens. The criteria are the ASED criterion, the MTS criterion, the GMTS criterion, the SED criterion, and the G criterion. They will be throughout described in the next section. These criteria are applied to several materials, belonging to the classes of Rocks, Polymers, Ceramics, and Steels. They are materials completely different from each other, to rank the performances of each criterion in different situations. Nevertheless, to apply the theoretical criteria, the materials have to respect some hypotheses: they have to be homogeneous and isotropic, they have to show a linear elastic behavior, and to present brittle fracture. Steels are ductile materials, but they will be studied at low temperatures when they become brittle.
The main purpose of this thesis is to validate the ASED criterion. This criterion can predict the failure load of a component. *ASED* stands for Average Strain Energy Density because the strain energy density is the parameter that this criterion uses to monitor the deformation of the crack, till the fracture. The energy is average in a control volume centered in the crack tip. The prediction is based on the following proportion:

$$P_f : \sqrt{W_c} = P : \sqrt{\overline{W}} \tag{3}$$

P_f is the failure load, W_c is the critical value of the strain energy density and it corresponds to the failure. It is a material property. The terms P and $\overline{W}$ are respectively the load applied to the specimens and the average strain energy density corresponding to a comparative case. This means that to predict the failure load of a cracked specimen it is sufficient to know the material properties of the specimen and to simulate a comparative case: the results of the analysis are used in eq. (3). In this study, the simulations are made with the FE software Abaqus. In the simulations, the specimen is modelized with the appropriate geometry and material properties. Also, the crack is modelized in the right position. Then the model is stressed with a loading configuration that in this case is an AFPB test configuration. The intensity of the applied load is an arbitrary choice. For simplicity, the total load is $1\,N$. Then it is sufficient to run the analysis: one of the outputs of the simulation is the average strain energy density $\overline{W}$, to use in eq. (3). This is how it is possible to predict the failure load with the ASED criterion, without testing the material with experimental tests.
The purpose of the thesis is not merely to use the criterion to predict failure loads for a long series of specimens, but also to validate it. The validation is based on the comparison between the simulation's results and experimental results: in the field of this work, it was not possible to carry out laboratory tests. It is necessary to use data already obtained by

other scientists. In the literature, several studies on AFPB tests are available, on several materials. The first step of the work is to find these experimental test reports. Then it is possible to simulate the same specimens used for the lab tests to predict the failure loads. At this point the comparison is possible.

The validation of the ASED criterion is fundamental for several reasons. The relevance of the topic derives from the necessity of verifying the structural resistance of a component without testing it. Real tests are expensive and not always feasible. It could also happen that an experimental test does not simulate properly the reality, and therefore the results are useless. For all these reasons and more, finding reliable theoretical criteria able to predict the fracture behavior of a component is important. The ASED criterion is one of the most recent, but in the last century, several criteria were formulated. Each criterion proposes a different parameter as an indicator of the crack deformation state. The criteria are stress-based or energy-based, according to the parameter used. This parameter should be defined in the most general way and it has to be easy to obtain. Then, it is necessary to find the critical value of this parameter that represents the failure of the component. The ASED predictions are compared not only with the experimental results but also with other criteria predictions. From the side of stress-based criteria, the MTS and the GMTS criteria were used. They both use as the fracture parameter the tangential stress at the crack tip. Then it has been used the SED criterion, based on the strain energy density. It seems similar to the ASED criterion, but according to this one, the strain energy density is not average in a control volume. The last one is called G Criterion and it is based on the energy release rate, G.
The secondary purpose of this thesis is to see which criterion is the best for studying different classes of materials. They are also important because with these criteria it is possible to predict the initiation angle of the crack. The specimens used are pre-cracked but subjected to stress, the crack propagates until the rupture. When the crack starts propagating from the tip of the pre-crack, it takes a direction that depends on the mixed-mode. In the case of pure mode I the crack keeps opening from the crack tip in the same direction, but with pure mode II, the direction is close to 70°. The initiation angle can not be obtained with the ASED criterion, but it is an important aspect to consider when studying the propagation of a crack.

To conclude, the results for what concerns the ASED criterion are satisfactory and encouraging. ASED predictions are in general extremely precise, with the majority of materials tested. This criterion considers the fracture toughness K_{Ic} a material property, therefore, a constant. With this assumption, it is not unexpected that the predictions for the failure load corresponding to pure mode I fracture are almost perfect. The discrepancy

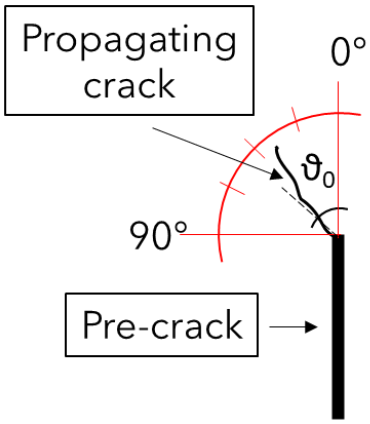

Figure 5: Initiation angle of a crack, general scheme

between prediction and real load is tiny. But the discrepancy increases while approaching pure mode II.
In the present work there are also materials for which the ASED criterion does not work. But in these cases, additional problems were observed: for example, if the scientists who carried out the test were not able to define the proper value of K_{Ic}, this is an uncertainty that affects the ASED predictions. These particular situations will be described properly in the following chapters.
For what concerns the other criteria, they are all well-known criteria, which validation is undeniable. But it is interesting to observe that for each class of materials they work differently. Even if with every material it is possible to recognize similarity, the best criterion is never expected. For example, it is always true that the MTS and the GMTS predictions are close to each other, and it is assumed that the GMTS criterion is the most accurate. Nevertheless, it is not always the best in fitting the reality, as it will be shown. This study was not needed to validate these criteria, which are milestones of Fracture Mechanics, but it allows us to discover more about their behavior with different types of materials.

The work structure is presented hereafter:

- Chapter 1: In the first chapter, the theoretical background is described. The thesis field is Linear Elastic Fracture Mechanics. This theory is described thoroughly. Also the theoretical criteria are presented.

- Chapter 2: the second chapter presents the numerical procedure followed. It is focused on the FE model used for the simulation in Abaqus, in particular on the

boundary conditions and the mesh used.

- Chapter 3: it is the kernel of the thesis. After a description of the loading configuration used, AFPB, all the materials tested are listed. The results of the application of the ASED criterion and the other ones are presented and discussed.

- Chapter 4: the last chapter contains the report of how some Zirconia specimens were tested with an AFPB fixture. Data obtained are then used to apply the theoretical criteria.

- Conclusion and recommendations: in the last section, some interesting observations on the thesis results are discussed.

Chapter 1

THEORETICAL BACKGROUND

Linear Elastic Fracture Mechanics (LEFM) is the framework of the present study. In the first section of the following chapter, an overview of LEFM theory and applications is presented.
With LEFM, the integrity of a crack specimen is measured with parameters called *stress intensity factors*. Even before the formulation of LEFM, scientists and researchers tried to identify the most indicative parameter to monitor in order to predict the behavior of a cracked specimen.
Several theoretical criteria were proposed during the last century. In this chapter, a detailed description of some of them is proposed. The criteria used in the present work are the following: the ASED criterion, the most recent one; the MTS criterion and a variation of it, the GMTS criterion, both based on the stress field study; the SED criterion and the G criterion, that are energy-based criteria.

1.1 Linear Elastic Fracture Mechanics

In the field of Fracture Mechanics, it is possible to study a crack with several approaches. In the present work, only linear elastic materials are considered: this means that in the proximity of a crack there is not a plastic zone or, eventually, it is negligible. Under this hypothesis, it is possible to use Linear Elastic Fracture Mechanics to study the way cracks lead to the failure of loaded specimens. Otherwise, other approaches should be preferred, as EPFM, Elastic-Plastic Fracture Mechanics.

Regarding the LEFM theory, the stress field near a crack tip can be described with the equations proposed by G.R. Irwing and M.L. Williams in 1957. Under some strict

hypothesis, the stress field assumes the form presented in eq. (1.1) ([1]).

$$\sigma_x = \frac{K_1}{\sqrt{2\pi r}} cos\frac{\theta}{2}\left(1 - sin\frac{\theta}{2}sin\frac{3\theta}{2}\right) + ... \tag{1.1a}$$

$$\sigma_y = \frac{K_1}{\sqrt{2\pi r}} cos\frac{\theta}{2}\left(1 + sin\frac{\theta}{2}sin\frac{3\theta}{2}\right) + ... \tag{1.1b}$$

$$\tau_{xy} = \frac{K_1}{\sqrt{2\pi r}} sin\frac{\theta}{2}\left(cos\frac{\theta}{2}cos\frac{3\theta}{2}\right) + ... \tag{1.1c}$$

$$\begin{cases} \sigma_z = 0 \quad plane\, stress \\ \sigma_z = \nu(\sigma_x + \sigma_y) \quad plane\, strain \end{cases} \tag{1.1d}$$

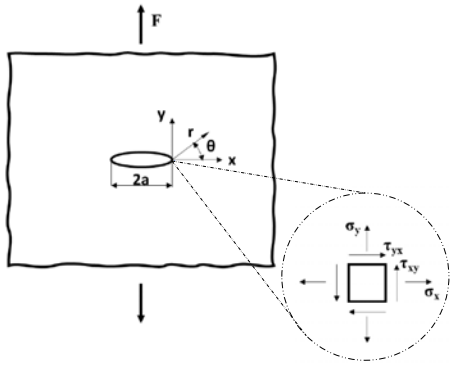

Figure 1.1: A generic crack subjected to Mode I loading

Fig. 1.1 clarifies the terms used in eqs. (1.1). The parameter K_1 is called *stress intensity factor*. More details on this parameter will be presented later. The equations are incomplete because the stress field presents also some non-singular terms that, by now, it is possible to ignore.

According to the classic mechanics, a flaw on a specimen is a concentrator of stress. The stress is higher if the flaw is sharper. Therefore, considering a sharp crack, near the tip the tension should increase to infinity. This is shown in fig. 1.2, where the stress component σ_y is plotted according to eqs. (1.1) both on a normal scale and a logarithmic scale. The stress field presents an asymptote to ∞ (fig. 1.2a). It is an impossible condition to reach: a real material will break in a brittle way if the stress reaches the tensile strength at a certain distance from the crack tip, therefore it can never present stress components that tend to ∞. The above-mentioned distance, r_p, characterizes the plastic zone. If the distance is short, the plastic zone is small and the material plastic behavior can be ignored. In fig. 1.3 the stress trend of an ideally linear material is compared with a real

material (the dashed curve). The distance r_p represents the plastic deformation zone. If r_p is similar to r_y, it is possible to consider the real material behavior perfectly linear. This is the situation in which LEFM theory can be applied, with all the advantages connected to it. In particular, in a linear elastic field, the principle of superposition is valid.
As said before, eqs. (1.1) can be used under some hypothesis: first of all the cracked specimen should be loaded in a pure mode I configuration. This means that only plane fields can be considered, plane stress field or plane strain field. Besides, a limit on the plastic zone should be considered. To apply the LEFM theory the radius that characterized the plastic zone should be closed to the crack tip. The last condition is about the stress field far from the crack: the gross stress should be smaller than half of the tensile strength of the specimen ($\sigma_g \leq 0.5\sigma_t$), else the stress field would be excessively intensive to ignore the plastic zone.

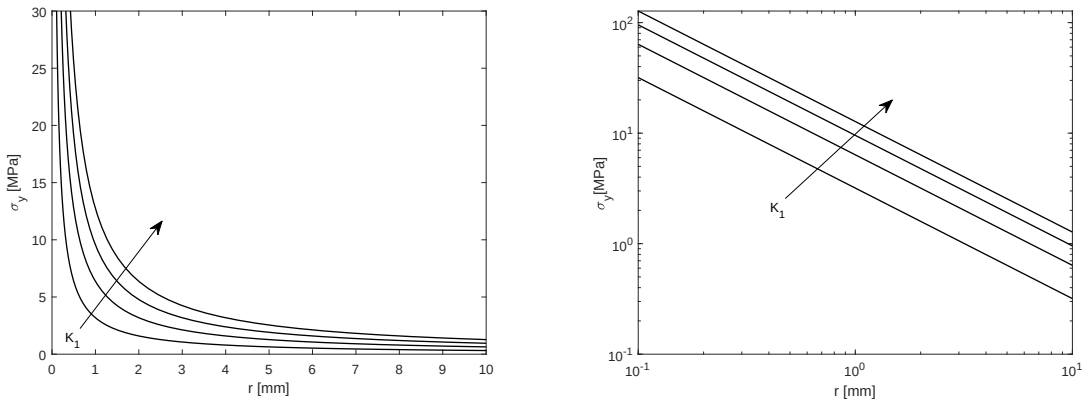

Figure 1.2: Stress field near the crack tip according to LEFM

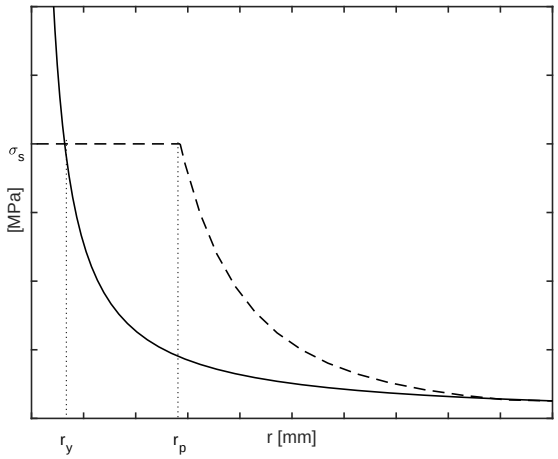

Figure 1.3: Comparison between a linear material stress field and a real material one.

According to equations (1.1), the tension field is represented in the diagrams in fig. 1.2.

As said before, the tension has a vertical asymptote when too close to the tip, as to say that the field is *singular*. Using a logarithmic scale, the trend appears as a straight line with a slope of 0.5. This is an important aspect to highlight. Irwing tension field is characterized by the ratio of $1/r^{0.5}$ in the first term of each equation. The exponent 0.5 represents the singularity of the field and it is a property of LEFM theory. In the next chapters, it will be explained that to classify a crack with his singularity factor means to choose how to consider the stress field around it, if perfectly linear or elastic-plastic.

The parameter K_1 is the most important one when dealing with cracks because it gives the measure of the intensity of the damage. It depends on the tension applied to the specimen and from the crack's initial length. It is measured in $[MPa/\sqrt{m}]$. The definition of K_1 is:

$$K_1 = 2\pi \lim_{x \to 0} \sigma_{yy}(r, \theta = 0) r^{0.5} \tag{1.2}$$

Looking to fig. 1.2a it is clear that the limit gives an indeterminate form. If $x \to 0$ it is not possible to determine the value of σ_y. For this reason, there are correlations to calculate K_1 with the following generic form:

$$K_1 = \alpha \sigma_g \sqrt{\pi a} \tag{1.3}$$

The components of (1.3) are:

- α, the shape factor. It depends on the geometry of the cracked specimen and the loading configuration.
- σ_g, the gross tension, it is the tension in a section of the specimen far from the flaw.
- a, the crack initial length.

To find α there are several handbooks and manuals available, one of the most famous is the handbook used in the present work: *Stress Intensity Factors Handbook*, by Murakami [2]. Anyway, there are also several empirical correlations to calculate K_1 in specific situations.

LEFM can be used both for static problems and fatigue problems. In the present work, only static problems are studied, therefore, in this chapter, there is no focus on the fatigue approach. According to LEFM theory, if the static load on a specimen increases, the stress intensity factor increases too. When K_1 reaches a critical value the crack has

overwhelmed the specimen and the fracture occurs.
The critical value above-mentioned is called *Fracture Toughness*, K_{Ic}, and it is a property of the material. The fracture toughness depends on the following factors: the first one is the temperature. It is easier for a crack to propagate when the temperature is low; the second one is material tensile strength, or more in general, the material characteristics; the last one is the thickness of the specimen that affects tension and deformation fields, and, as a consequence, the fragility of the specimen.

In the previous section, it was shown how important it is to study the fragility of cracked specimen loaded with realistic configurations. In the present work all the specimens studied are subjected to mixed-mode loading configuration, mode I + mode II combinations. When an in-plane load is applied to the specimens, the description of the stress field is more complicated and new terms must be added to equations (1.1). The result is the following stress field, proposed by William in 1959. Eqs. (1.4), represents the mode I + mode II stress field for a generic notch. It is valid also for V-notches, with an opening angle of $2\alpha \neq 0$. The equations show some new terms: Williams'eigenvalues, λ_1 and λ_2 depend on the opening angle of the notch.

$$\sigma_x = \frac{K_1}{(2\pi r)^{1-\lambda_1}} cos\frac{\theta}{2}\left(1 - sin\frac{\theta}{2}sin\frac{3\theta}{2}\right) - \frac{K_2}{(2\pi r)^{1-\lambda_2}} sin\frac{\theta}{2}\left(2 - cos\frac{\theta}{2}cos\frac{3\theta}{2}\right) + ... \tag{1.4a}$$

$$\sigma_y = \frac{K_1}{(2\pi r)^{1-\lambda_1}} cos\frac{\theta}{2}\left(1 + sin\frac{\theta}{2}sin\frac{3\theta}{2}\right) + \frac{K_2}{(2\pi r)^{1-\lambda_2}} sin\frac{\theta}{2}cos\frac{\theta}{2}cos\frac{3\theta}{2} + ... \tag{1.4b}$$

$$\tau_{xy} = \frac{K_1}{(2\pi r)^{1-\lambda_1}} sin\frac{\theta}{2}\left(cos\frac{\theta}{2}cos\frac{3\theta}{2}\right) + \frac{K_2}{(2\pi r)^{1-\lambda_2}} cos\frac{\theta}{2}\left(1 - sin\frac{\theta}{2}sin\frac{3\theta}{2}\right) + ... \tag{1.4c}$$

$$\begin{cases} \sigma_z = 0 \quad plane\, stress \\ \sigma_z = \nu(\sigma_x + \sigma_y) \quad plane\, strain \end{cases} \tag{1.4d}$$

Again, non-singular terms are ignored. In equations (1.4) there is another protagonist, K_2. This is the second stress intensity factor and the same considerations made for K_1 are valid.
When dealing with ideal cracks, with opening angle $2\alpha = 0$, the Williams'eigenvalues are both equal to 0.5. Eqs. (1.4) assume the following form, for what concerns σ_x, σ_y and τ_{xy}. These are the equations to which this study will refer to when considering a cartesian reference frame.

$$\frac{K_i}{(2\pi r)^{1-\lambda_i}} \quad \rightarrow \quad \frac{K_i}{(2\pi r)^{0.5}} \quad i = 1, 2 \tag{1.5}$$

$$\sigma_x = \frac{K_1}{\sqrt{2\pi r}} cos\frac{\theta}{2}\left(1 - sin\frac{\theta}{2}sin\frac{3\theta}{2}\right) - \frac{K_2}{\sqrt{2\pi r}} sin\frac{\theta}{2}\left(2 - cos\frac{\theta}{2}cos\frac{3\theta}{2}\right) + ... \tag{1.6a}$$

$$\sigma_y = \frac{K_1}{\sqrt{2\pi r}} cos\frac{\theta}{2}\left(1 + sin\frac{\theta}{2}sin\frac{3\theta}{2}\right) + \frac{K_2}{\sqrt{2\pi r}} sin\frac{\theta}{2}cos\frac{\theta}{2}cos\frac{3\theta}{2} + ... \tag{1.6b}$$

$$\tau_{xy} = \frac{K_1}{\sqrt{2\pi r}} sin\frac{\theta}{2}\left(cos\frac{\theta}{2}cos\frac{3\theta}{2}\right) + \frac{K_2}{\sqrt{2\pi r}} cos\frac{\theta}{2}\left(1 - sin\frac{\theta}{2}sin\frac{3\theta}{2}\right) + ... \tag{1.6c}$$

1.2 The ASED Criterion

The first and the main criterion used in this thesis is the ASED criterion. This is an energy-based criterion. It was first used for V-notches, with an opening angle different from 0, by Lazzarin and Zambardi in 2001 [3]. It can be used both for static and fatigue problems. Dealing with the fatigue analysis of notched components, this criterion presents several advantages: the value of ASED can be calculated for notches with different opening angles and subjected to different loading conditions, mode I, or mixed-mode (mode I+mode II). Therefore, using ASED it is possible to compare different notches to understand which one is the most critical. This was not possible using a stress approach because only similar notches under similar loading configurations can be compared together.
In the present work, static loads are considered, hence, hereafter, only static aspects are presented.
According to this criterion, the fracture occurs when the average strain energy density near the crack tip reaches a critical value: $\overline{W} = W_c$.
In this section the parameter $\overline{W}$ is obtained step by step, starting with the strain energy. Something similar is presented in the article [4], by Razavi, Aliha, and Berto, where a clear and incisive description of how to apply the ASED criterion to rock materials is proposed. In particular, it explains how to obtain analytically the *ASED*. The strain energy is the energy released after deformation and it is the area subtended by the load-deformation curve (fig.1.4). The integer in (1.7) is the general form of the strain energy, but if the material has a linear elastic behavior, the relation becomes the (1.8), much easier.

$$U = \int_0^{x_1} P dx \tag{1.7}$$

$$U = \frac{1}{2} P_1 x_1 \tag{1.8}$$

The strain energy density is simply the strain energy calculated for a unit of volume (see (1.9)). For a generic tri-axial stress field the result is in eq. (1.10), using cylindrical

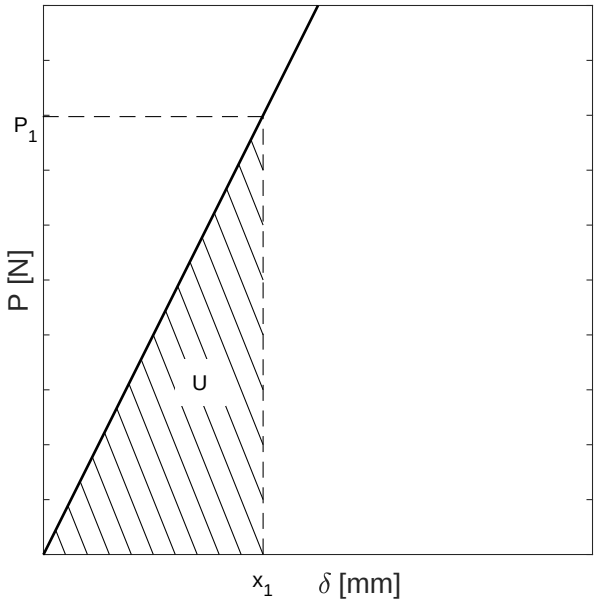

Figure 1.4: Load-displacement curve with strain energy area dashed

coordinates.

$$W = \frac{U}{Vol} = \int_0^{\varepsilon_1} \sigma d\varepsilon \tag{1.9}$$

$$W = \frac{1}{2}\sigma_{rr}\varepsilon_{rr} + \frac{1}{2}\sigma_{\theta\theta}\varepsilon_{\theta\theta} + \frac{1}{2}\sigma_{zz}\varepsilon_{zz} + \frac{\tau_{r\theta}}{2G} \tag{1.10}$$

To calculate the average strain energy density, it is sufficient to average the strain energy density just obtained, in a control volume. According to the ASED criterion, the control volume is a circle or a cylinder, depending on the model type, 2D, or 3D. The radius is a material property, and the volume is centered in the crack tip. Fig. 1.5 shows a generic crack, with an opening angle that ideally tends to zero, with the circular control volume. The radius depends on the tensile strength and the mode I fracture toughness of the material. There are two different equations available depending on the stress and deformation fields on the component:

$$R_c = \frac{(1+\nu)(5-8\nu)}{4\pi}\left(\frac{K_{Ic}}{\sigma_t}\right)^2 \quad \text{plane strain} \tag{1.11}$$

$$R_c = \frac{(5-3\nu)}{4\pi}\left(\frac{K_c}{\sigma_t}\right)^2 \quad \text{plane stress} \tag{1.12}$$

The idea of using a control volume is not completely new. According to the Irwing and Williams equations reported in the previous section, the stress field is singular near the crack tip. Hence, to evaluate a crack and the material behavior it is not possible to focus only on the proximity of the crack tip. To avoid the plastic zone around the tip, several

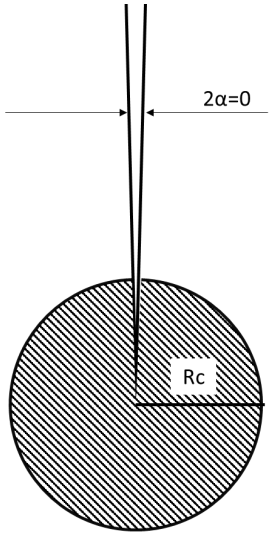

Figure 1.5: Control volume centered in the crack tip

criteria established that the material conditions of a cracked specimen (like the stress field components or the strain energy density) have to be evaluated at a proper distance from the tip. The innovation of the ASED criterion is to define not only a distance but a control volume in which the strain energy density is averaged.
After calculating the strain energy density, it is possible to obtain ASED as W/V_c, where V_c is the control volume. The result, considering an in-plane loading combination, is presented in eq. (1.13).

$$\overline{W} = \frac{e_1}{E}\left(\frac{K_1^2}{R_c^{(1-\lambda_1)}}\right) + \frac{e_2}{E}\left(\frac{K_2^2}{R_c^{(1-\lambda_2)}}\right) \tag{1.13}$$

It is immediate to extend this approach to extra plane loading combinations by the addition of the term related to K_3, the mode III stress intensity factor. The terms e_1 and e_2 are geometric constants that depend on the geometry of the crack and the Poisson's ratio. Dealing with an ideal crack, with opening angle of $2\alpha = 0$, $e_1 = 0.133$ and $e_2 = 0.34$. The exponents λ_1 and λ_2 depend on the notch configuration and they are already discussed in the previous section. They are called Williams'eigenvalues and for an ideal crack, they are both equal to 0.5.
With (1.13) it is possible to obtain analytically the value of ASED. But using a FE software like Abaqus, the one used in this work, it is also possible to get ASED as an output of the analysis, if, previously, the control volume is defined.
The last step of the formulation of the ASED criterion is the comparison between the calculated ASED and the critical value of it, corresponding to the rupture. The critical value is a material property equal to:

$$W_c = \frac{\sigma_t^2}{2E} \tag{1.14}$$

where σ_t is the tensile strength and E the Young modulus. Actually, this is true only if the material is ideally brittle.

The power of this criterion is that there is proportionality between the strain energy density and, through the stress intensity factor, the load applied to the specimen. Therefore, it is possible to predict the fracture load with the following crucial relation:

$$P_f = P\sqrt{\frac{W_c}{\overline{W}}} \tag{1.15}$$

It is sufficient to simulate a comparative case with a cracked specimen subjected to a particular loading configuration. The applied total load is arbitrary, and it is the term P (1.15). The term $\overline{W}$ is obtained as an output of the simulation. At this point, all the terms present in equation (1.15) are available, and it is possible to predict the load that lead the specimen to the fracture. This is an incredibly powerful result. In the next chapter, the ASED criterion will be applied to several specimens of different materials to demonstrate that the method can be extremely precise in predicting failure loads.

Moreover, as just said, stress intensity factors depend on the stress and therefore on the applied load. With the predicted load is possible to calculate also the toughness of the specimen, to characterize properly the fracture behavior of a component.

In the present work, the ASED criterion is applied to brittle materials that are tested with the loading configuration called Asymmetric Four-Point Bending (AFPB). Further details on this configuration will be propesed later (3.0.1). Nevertheless, the criterion can be applied also to different shapes of specimens. Some examples are reported in paper [5], by Razavi, Ayatollahi, and Berto.

1.3 The MTS Criterion

The second criterion used in the present work is the Maximum Tangential Stress Criterion. This criterion was first proposed by Erdogan and Sih in 1963 [6]. According to the MTS criterion, the fracture propagates along the direction where $\sigma_{\theta\theta}$ is maximum. The rupture will occur when the tangential stress reaches a critical value at a distance from the tip called critical distance r_c. Usually, r_c delimits the plastic zone around the tip but more in general it defines the so-called process zone, characterized by dislocation motion and other defects. It is a non-linear deformation region.

Using cylindrical coordinates, the stress field around the crack tip can be described with equations (1.16). Fig. 1.6 helps to understand the terms. To perform the MTS criterion it is sufficient to consider the singular terms of the field, ignoring the first non-singular term and the higher-order terms of the equations.

$$\sigma_{rr} = \frac{K_1}{\sqrt{2\pi r}} cos\frac{\theta}{2}\left(1 + sin^2\frac{\theta}{2}\right) - \frac{K_2}{\sqrt{2\pi r}}\left(-\frac{5}{4}sin\frac{\theta}{2} + \frac{3}{4}sin\frac{3\theta}{2}\right) + ... \tag{1.16a}$$

$$\sigma_{\theta\theta} = \frac{K_1}{\sqrt{2\pi r}} cos\frac{\theta}{2}\left(1 - sin^2\frac{\theta}{2}\right) - \frac{K_2}{\sqrt{2\pi r}}\left(-\frac{3}{4}sin\frac{\theta}{2} - \frac{3}{4}sin\frac{3\theta}{2}\right) + ... \tag{1.16b}$$

$$\tau_{r\theta} = \frac{K_1}{\sqrt{2\pi r}} sin\frac{\theta}{2}cos^2\frac{\theta}{2} + \frac{K_2}{\sqrt{2\pi r}}\left(\frac{1}{4}sin\frac{\theta}{2} + \frac{3}{4}sin\frac{3\theta}{2}\right) + ... \tag{1.16c}$$

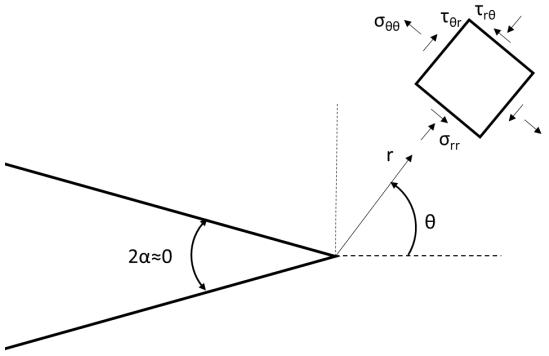

Figure 1.6: William stress field in a cycilidrical reference system

To find the maximum of $\sigma_{\theta\theta}$, it is necessary to set an optimization problem as shown in the following group of equations (1.17): the first condition is necessary to find a stationary point. In the second line, the imposition on the second derivative sign is the sufficient condition to ensure that the point is a maximum, not a minimum neither a point of flex.

$$\begin{cases} \dfrac{\partial \sigma_{\theta\theta}}{\partial \theta} = 0 \\ \\ \dfrac{\partial^2 \sigma_{\theta\theta}}{\partial \theta^2} < 0 \end{cases} \tag{1.17}$$

It is possible to solve the problem numerically, using software like Matlab, but the first equation of the previous system is equivalent to eq. (1.18), easy to solve analytically to find θ_0, the initiation angle. Furthermore, being one of the most famous and precise criteria, the MTS is also implemented in Abaqus. This means that it is possible to ask the software the initiation angle of a propagating crack according to the MTS criterion during an analysis.

$$K_{1f} sin\theta_0 + K_{2f}(3cos\theta_0 - 1) = 0 \tag{1.18}$$

In (1.18) K_{1f} and K_{2f} are the stress intensity factors calculated near the crack tip in a cracked specimen that undergoes a particular loading condition when the fracture occurs. If the way of crack-deformation is pure mode I, $K_{2f} = 0$ and $\theta_0 = 0$. When the loading condition is really close to pure mode II and K_{1f} tends to 0, typical values for θ_0 are around 70°.
If θ_0 has been found, it is possible also to calculate the toughness K_{Ic} related to the configuration under consideration. It is well known that, in a pure mode I configuration, $K_{Ic} = \sigma_c\sqrt{2\pi r_c}$, where σ_c is the critical value of $\sigma_{\theta\theta}$ and r_c the critical distance above mentioned. Substituting this equation in the eq. (1.16c), it is possible to find the value of the fracture toughness of the specimen if the stress intensity factors and the angle θ_0 are known. Eq. (1.19) shows how:

$$K_{Ic} = cos^2\frac{\theta_0}{2}\left(K_{1f}cos\frac{\theta_0}{2} - \frac{3}{2}K_{2f}sin\theta_0\right) \tag{1.19}$$

It is worth to precise that the parameter K_{1f} and K_{2f} are the stress intensity factors related to a mixed-mode loading configuration when the fracture occurs. If the applied load respect the pure mode I fracture deformation, $K_{1f} = K_{Ic}$, mode I fracture toughness, while $K_{2f} = 0$.
The MTS criterion is not the only one able to predict both the initiation angle and the K_{Ic}. Three other criteria will be presented, and, in the next chapter, they will be compared through two plots for each material studied: the first one is the comparison of the initiation angles find out in different mixed-mode loads. The second one compares the trend of the normalized stress intensity factors K_1/K_{Ic} and K_2/K_{Ic}. For the MTS criterion, the toughness is calculated according to eq. (1.19) and a similar correlation will be proposed for each criterion.

1.4 The GMTS Criterion

It is known that the MTS criterion is one of the most used criteria to predict the initiation angle of a crack. But the predictions are not always precise. The limitation of the classical MTS is that it considers only the singular terms of William's stress field. But it is shown that ignoring the non-singular term of the field can affect significantly the precision of the prediction. For this reason, a new criterion was recently proposed (firstly by Smith et al. in 2001, [7]), called Generalized Maximum Tangential Stress Criterion, or Modified MTS Criterion.
The complete equation for the tangential component of the stress field is presented below in (1.20): after the singular terms, there is the first non-singular term called $T - stress$. In the complete equations, there are also higher-order terms, but they are negligible.

$$\sigma_{\theta\theta} = \frac{K_1}{\sqrt{2\pi r}} cos\frac{\theta}{2}\left(1 - sin^2\frac{\theta}{2}\right) - \frac{K_2}{\sqrt{2\pi r}}\left(-\frac{3}{4}sin\frac{\theta}{2} - \frac{3}{4}sin\frac{3\theta}{2}\right) + Tsin^2\theta + O(r^{1/2}) \tag{1.20}$$

The GMTS, as the MTS criterion, states that a crack initiates along the direction where the tangential stress, calculated using 1.20, is maximum. Therefore, equations (1.18) and (1.19) are transformed in the following:

$$K_{1f}sin\theta_0 + K_{2f}(3cos\theta_0 - 1) - \frac{16T_f}{3}\sqrt{2\pi r_c}cos\theta_0 sin\frac{\theta_0}{2} = 0 \tag{1.21}$$

$$K_{Ic} = cos^2\frac{\theta_0}{2}\left(K_{1f}cos\frac{\theta_0}{2} - \frac{3}{2}K_{2f}sin\theta_0\right) + \sqrt{2\pi r_c}T_f sin^2\theta_0 \tag{1.22}$$

Eq.(1.21) is useful to find θ_0 while with (1.22) the fracture toughness is obtained.
T-stress is difficult to calculate analytically. In very simple loading configurations T-stress is easy to obtain along with particular directions like 0°. In the article [8] some typical solution are presented. To avoid the propagation of uncertainty it is better to obtain T-stress directly from the software Abaqus.
The critical distance r_c has already been described, it is the distance from the crack tip that delimits the process zone. As already said, to respect the LEFM theory, the plastic zone around the tip should be small. This means that the critical distance should be short: typical magnitude for r_c is $10^{-5}\,m$. To evaluate it, there are several correlations available in the literature. In the present work the Schmidt's correlation was usually used [9], [10], [11]:

$$r_c = \frac{1}{2\pi}\left(\frac{K_{Ic}}{\sigma_t}\right)^2 \tag{1.23}$$

As for the MTS criterion, it is not necessary to solve an optimization problem because eq. (1.21) is resolvable analytically.
Usually, in the literature [7],[9], [10], [11], another approach is used to express the equation to find θ_0, that implies the use of normalized expressions:

$$K_{Ic} = cos^2\frac{\theta_0}{2}\left(K_1 cos\frac{\theta_0}{2} - \frac{3}{2}K_2 sin\theta_0\right) + B\alpha K_{eff}sin^2\theta_0 \tag{1.24}$$

with the terms proposed below (1.25). The parameter a is the initial crack length.

$$K_{eff} = \sqrt{K_1^2 + K_2^2} \tag{1.25a}$$

$$B = \frac{T\sqrt{\pi a}}{K_{eff}} \tag{1.25b}$$

$$\alpha = \frac{\sqrt{2r_c}}{a} \tag{1.25c}$$

The T-stress affects both the toughness and the value of θ_0 of a component. The sign of T-stress depends on the geometry and loading configuration. A negative T-stress means increasing the mixed-mode fracture toughness and the value of the initiation angle. Instead, the magnitude gives an idea of the severity of the flaw in the specimen.

1.5 The SED Criterion

The SED criterion is the fourth theoretical criterion used in the present work. The acronym SED stands for strain energy density, the same parameter calculated to perform the ASED criterion. This criterion was first formulated by Sih, in 1973 [12]. This is an energetic criterion, like the ASED criterion. The parameter used to study the onset of the fracture is the strain energy density factor S. It is simply the strain energy density, already calculated in the previous section, multiply for the critical distance r_c. This distance usually represent the *core region*, a small region around the crack tip where the material is not perfectly elastic but it shows flaws and dislocations.
Factor S can be written with the following equation:

$$S = r_c \frac{\partial W}{\partial V} = a_{11}(\theta)K_1^2 + a_{12}(\theta)K_1K_2 + a_{22}(\theta)K_2^2 \tag{1.26}$$

The angular functions a_{11}, a_{12} and a_{22} are obtained as follows. The parameter κ changes if the specimen stress and deformation fields are plane. In the present work, only thick specimens were analyzed. Therefore it is always used the plane strain model. The parameter ν is the Poisson's ratio.

$$a_{11}(\theta) = \frac{1}{16G}[(1 + cos\theta)(\kappa - cos\theta)] \tag{1.27a}$$

$$a_{12}(\theta) = \frac{1}{16G} sin\theta[2cos\theta - (\kappa - 1)] \tag{1.27b}$$

$$a_{22}(\theta) = \frac{1}{16G}[(\kappa + 1)(1 - cos\theta) + (1 + cos\theta)(3cos\theta - 1)] \tag{1.27c}$$

$$\begin{cases} \kappa = 3 - 4\nu & plane\,strain \\ \kappa = (3-\nu)/(1+\nu) & plane\,stress \end{cases} \tag{1.27d}$$

The SED criterion states that the crack will initiate along the direction of the minimum strain energy density factor. The fracture will occur if, along this direction, at a distance from the crack tip equal to r_c, the factor S reaches a critical value S_c.
The critical value of the S factor depends on the loading configuration and it is considered, as r_c, a material constant. To find the stationary value of $\frac{\partial S}{\partial \theta}$ it was used the software Matlab that offers several built-in functions to minimize a function. Once the value of θ_0 is found, it's possible to calculate also the fracture toughness of the specimen with equation (1.28).

$$K_{Ic} = \left[\frac{8}{\kappa - 1} \left(\frac{1}{16}(\kappa - cos\theta_0)(1 + cos\theta_0)K_1^2 + \frac{1}{8} sin\theta_0 (2cos\theta_0 - (\kappa - 1))K_1 K_2 + \right. \right. \\ \left. \left. \frac{1}{16}(\kappa + 1)(1 - cos\theta_0) + (1 - cos\theta_0)(3cos\theta_0 - 1)K_2^2 \right) \right]^{0.5} \tag{1.28}$$

1.6 The G Criterion

The G criterion is the last theoretical criterion used in the present work. The G criterion states that the crack will propagate in the direction along which the energy release rate G is maximum, and the fracture will occur when G reaches a critical value. More details will be discussed later. But first, the parametric form of G is presented below. In order to apply the criterion, eq. (1.29) is implemented in Matlab to find the maximum of G. Once the initial angle is defined, it is possible to calculate the fracture toughness with eq. (1.30). Abaqus can calculate the initiation angle according to this criterion, which is called also $MERR$, Maximum Energy Release Rate [13]. It is also possible for the MTS criterion. While for the MTS criterion Abaqus results are in good accordance with the values of θ_0 obtained analytically, with the MERR criterion the software is less precise. Therefore both the numerical solutions and Abaqus solutions are considered. Even from the point of view of the numerical implementation of the G criterion, there are more troubles: it seems that the function has several stationary points, and it is necessary to indicate to Matlab the right interval in which looking for the maximum. Else, Matlab gives unreliable angular values.

$$G = \frac{4}{E} \left(\frac{1}{3 + cos^2\theta} \right) \left(\frac{1 + \theta/\pi}{1 - \theta/\pi} \right)^{\frac{-\theta}{\pi}} \left[(1 + 3cos^2\theta)K_1^2 + 8sin\theta cos\theta K_1 K_2 + (9 - 5cos^2\theta)K_2^2 \right] \tag{1.29}$$

$$K_{Ic} = \left(\frac{2}{3 + cos^2\theta_0} \right) \left(\frac{1 + \theta_0/\pi}{1 - \theta_0/\pi} \right)^{\frac{-\theta}{2\pi}} \left[(1 + 3cos^2\theta_0)K_1^2 + 8sin\theta_0 cos\theta_0 K_1 K_2 + (9 - 5cos^2\theta_0)K_2^2 \right]^{0.5} \tag{1.30}$$

It is worth to discuss the origin of this criterion. The G criterion is a generalization of the so-called Griffith-Irwing's criterion [14] and G is literally the elastic energy release per unit crack extension. Griffith, in 1920, stated that a crack will propagate if "the release of available stored elastic strain energy due to crack extension is larger than the energy required to create new crack surfaces" [15, pp. L–39]. This means that according to Griffith, the parameter to monitor is the superficial potential energy. While Griffith considered only ideally brittle material, Irwing extended the criterion to ductile materials. It is clear that the MERR criterion, or G criterion, is directly derived from the Griffith approach.

The parametric form described above is the result of the necessity of describing G for deflected crack: there are other correlations in the literature which links G to stress intensity factors [14]. But it is well known that under combined mode I and mode II loads, a crack will propagate outside the crack plane, with a deflection angle that depends on the loading configuration. Hence, the classical correlations are not useful and the parametric form for G was derived using path-independent integrals, like Rice's integral [16], that doesn't consider the motion of the crack.

Chapter 2

NUMERICAL PROCEDURE

The present work is based on the numerical procedure described hereafter. As already explained in the previous chapters, the heart of the thesis is the comparison between theoretical predictions and experimental results to validate several criteria dealing with the fracture behavior of cracked specimens. To apply the criteria it is necessary to simulate an AFPB test with a FE software. It is sufficient to stress a little the specimen, without lead it to the rupture. The results of the analysis are then scaled and used to predict the behavior of the specimen when the fracture occurs.
In a few words, the method consists of the following steps. The first one is a review job. It was necessary to look in the literature for datasets obtained through experimental tests carried out for other purposes. The articles under consideration have to respect some restrictions: first of all, they have to deal with the static fracture of pre-cracked AFPB specimens, loaded under mixed-mode (I + II) conditions. Failure loads and stress intensity factors depend on the geometry of the specimen and the loading configuration. Therefore, it would be a mistake to use data obtained through tests different from the AFPB, the one chosen for this work. To prepare the simulations, a large amount of information is needed: the articles used have to be detailed enough to provide the necessary inputs for the numerical procedure.
As disclosed before, the numerical procedure is based on the simulation of the behavior of cracked specimens with precise boundary conditions through FE software. Data obtained from the analysis are then processed to perform theoretical criteria and predict the fracture behavior of the specimens.
A detailed description of the FE model and the procedure to process data are presented in the next sections. The FE model has to respect the characteristics of the real tests. This is the reason why it was said that a large quantity of information about experimental tests has to be available: above all, failure loads for each configuration have to be registered. Furthermore, the specimen's dimensions, the test's parameters, and the material's properties have to be provided.

Once this information is collected, it is possible to begin with the simulation part. The FE software used in this work is Abaqus.

2.1 The FE Model

2.1.1 Geometry and Material

First of all, the simulation requires the construction of a good model. The geometry of specimens used in AFPB tests is simple, they are classic SEN specimens, as shown in fig. 2.1; for this, they are modeled as rectangular bars. The three dimensions, length, width, and thickness, have to be known. The part is modeled in 2D with the hypothesis of plane strain field. All the specimens studied have an average thickness of $10\,mm$, hence a plane stress field was not applicable. For what concerns the material, ideal isotropic and linear-elastic materials are considered. Therefore, it is enough to provide Abaqus with the Young modulus and Poisson's ratio of the material used.
As shown in fig. 2.1, on the model it is sketched a simple partition: it has several functions. First of all, to model the crack as described later, it is necessary to draw it with a partition. Then, centered in the crack tip, the circular control volume is sketched. There is usually a cross in it to facilitate the construction of the swept mesh inside it. In the end, extra edges are created far from the crack to guarantee a nice structured mesh at the extremity of the specimen.

2.1.2 Definition of the Crack in the FE Model

In Abaqus, the crack is modeled as a seam: that means that the crack is ideal, sharp, with an opening angle equal to zero. Abaqus is provided with different models to evaluate a crack. For the aim of this work, the model used is *Contour Integrals*.
Particular attention was paid to the singularity of the crack. The work is based on the LEFM theory and the model of Williams (section 1.1) for the stress field: the singularity of the stress field is $1/\sqrt{r}$. To respect this point, a proper characterization of the crack should be done in the software: first, the nodes of the mesh's elements next to the crack tip should be collapsed in one, which will be perfectly overlapped with the tip itself. This is easier to understand looking at fig. 2.6a. The elements used are 8-nodes biquadratic plane strain elements, but the mesh description will be proposed later on.
Second, mid-side nodes of the sides of these elements linked to the tip should move to the quarter points of the sides, towards the tip. In this way, it is possible to have suitable degenerated *quad* elements around the tip. In fig. 2.1 the geometric model in Abaqus is shown. In this case, the crack starts from the bottom side of the specimen and it is

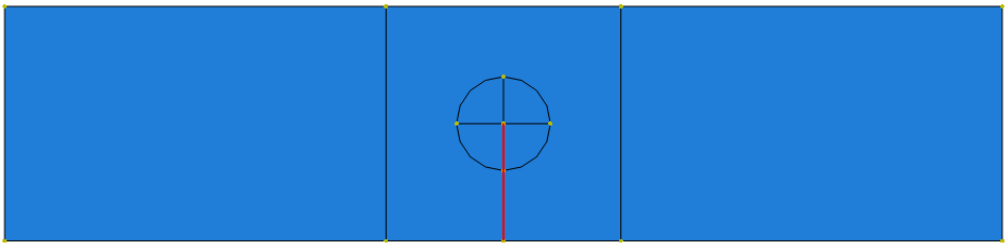

Figure 2.1: Geometric model in Abaqus

highlighted in red.

2.1.3 Boundary Conditions

The proper definition of the boundary conditions is fundamental to perform the ASED criterion correctly.
The first thing to know is that, in the simulations, specimens are loaded with a force of $1\,N$. In this condition, the specimen is not lead to the fracture. Anyway, the analysis is useful in predicting the fracture behavior of the material because, as told at the beginning, the theory used in this thesis for the evaluation of the crack is the LEFM theory. This means that *the Principle of Superposition* is valid. Therefore, what happens to the specimen with a load of $1\,N$ can be appropriately scaled to what happens when the fracture occurs. The consequence is that the prediction of the failure load with the ASED criterion is based on the simple equation already proposed in section 1.2: $P_f = P\sqrt{\frac{W_c}{\overline{W}}}$. From the FE software, it is possible to know the value of the strain energy density averaged in the control volume when a load of $1\,N$ is applied ($\overline{W}$). It is necessary to calculate the critical value of the strain energy density (W_c), but it depends only on material properties and it is easy to obtain. Therefore the only unknown variable in the equation is the failure load (P_f).
After discussing the intensity of the load applied, it is worthly to focus on the boundary conditions. In this regard, it is useful to outline the setting of an AFPB test fixture, as shown in fig. 2.2.
The specimen is kept in the right position using 4 rollers. Two of them on the upper side and two on the lower side. In the FE model, the lower rollers are represented as constraints to fix the specimen in the space. Dealing with a 2D model, to guarantee the static equilibrium, only 3 *d.o.f.*, degrees of freedom, have to be blocked. For these simulations, displacements along X and Y-axis on the left support and displacements along

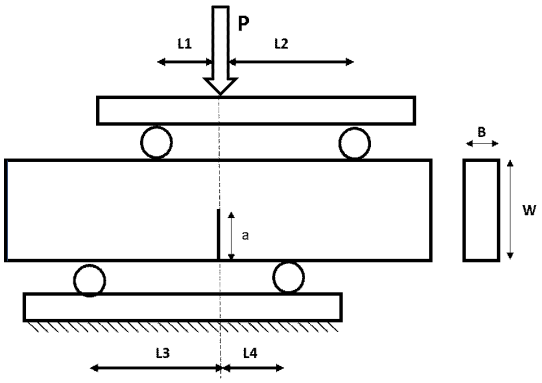

Figure 2.2: AFPB test's scheme

Y-axis on the right support are disabled.
For what concerns the load, the specimen is loaded from the top to the bottom, and the force is split into two components which points of application are located at the place of the upper rollers. These forces are treated as concentrated loads. Their intensity is calculated to have a bending moment equal to zero on the symmetry plane of the sample, to preserve the static equilibrium.
The distances called L_1, L_2, L_3, and L_4 in fig. 2.2, are not random. Changing these distances it is possible to vary the value of the mixed-mode coefficient Me. Me is calculated with the eq. (2.1) and it indicates the influence of mode I in the fracture mechanism concerning mode II. Me is included in $[0, 1]$, where 0 corresponds to pure mode II and 1 to pure mode I.

$$Me = \frac{2}{\pi} arctg\Big(\frac{K_1}{K_2}\Big) \tag{2.1}$$

Dealing with 4-points bending tests, to obtain pure mode I it is necessary to simulate a Symmetric Four-point bend test. The scheme of this configuration is shown in fig. 2.3a. Distances have to respect these constraints: $L1 = L2$ and $L3 = L4$. The crack is in the symmetry plane of the sample.
To obtain mode II the Asymmetric Four-Points bending configuration has to be simulated. This time $L1 = L4$ and $L2 = L3$. The crack is in the symmetry plane. (fig. 2.3b).

To simulate mixed-mode (I+II) there are two possibilities. The first one is the solution used for example with Takkab Granite, (section 3.1.3). In this case, to change the value of Me, it is sufficient to change the distance of a boundary condition. In fig. 2.4a $L4$ changes to vary the mixed mode. Starting with the configuration $L1 = L4$ (mode II), $L4$ decreases gradually and the constraint is closer to the crack. This means that the

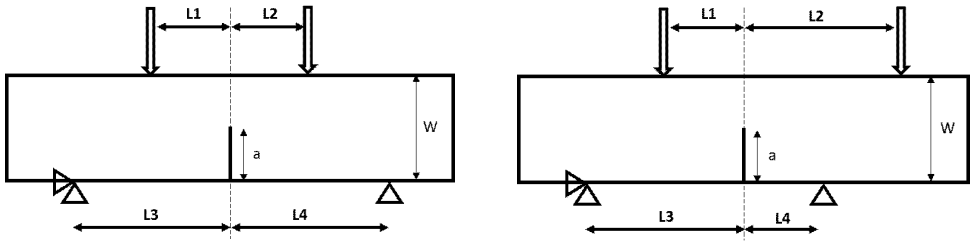

(a) SFPB, Mode I (b) AFPB, Mode II

Figure 2.3: Loading configurations

influence of mode I will be stronger in the fracture mechanism.
Another way to obtain mixed modes is to move the specimen, and therefore also the crack's plane, instead of the boundary conditions. Loads and constraints are kept in the same position in every simulation. But the crack moves towards the closer load of a distance called S (fig. 2.4b). The longer is S the higher is the coefficient Me. S can be calculated, if not provided, using eq. (2.2). This should be always possible because stress intensity factors registered during tests should be available. $F1$ and $F2$ in the equation are the geometry factors used to calculate SIFs.

$$S = W\left(\frac{F_2}{F_1}\right)\left(\frac{K_1}{K_2}\right) \tag{2.2}$$

Special attention should be paid to the loading distances $L1$, $L2$, $L3$ and $L4$. The most important thing is that $L1$ has to be "far enough" to the crack tip. This information is translated in the following condition: it is appropriate to never let $L1/W < 0.5$. Otherwise, the intensity of mode I in the fracture mechanism will be high even with the AFPB configuration. In this eventuality, mode II will not be obtained because $K1$ will not be zero, either approximated to zero. These considerations are reported in the papers [11] and [17]. Even in this work, similar problems were found in the analysis of Indiana and Westerly granite (sections 3.1.5 and 3.1.6).

2.1.4 Output Requests

As already explained, the input required to perform the ASED, MTS, GMTS, SED and G criteria can be obtained through simulations. In particular, to perform the ASED criterion it is necessary to calculate the Average Strain Energy Density. From the software, it is possible to obtain the output requests called *ELSE* and *EVOL* in the circular control

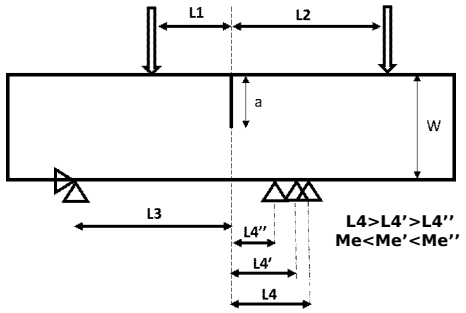

(a)

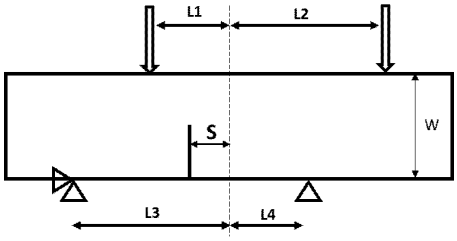

(b)

Figure 2.4: Loading configurations to simulate mixed modes

volume sketched in the partition. *ELSE* is literally the *Total Elastic Strain Energy in the Element*, while *EVOL* is the *Current Element Volume*. They are both required for all the elements in the control volume. To calculate $ASED$ it will be sufficient to divide *ELSE* by *EVOL*.

These are not the only useful outputs. From Abaqus, Stress Intensity Factors at the crack tip can be extracted. The software is provided with different algorithms to calculate the SIFs. In the interest of this work, both Maximum Tangential Stress and Maximum Energy Release Rate were used, because the software gives also the prediction of the direction along which the crack will start, according to these criteria. These directions will also be obtained numerically, to have a double-check of the results. The last output necessary in the procedure is the *T-stress*. This is the first non-singular term of the stress field, according to William's theory, and it is used in the GMTS criterion. To apply the criterion, it is needed the *T-stress* when the fracture occurs and it is obtained multiplying *T-stress* from the simulation with $1N$ load (that is an output request) for the predicted failure load.

2.1.5 The Mesh

The element type used in the analysis is $CPE8$: 8 nodes plain strain element. These elements are suitable for the type of analysis, primarily because of the hypothesis of plain strain field, and secondly because quadratic elements are in general more stable and easy to manage. To have a nice mesh, the partition shown in fig. 2.1 was sketched to delimit different mesh control areas. For example, in the extreme parts of the sample, a simple *structured* mesh with *quad* elements was required. In the middle area, the geometry is more complex and the most convenient mesh is the *free* one, with algorithm of construction *Medial Axis* and *quad* elements.
The most important area is the control volume. The control volume has the shape of a circle, for this, it is required a *swept* mesh with *quad dominated* elements. With the characterization of the crack' singularity described in the previous section, these *quad* elements will degenerate in *triangulare* elements in the first contour around the tip. To improve the seeding, a cross was sketched inside of the control volume, perpendicular to the crack. In the four edges of the cross, a *single bias seeding* is requested. The element size in the control volume has to be chosen carefully.
It was appropriate to do a sensitive analysis of the mesh. The resulting mesh is shown in

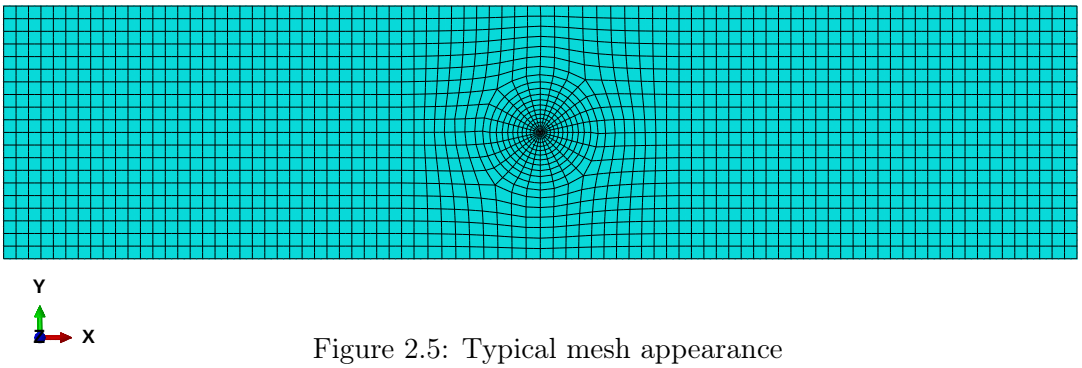

Figure 2.5: Typical mesh appearance

2.1.6 Mesh Sensitivity Analysis

A sensitivity analysis was performed to understand the importance of the mesh seeding to the aim of this work. The analysis was performed with the FE model build to study Takkab Granite fracture behavior. First, mode I was analyzed, with three different mesh. For an overall analysis, all the output requests were observed: this means $ASED$, K_1, the directions of crack's initiation according to the MTS and the G criteria, and the T-stress. The results of this sensitivity analysis are the expected ones: it is well known that the value of $ASED$ is not mesh-dependent. In fact, with gross meshes, the value

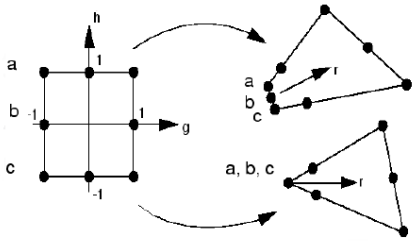

(a) Collapsed elements'nodes near the crack tip.

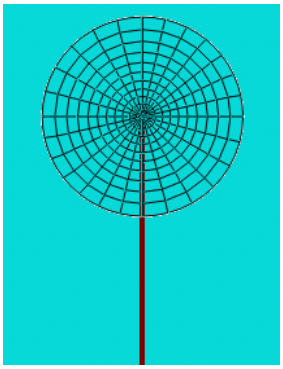

(b) Enlargement of the swept mesh in the control volume.

Figure 2.6: Details of the mesh's elements near the crack tip.

does not change. Instead, stress intensity factors are known to be sensitive to the finesse of the mesh, and this is what is seen in the tab. 2.1, where there is a tiny difference between the three values of K_1. No differences were registered in the directions and for the *T-stress*. *T-stress* is less sensitive to the mesh than stress, but not strongly mesh-independent as the strain energy density. For this reason it worth checking them too. To have a double-check, a sensitivity analysis was performed also on the model when the mixed-mode coeff
is strongly mesh-i
concerns direction

MESH PATTER

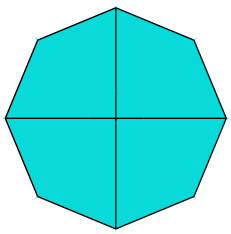

$ASED$	$[mJ/mm^3]$	$1.44E-09$	$1.44E-09$	$1.38E-09$
$K1\,(1\,N)$	$[MPa\sqrt{mm}]$	0.044705	0.044700	0.052663
$T-stress$	$[MPa]$	0.0016044	0.0016044	0.00031365

Table 2.1: Mesh sensitivity analysis, pure mode I

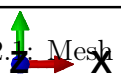

MESH PATTER		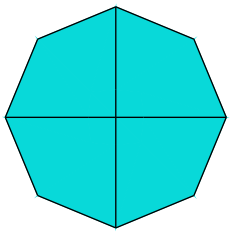		
$ASED$	$[mJ/mm^3]$	$1.98E-10$	$1.98E-10$	$1.81E-09$
$K1\,(1\,N)$	$[MPa\sqrt{mm}]$	0.01264900	0.012648000	0.060940
$K2\,(1\,N)$	$[MPa\sqrt{mm}]$	0.00644950	0.00644910	0.0023022
$T-stress$	$[MPa]$	0.000507780	0.000507280	0.0016746

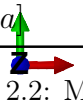

Table 2.2: Mesh sensitivity analysis, $Me = 0.7$

2.2 Data Processing

2.2.1 The ASED Criterion Application

Once all necessary data are available, it is possible to work with the criteria. The description of the steps to perform the ASED criterion is presented here. As already said, from Abaqus simulations, *ELSE* and *EVOL* can be extracted. This means that *ASED*, the Average Strain Energy Density, can be calculated as $ASED = ELSE/EVOL$. The common symbol for the average strain energy density is $\overline{W}$, and from here on out it will be called in this way. To obtain the failure load in each configuration, the critical value of the strain energy density is calculated, as $Wc = \sigma_t^2/2E$. The last equations are already discussed in section 1.2, where the criterion is presented. The load used in the simulations to simulate the comparative case is unitary, for simplicity, and the failure load is obtained with: $Pf = \sqrt{\frac{W_c}{\overline{W}}}$. In this way, the first important parameter of the study, the failure load, is provided.

At this point, it is sufficient to compare failure loads predicted with the ASED criterion with the experimental ones presented in the paper used as a reference for each material. Sometimes in the articles, failure loads are not provided directly, but there are the stress intensity factors registered when the fracture occurs for every mixed-mode loading configuration. In this case, failure loads can be obtained with the general equations here below (eq. (3.3) and (3.4)), where M and Q are respectively the bending moment and the shear on the crack plane. As said before, the geometry factors F_1 and F_2 can be found in the literature.

$$K_1 = \frac{M}{tW^{1.5}} F_1(a/W) \tag{2.3}$$

$$K_2 = \frac{Q}{tW^{0.5}} F_2(a/W) \tag{2.4}$$

The procedure behind this thesis is based on the fact that the fracture toughness of the material is a material property, a constant. This means that also simulating the model, the fracture toughness obtained should be the same that is presented in the paper as a property of the material. It is important to check this equality because if the K_{Ic} obtained through the simulation is different, it means that there are mistakes and the results obtained are not valid.

As said before, the simulations present a total applied load of $1\,N$, therefore the specimen is far from the rupture. For pure mode I, the value of the first stress intensity factor K_1 obtained, does not correspond to the facture toughness K_{Ic}. To calculate the fracture toughness there are several ways. One of the possibilities is to use a correlation that links K_{Ic} to the failure load predicted for mode I with the ASED criterion. Usually, in the papers, specific correlations and geometry factors suitable for the tests under consideration are presented. But it is always possible to use the theory of Murakami [2]. Most of the time, mode I is obtained with the Symmetrical Four-Points Bending test (SFPB), sometimes with a Three-Points Bending test (3PB). For the SFPB, equations from the masterpiece of Murakami are presented here below. For the nomenclature of the parameters, see fig. 2.7:

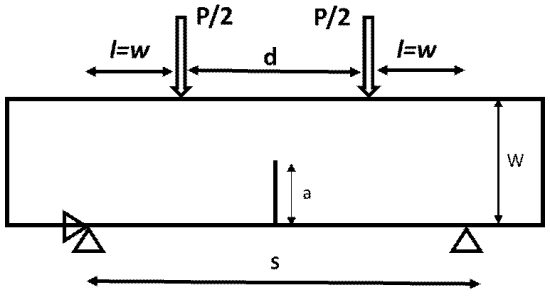

Figure 2.7: SFPB scheme from Murakami handbook

$$K1c = \frac{3Pl}{tW^2} \sqrt{\Pi a}\, F\Big(\frac{a}{W}\Big) \tag{2.5}$$

$$F\Big(\frac{a}{W}\Big) = 1.122 - 1.121\Big(\frac{a}{W}\Big) + 3.740\Big(\frac{a}{W}\Big)^2 + 3.873\Big(\frac{a}{W}\Big)^3 - 19.05\Big(\frac{a}{W}\Big)^4 + 22.55\Big(\frac{a}{W}\Big)^5 \quad (2.6)$$

Otherwise, to calculate K_{Ic}, it is possible to take advantage of the relation between stress intensity factors and applied load. This is valid not only for K_{Ic}, but also for the stress intensity factors corresponding to mixed-mode with $Me < 1$, when the fracture occurs. They will be indicated as K_{1f} and K_{2f}. In eqs. (3.3) and (3.4) the following relation is indicated:

$$K_1 \propto M \qquad K_2 \propto Q \quad (2.7)$$

But both the bending moment M and the shear Q depends directly on the load applied. It is possible to establish the following proportion:

$$K_1 : P = K_{1f} : P_f \qquad K_2 : P = K_{2f} : P_f \quad (2.8)$$

keeping in mind that if $Me = 1$, $K_2 = 0$ and $K_{1f} \equiv K_{Ic}$. Using eqs. (2.8) it is possible to calculate the stress intensity factors when the failure occurs without further difficult steps, as the calculations of the geometry factors. The terms K_1 and K_2 are given as results of the simulation, P is the load applied, that for simplicity is $1\,N$ and P_f has been obtained applying the ASED criterion.
The values of K_{1f} and K_{2f} will be used to apply the other theoretical criteria.

2.2.2 The MTS, GMTS, SED AND G Criteria Application

These theoretical criteria were already described in chapter 1. To recap, they can predict the direction along which the crack initiates and the value of K_{Ic}. Basically, the only inputs that they need are the stress intensity factors, when the fracture occurs. They are obtained with the procedure described in the previous section. Material properties are necessary, but it is supposed that at this point of the analysis they are well known. The GMTS criterion needs also the *T-stress*. To calculate the *T-stress* when the specimen fails it is sufficient to multiply the *T-stress* obtain from Abaqus, with $1\,N$ load, by the failure load predicted, taking advantage of the proportionality $T - stress \propto P$. This is exactly the method used to calculate K_{1f} and K_{2f}, and it is an advantage related to the LEFM theory.
All criteria are based on optimization problems: to obtain the initiation directions it is necessary to calculate the singular point of a function. For the MTS and the GMTS criteria, it is necessary to find the maximum of the tangential stress, while for the G criterion the energy release rate has to be maximalized. In the end, for the SED criterion, it is necessary to find the minimum of the strain energy density factor. To solve these problems, the software Matlab was used. Actually, as already explained in the previous

chapter, for the MTS and the GMTS criteria there are explicit equations to find the angle. For the other two criteria, it is possible to use a built-in function of Matlab to minimize a function numerically.
Abaqus can predict the initiation angle of a crack according to the MTS and the G criteria. These values are registered on purpose to compare them with the ones obtained from Matlab to see if the codes are working appropriately. This is a method to notice errors.
Once the four criteria are applied, it is possible to present the comparison. The results are presented in two plots: in the first one, the initiation angles are plotted for each Me, from pure mode I to mode II. For all the material the four criteria predicted angle trend are presented, but sometimes also the experimental values are available: this happens when, during the experimental tests, the scientists registered the initiation angles of the crack for each specimen, using visual instruments and a goniometer. In this case, it is possible to compare the reality with the criteria to see which one is the best in fitting the real trend.
In the second plot, a comparison between the stress intensity factor is shown. The SIFs are normalized, this means that the plot has K_1/K_{Ic} in the X-axis and K_2/K_{Ic} on the Y-axis. The SIFs used are obtain when the fracture occurs. In this plot not only the four criteria are presented but also the ASED predictions and the experimental results. There is more than one level of interest in this comparison: it is interesting first of all to see the difference between the ASED trend and the experimental one. Then it is also interesting to see how close are these four criteria between each other and between the ASED and experimental trends.
For every class of materials, more than one material was tested. This makes it possible to understand when a criterion is better than the other and to draw useful conclusions.

Chapter 3

RESULTS AND DISCUSSION

3.0.1 Asymmetric Four-Point Bend Configuration

The loading configuration used for this work is the Asymmetric Four-Point Bending configuration. Some details about this configuration have already been reported in the previous sections, in particular in sec. 2.1.3, where the Boundary Conditions of the FE model in Abaqus were described. As said before, in the present work, the experimental test results were found in the literature, and only articles regarding AFPB configurations were considered.
Schemes of the configuration have already been shown. Here it is proposed again the scheme for both the Symmetric Four-Point Bending configuration and the Asymmetric one. The shear and moment diagrams are showed (fig. 3.2).

With the SFPB configuration mode I fracture is obtained. In this case the two loads P_1 and P_2 are equal. The same result could be obtained with the Three-Point Bending configuration, shown in fig. 3.3. It is easier to use the SFPB, in the field of this work, because once the fixture with 4 rollers is attached to the traction/compression machine, it is better to use the four points configuration for all the specimens. In fig. 3.1 the fixture with the four rollers is shown. For what concerns the AFPB configuration, the loads have to be calculated to have bending moment $M = 0$ along the crack plane. The relation is:

$$P_1 \cdot L_1 = P_2 \cdot L_2 \tag{3.1}$$

$P_1 + P_2 = P$, that for the FE simulation is $P = 1\,N$, as already said. During the tests the specimen is lead to fracture and $P \equiv P_f$, the failure load.

What was not discussed till now, is why this particular configuration is considered. There are different possibilities to perform a similar study. In the literature several works on Brazilian Disks (BD) or Cracked Semi-Circular Bending Specimens (CSCB) are available. For example, in paper [18], by Majidia et al., the ASED criterion is applied to CSCB specimens that are obtained by welding two Aluminium alloys. In other papers, as [19] and

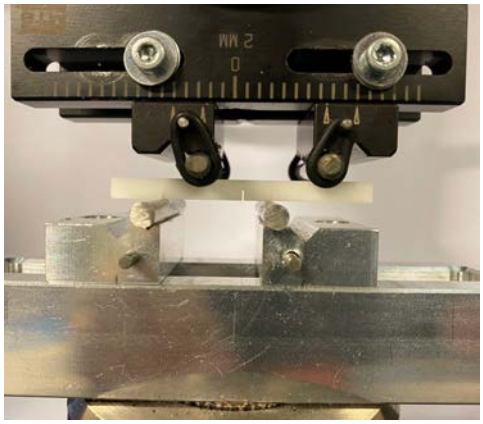

Figure 3.1: Four-points bending test configuration

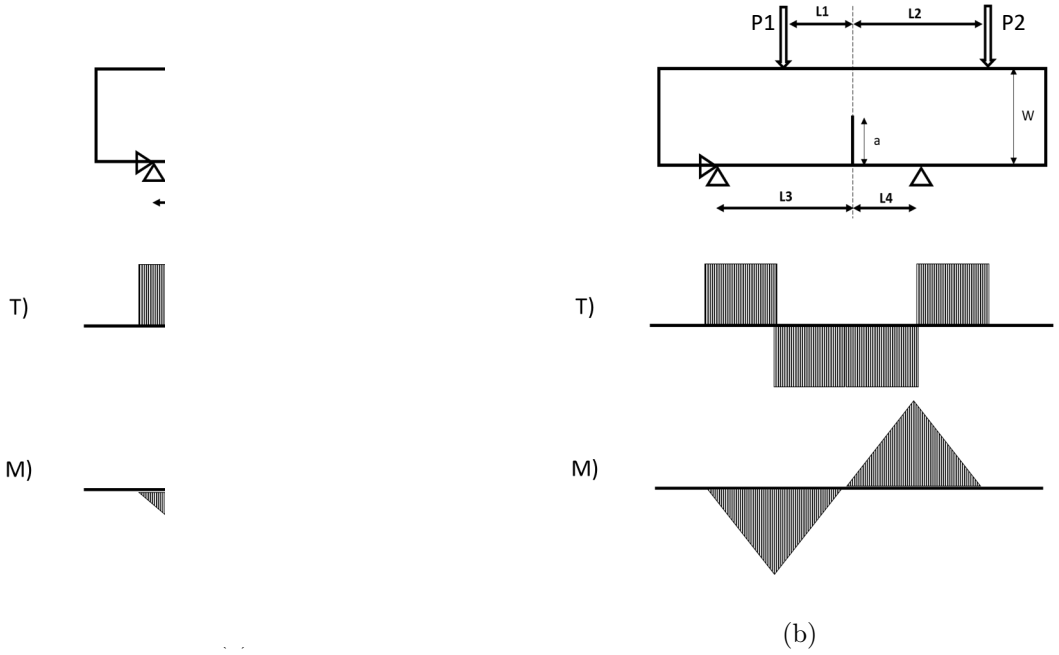

(b)

Figure 3.2: Diagrams of the shear and the bending moment for both SFPB and AFPB configurations

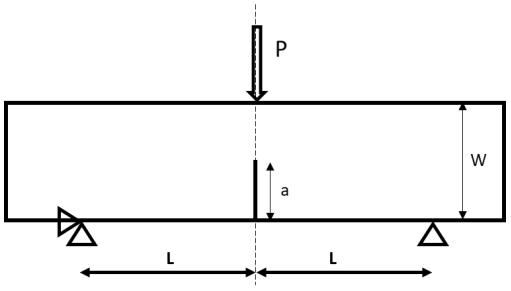

Figure 3.3: Three-Points Bending Configuration

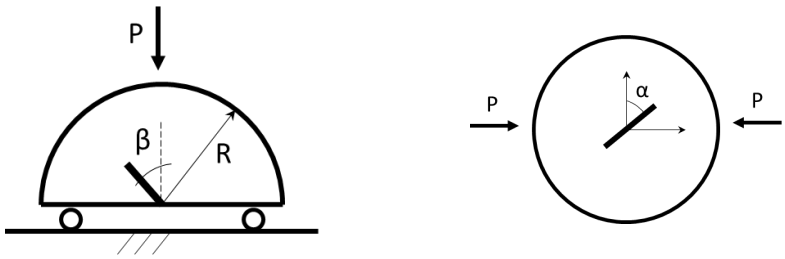

(a) CSCB (b) BD

Figure 3.4: Cracked Semi-Circular Bending specimen and Brazilian Disk specimen

[20], Brazilian Disks made of ceramic materials are tested with Diametral Compression. But the AFPB presents some undeniable advantages. First of all the specimen used is simple to manufacture and it does not require particular attention. It is basically a Single Edge Notch Specimen (SEN), a rectangular bar with a crack. It is visible in the fixture in fig. 3.1

The second advantage is related to the possibility of obtaining mixed-mode fractures (mode I +mode II only). With other specimens, the mixed-mode is affected by constructive details like the inclination of the flaw. This problem does not concern the AFPB test. It is also possible to simulate the pure mode II, that it is not expected, generally. Actually, with AFPB, particular attention is needed in the choice of the loading distances L_1 and L_2: if the loads are too close to the crack plane, even when performing mode II the contribution of the opening mode is not negligible, and the mixed-mode coefficient Me is not 0. But with proper distances, Me could be pretty close to zero.

In the following sections, several materials are analyzed with the same configuration, (AFPB). Sometimes there are differences, for example, the crack can be cut on the bottom side or on the upper side of the specimen, with a consequence on the sign of the initiation angle. All the eventual peculiarities will be exposed at the right point.

3.1 Rocks

3.1.1 An Overview

In the following sections the first class of material is analyzed: for the category of Rocks and Granites the materials studied are Yemeng black granite, Takkab granite, Dehbid marble, Indiana limestone, and Westerly granite.
Before starting, it is important to do a short overview of the more difficult aspects to manage during the study of Rocks.
To apply the ASED criterion, it is necessary to replicate every aspect of the experimental tests, to compare for each mixed-mode coefficient Me the right failure load. Unfortunately, to prepare the FE analysis, some approximations must be introduced in the model. This will for sure affect the accuracy of the results. For example, one of the main uncertainty was introduced when defining the material. This was already discussed in the previous chapter. The model used is an isotropic material with elastic behavior, so that only Young modulus and Poisson's ratio have to be defined. This is an ideal model, especially considering rocks and granite, naturally non-homogeneous materials. Furthermore, one of the biggest problems in the work is to define the material properties. To apply the ASED criterion, tensile strength, Young modulus, Poisson's ratio, and fracture toughness (mode I) are required. Luckily, for Yemeng black granite and Takkab granite, the experimental results were associated with papers in which it was possible to find all the properties. For the other materials, it was more difficult. Material properties were found in the literature, but it is well known that they depend on several factors, hence different values were proposed. An average value of these uncertain properties was used. This will certainly add approximation to the comparison. Finally, for almost all the rocks considered, more than one experimental test was carried out. The wisest thing to do was to compare ASED predictions to the average trend of failure loads reported for each material. For the values of K_1 and K_2, it was the same. There are some materials in particular where the failure loads do not follow a real trend. This condition will be discussed in detail later on.

3.1.2 Yemeng Black Granite

The first rock tested is the Yemeng black granite, a Chinese rock. The experimental results were provided in the article [11], by Wang, Zhu, and Liu. They tested with an AFPB set the rock with different mixed-mode combinations, ranging from mode I to mode II. For the construction of the FE model, the same dimensions of the experimental tests were used:

L=200 mm
w=40 mm
t=18 mm

The crack length a is $14\,mm$. The mechanical properties, reported in [11], are:

ν=0.21
E=82000 MPa
K_{Ic}=2.418 MPa$\sqrt{m}$
σ_t=16.6 MPa

The radius of the control volume was evaluated as $R_c = 6.78\,mm$.
In fig 3.5b, the configuration used for the AFPB tests in [11] is showed. The crack starts from the lower side of the specimen.

Once the part in Abaqus is prepared, different loading mode combinations were chosen to simulate different fracture modes.
Due to the fact that the AFPB tests were conducted 3 times for every mixed-modes, an average trend for failure load, K_{1f}, and K_{2f} was used for the comparison with ASED predictions.
The result of the comparison is shown in fig. 3.6 and tab. 3.1. The predictions are quite in good accordance with the failure loads values presented in [11]. The worst accordance is observed for pure mode II. This is quite typical because the ASED criterion fails also with other materials for mode II. As shown in the table, the discrepancy between experimental and predicted failure loads increases for Me approaching zero (mode II). The conclusion is that with Yemeng black granite, the ASED criterion works fine.

The discrepancy $\Delta\%$ is the relative error betwenn the two failure loads, and it is obtained as:

$$\Delta\% = \frac{P_{fASED} - P_{fEXP}}{P_{fASED}} \cdot 100 \tag{3.2}$$

Different criteria were used to predict K_{Ic} and the crack's initiation angle. It is interesting to compare them also with the ASED predictions and the real values of the angles

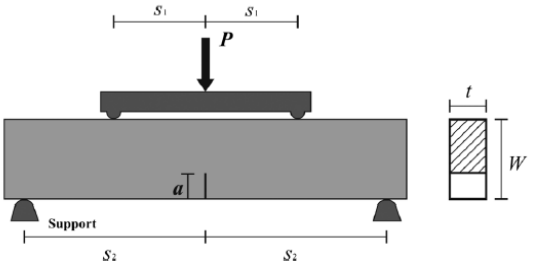

(a)

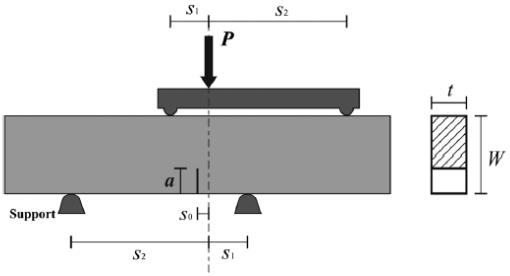

(b)

Figure 3.5: Yemeng granite: mixed-mode configuration used for the experimental tests in Ref. [11].

registered during the lab tests. The criteria used have been presented in the previous chapter and they are the MTS, GMTS, SED, and the G Criterion. In the following plot (3.7 and 3.8) the comparison for normalized stress intensity factors and initiation angles are presented. In both cases, the GMTS criterion is in better accordance with the experimental trend, but the MTS is not so far. This is because the GMTS is the only criterion that considers also the first non-singular term of the stress field near the crack tip. The GMTS derives from the MTS criterion. Therefore, they show similar trends, because T-stress has a small magnitude (that is why it is usually ignored). From the plot in fig. 3.7, it is clear that the worst results are obtained with the SED criterium. Precisely, it seems that the SED criterion overestimates the stress intensity factors.
A last interesting observation can be done. To calculate the failure loads, simulations with Abaqus are needed. It is necessary to know the strain energy density in the control volume. To do this the parameter called *ELSE* is calculated for all the mesh elements that belong to the control volume. It is also possible to plot it: the contour plots of *ELSE* in the control volume have a typical appearance shows in figure 3.9. It was observed that depending on the distance between the boundary conditions or more in general on the dimension of the specimen, the contour plots show differences. In general, the contours are symmetrical to the crack for pure mode I. Approaching mode II, the zone where *ELSE* is small (the blue part) assumes a shape called *peanut shape*, perpendicular to the load direction.

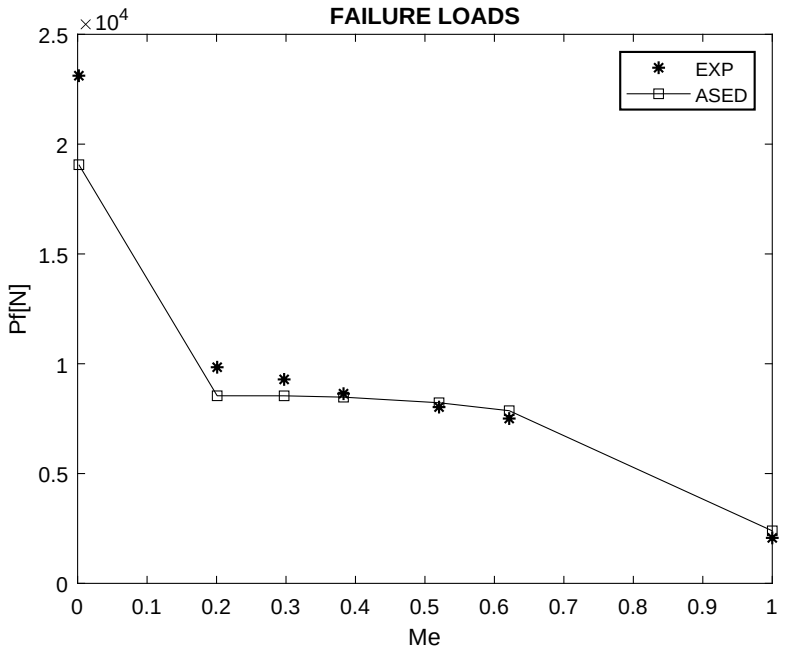

Figure 3.6: Yemeng granite: failure loads comparison. Experimental data were taken from Ref. [11]

FAILURE LOADS							
	ASED			EXP [11]			
Me	K_1 $MPa\sqrt{m}$	K_2 $MPa\sqrt{m}$	P_f N	K_1 $MPa\sqrt{m}$	K_2 $MPa\sqrt{m}$	P_f N	$\Delta\%$
1	2.418	0	2071	2.79	0	2392	-15.49
0.6213	1.654	1.12	7505	1.73	1.17	7862	-4.72
0.5203	1.344	1.261	8027	1.38	1.29	8224	-2.46
0.3828	0.97	-1.414	8637	0.95	1.39	8479	1.83
0.2973	0.781	1.548	9287	0.72	1.42	8540	8.05
0.2009	0.545	1.669	9841	0.47	1.45	8542	13.20
0.0018	0	1.807	23116	0	1.49	19064	17.53

Table 3.1: Yemeng granite: predicted and real failure loads

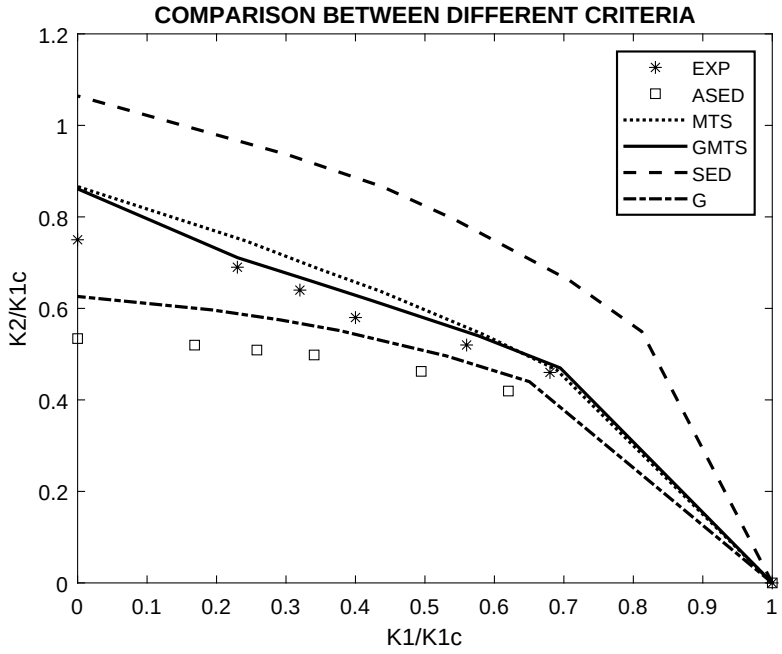

Figure 3.7: Yemeng granite: normalized stress intensity factors comparison. Experimental data were taken from Ref. [11]

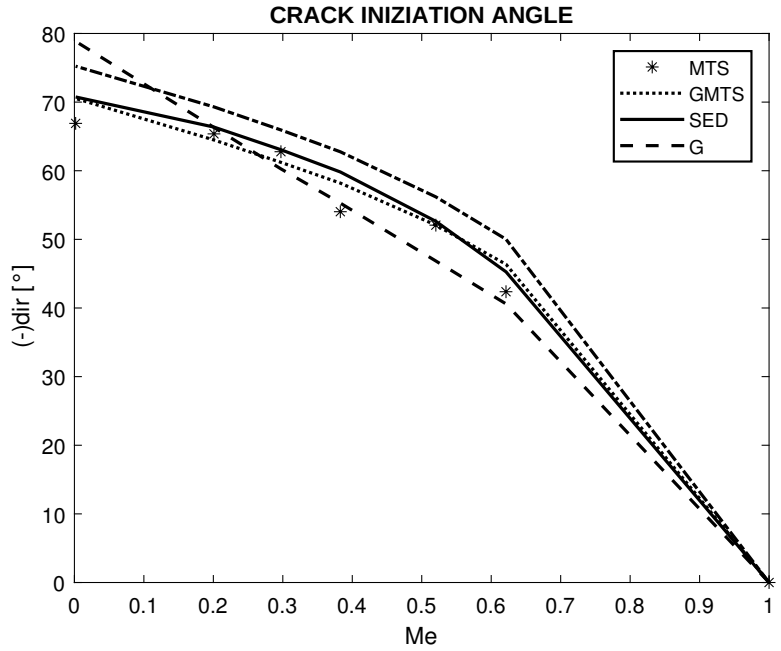

Figure 3.8: Yemeng granite: initiation angles comparison. Experimental data were taken from Ref. [11]

For Yemeng granite it is interesting to notice in fig. 3.9 that for pure mode II (fig. 3.9g) the peanut shape is not well defined because the blue part seems to be grabbed to the crack. This depends on the distances called S_1 and S_2 in the figure 3.5b, which are small in proportion with the width of the specimen. In the following sections, other contour plots will be shown, to see the differences. In addition, being Yemeng granite the first material studied, the following check was made. As already said, Abaqus can provide the initiation angle of the crack according to both the MTS criteria and the MERR criteria. This last one coincides with the so-called G criterion. To verify that the Matlab codes work properly and that they are reliable, the comparison between prediction from Abaqus ans numerical results are shown in the tables here below. They are compared also with the experimental values of the angles. For both criteria Abaqus predictions and Matlab solutions are in very good accordance, but they both overestimate the experimental values

MTS			
Me	$Abaqus$ $^\circ$	$Matlab$ $^\circ$	EXP [11] $^\circ$
1	0	0	0
0.6213	46.37	46.37	42.37
0.5203	52.13	52.08	52.07
0.3828	58.16	58.2	54.03
0.2973	61.27	61.22	62.77
0.2009	64.44	64.47	65.37
0.0018	70.48	70.53	66.90

(a)

MERR			
Me	$Abaqus$ $^\circ$	$Matlab$ $^\circ$	EXP [11] $^\circ$
1	0	0	0.00
0.6213	48.96	50.02	42.37
0.5203	55.44	56.19	52.07
0.3828	62.21	62.76	54.03
0.2973	65.7	65.94	62.77
0.2009	69.19	69.29	65.37
0.0018	75.71	75.23	66.90

(b)

Table 3.2: Yemeng granite: comparison between initiation angles obtained numerically and predicted with Abaqus

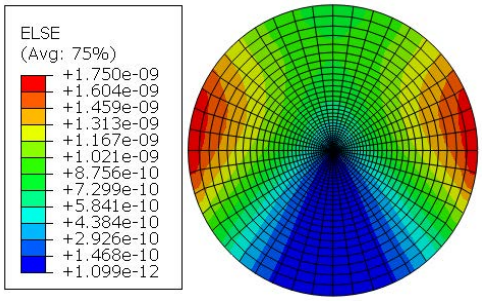

(a) Me=1

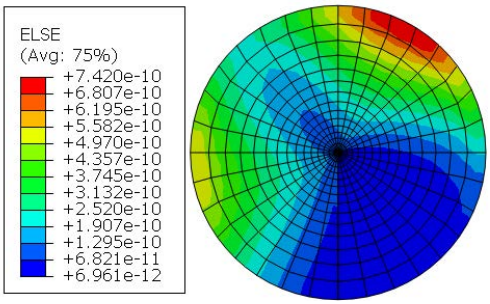

(b) Me=0.6213

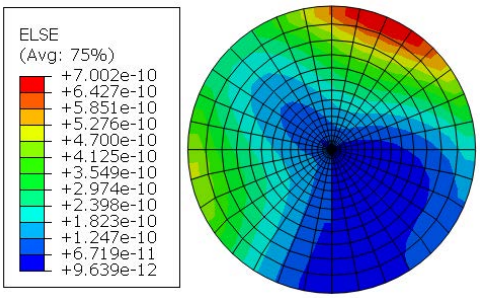

(c) Me=0.5203

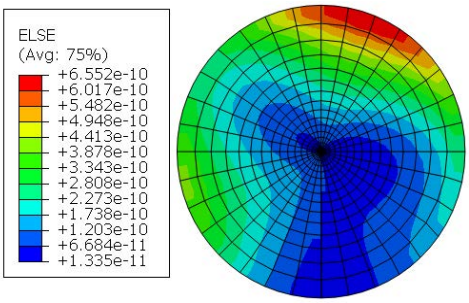

(d) Me=0.3828

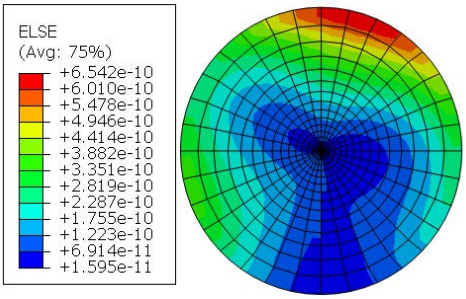

(e) Me=0.2973

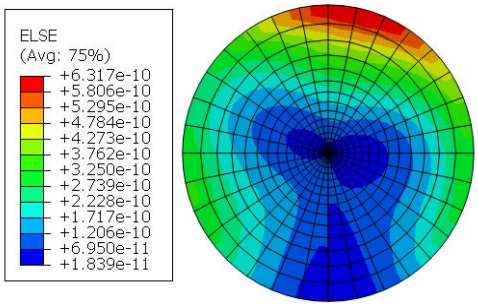

(f) Me=0.2009

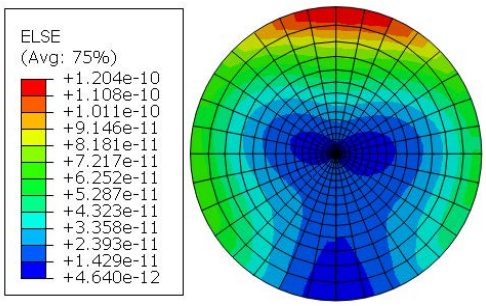

(g) Me=0.0018

Figure 3.9: Yemeng granite: ELSE contour plots in the model

3.1.3 Takkab Granite

For this granite rock, the same procedure adopted for Yemeng granite was followed. It is an Iranian granite extracted in the region of Takkab. The experimental results were taken from the papers [4] and [21]. The dimensions of the FE model and the properties of Takkab granite are the following:

L=220 mm
w=40 mm
t=20 mm
ν=0.28
E=45000 MPa
K_{Ic}=1.39 MPa$\sqrt{m}$
σ_t=12.2 Mpa

The radius of the control volume is $R_c = 3.67\,mm$. Considering the properties, this granite is quite similar to the Yemeng material. There is a difference between the specimens, concerning the previous material. The crack starts from the upper side of the rectangular SEN specimen and to simulate mixed modes it is sufficient to change the dimension called L_3 in the picture 3.10.
The comparison between failure loads predicted with the ASED criterion and the real values obtained with the experimental tests is presented in fig. 3.11 and tab. 3.3 The

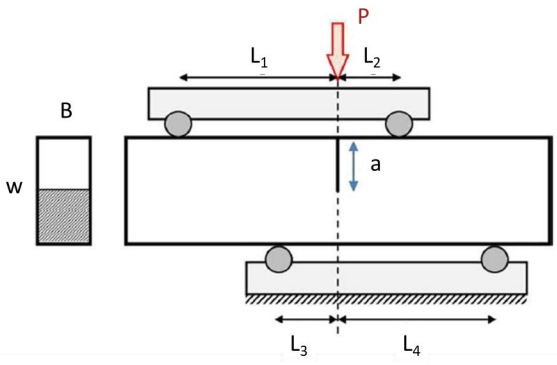

Figure 3.10: Takkab granite: mixed-mode configuration used for the experimental tests in Ref. [4]

results are the expected ones: a proper agreement between predictions and reality for mixed-mode loading configurations, a higher discrepancy for pure mode I and pure mode II, especially for the latter one. For Takkab granite too, it was interesting to compare

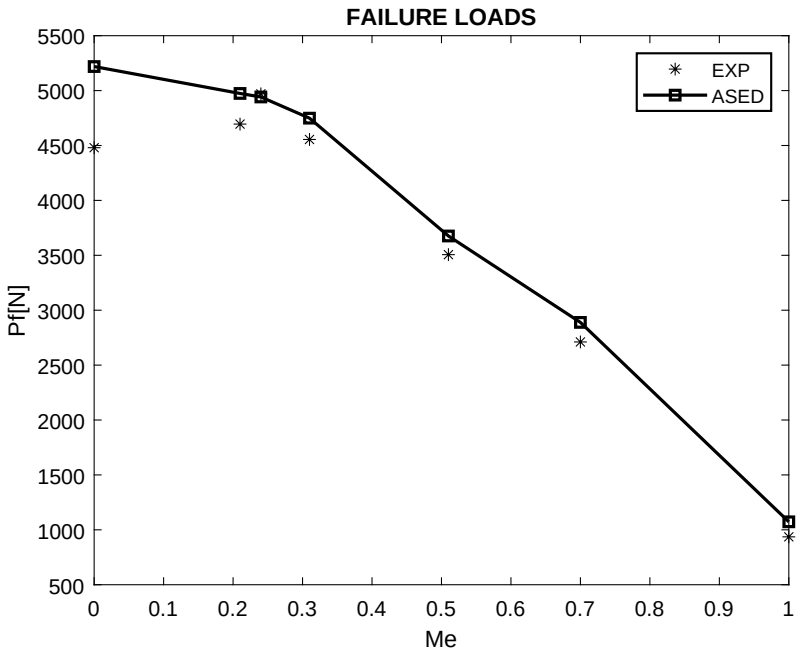

Figure 3.11: Takkab granite: failure loads comparison. Experimental data were taken from Ref. [4]

FAILURE LOADS							
	ASED			EXP [4]			
Me	K_1 $MPa\sqrt{m}$	K_2 $MPa\sqrt{m}$	P_f N	K_1 $MPa\sqrt{m}$	K_2 $MPa\sqrt{m}$	P_f N	$\Delta\%$
1	1.52	0.00	1073	1.394	0.000	936	-14.68
0.7	1.16	0.59	2889	1.140	0.582	2711	-6.58
0.51	0.93	0.71	3676	0.710	0.697	3506	-4.85
0.31	0.46	0.86	4749	0.465	0.866	4555	-4.27
0.24	0.48	0.89	4942	0.347	0.930	4970	0.56
0.21	0.30	0.88	4974	0.303	0.876	4695	-5.93
0	0.00	0.90	5219	0.000	0.813	4480	-16.49

Table 3.3: Takkab granite: predicted and real failure loads

theoretical criteria to predict the trend of the normalized values K_1/K_{Ic} and K_2/K_{Ic} and the initiation angle of the growing crack.

The GMTS criterion is again one of the best, but it is remarkable how proper is the G criterion in fitting the experimental trend. Once more, as with Yemeng granite, the SED criterion is the most far from the real curve, overestimating the values.

It is strange to notice the little drop in the curve of the SED and the G criterion for the initiation angle when $Me = 0.24$. Between $Me = 0.21$ and 0.24, there's not a considerable difference, however, the angle must increase while approaching mode II. This is better predicted by the other two stress criteria and also by Abaqus both for the MTS and the G criterion. Simply to compare the *ELSE* magnitude in the control volume with the Yemeng granite, figure 3.14 is presented. The contour plots are obviously upside down concerning Yemeng ones because the crack starts from the opposite side. The *peanut shape* in fig. 3.14g looks more defined.

This is one of the first materials tested, therefore it was thought convenient to investigate deeper what happens near the crack tip, where Linear Elastic Fracture Mechanics is not valid. This is a plastic deformation area and it is usually identified with a distance called r_c.

This distance is what is used to apply the GMTS criterion. For Takkab granite the distance is calculated as $r_c = 2.08\,mm$, considering the properties of the material described above. The contour plots of the Von Mises stress are reported for each mixed-mode. Keeping in mind that the material is considered perfectly linear and that the tensile strength is $12.2\,MPa$, the plastic zone is highlighted with the color blue. It is visible the peanut shape mentioned before. This time the peanut is perpendicular to the crack for pure mode I. The dimensions of the peanut were calculated. For pure mode I the radius of the region is around $1.84\,mm$, almost equal to the Schmidt prediction, used for the GMTS criterion. The peanut zone becomes bigger while increasing the contribution of mode II, until a maximum value around $3\,mm$.

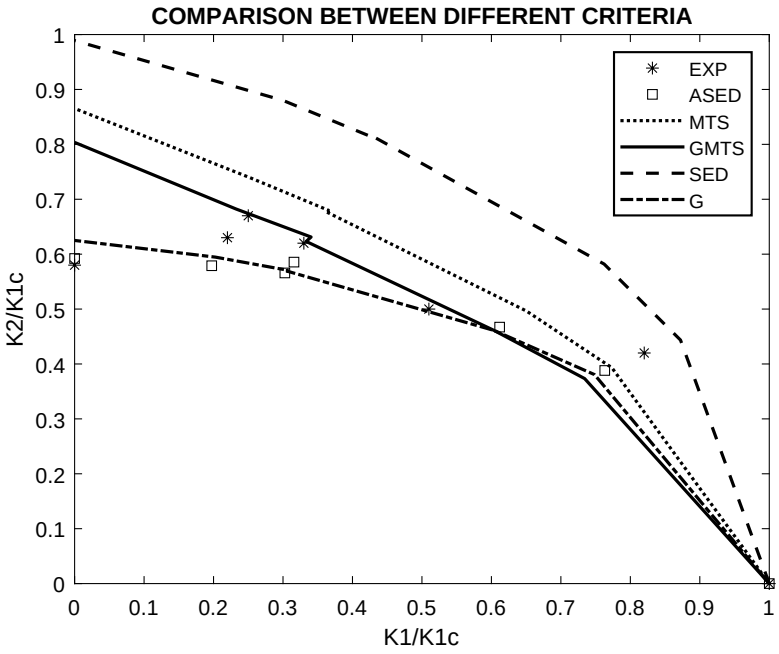

Figure 3.12: Takkab granite: normalized stress intensity factors comparison. Experimental data were taken from Ref. [4]

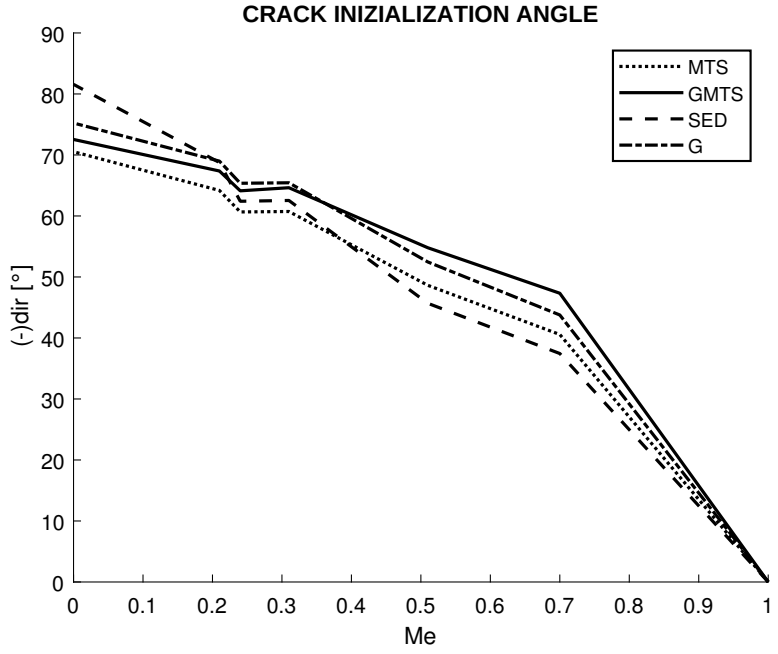

Figure 3.13: Takkab granite: initiation angles comparison

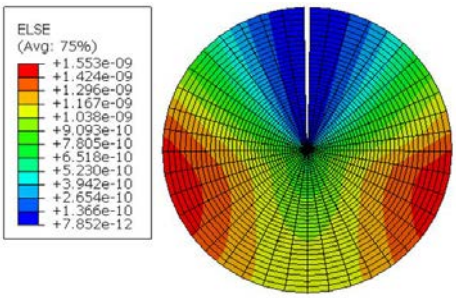

(a) Me=1

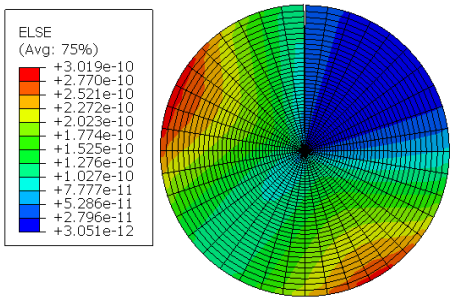

(b) Me=0.7

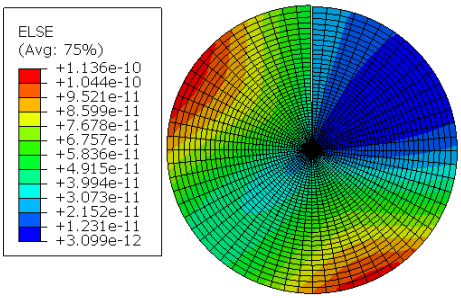

(c) Me=0,51

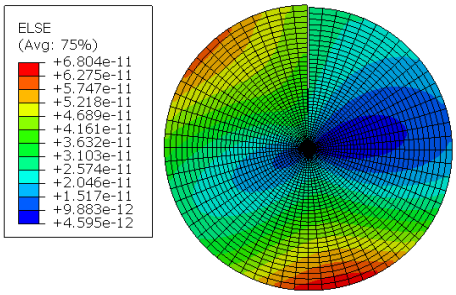

(d) Me=0,31

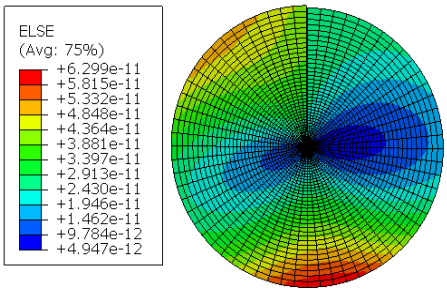

(e) Me=0,24

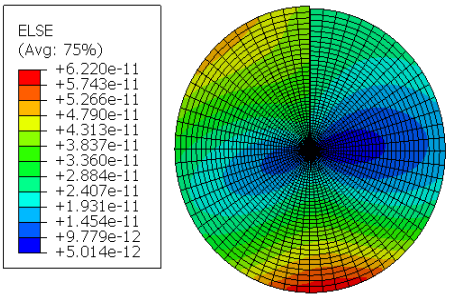

(f) Me=0,21

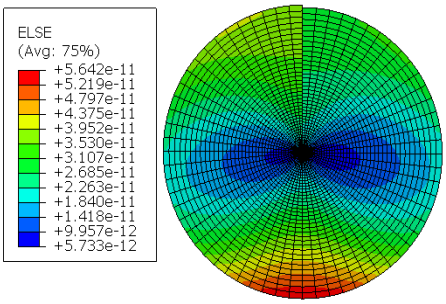

(g) Me=0

Figure 3.14: Takkab granite: ELSE contour plots in the model

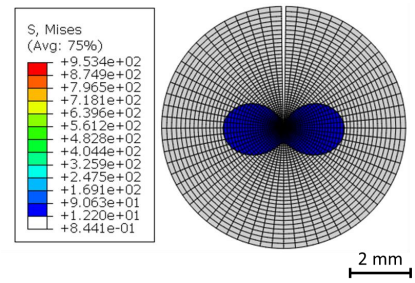

(a) Me=1

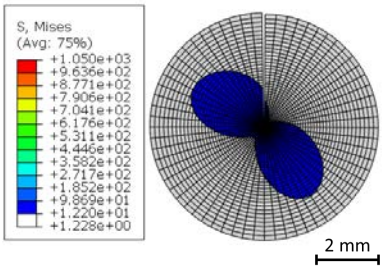

(b) Me=0.7

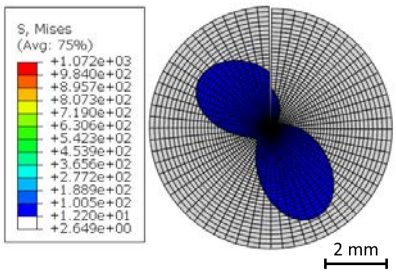

(c) Me=0,51

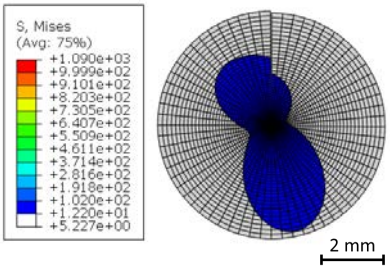

(d) Me=0,31

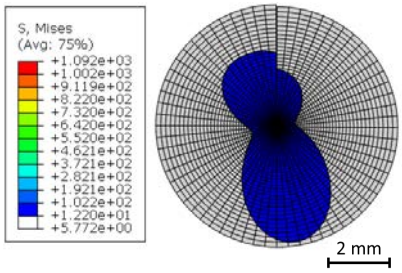

(e) Me=0,24

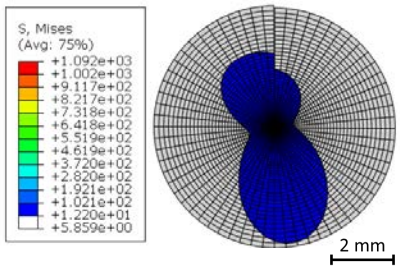

(f) Me=0,21

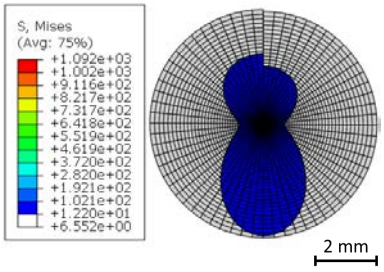

(g) Me=0

Figure 3.15: Takkab granite: plastic zone contour plots

3.1.4 Dehbid Marble

Dehbid marble is another Iranian rock with mechanical properties similar to the Takkab granite. The study on this material presents some singularities, compared to the previous. The first peculiarity was about the radius of the control volume: considering the following mechanical properties, the radius is $R_c = 9.7\,mm$, which means quite a large control volume.

L=220 mm
w=40 mm
t=16 mm
ν=0.27
E=35000 MPa
K_{Ic}=1.35 MPa$\sqrt{m}$
σ_t=7.35 MPa

The paper used to find mechanical properties of the specimens tested and the failure loads is reference [22], by Aliha and others.
The configuration of loads and boundary conditions is the same used for Takkeb granite. The comparison between failure loads is showed in fig. 3.16 and tab. 3.4.
There is a huge problem with mode I and mode II. Concerning mode II the discrepancy

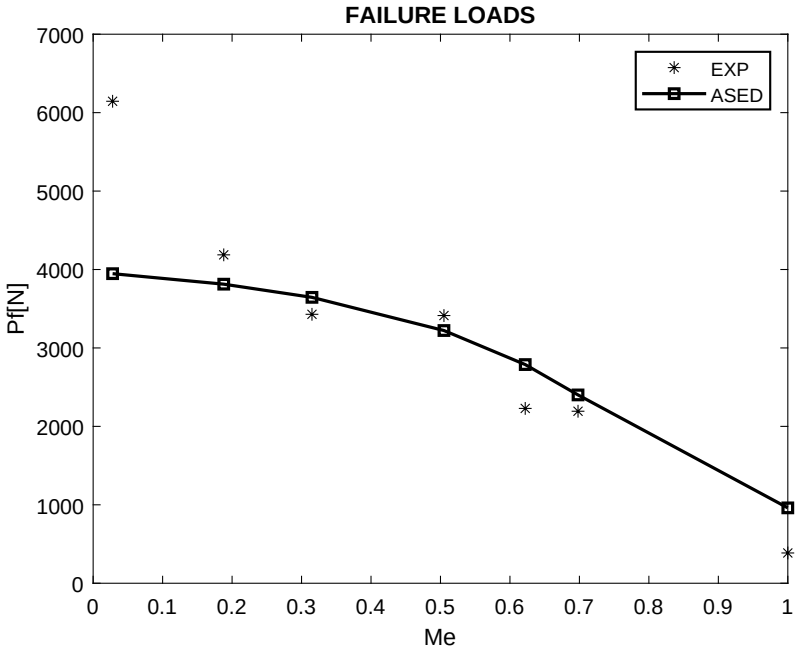

Figure 3.16: Dehbid marble: failure loads comparison. Experimental data were taken from Ref. [22]

is less surprising because this happened also with other materials. Hence the focus was

FAILURE LOADS							
	EXP [22]			ASED			
Me	K_1 $MPa\sqrt{m}$	K_2 $MPa\sqrt{m}$	P_f N	K_1 $MPa\sqrt{m}$	K_2 $MPa\sqrt{m}$	P_f N	$\Delta\%$
1	1.39	0.00	386	1.70	0.00	961	-148.921
0.698	1.10	0.55	2193	1.19	0.61	2401	-9.47397
0.622	0.88	0.58	2229	1.02	0.69	2788	-25.0979
0.505	0.88	0.85	3413	0.77	0.76	3222	5.58496
0.315	0.45	0.82	3429	0.44	0.82	3645	-6.29499
0.188	0.20	0.95	4187	0.26	0.84	3813	8.941464
0.028	0.00	1.16	6145	0.04	0.85	3947	35.77409

Table 3.4: Dehbid marble: predicted and real failure loads

to improve mode I discrepancy.

Different attempts were made with no success. Trying to increase the control volume (considering smaller tensile strength) did not give the desired improvement. Neither changing the Young modulus because both Wc (critical energy density) and $\overline{W}$ (energy density) are proportional to E, hence the failure load does not change. Once it was checked that the reason behind the incongruity was not related to the properties used, the configuration was studied. The configuration used to simulate mode I, which gave as failure load $961\,N$ is the same used for Takkab granite. A possible option is to use the geometrical rules of the Murakami SFPB specimen, but in this case, the failure load is around 766 N, therefore this wasn't the configuration used in paper [22] to find the first failure load. The last attempt was made with a 3PB configuration, that gave $P_f = 599\,N$, really far from the experimental value. The possibility that the data was registered wrongly is to exclude because experimental tests were carried out three times for each Me. In conclusion, it is still an open question to know what configuration was used to break the Dehib marble specimen under mode I loading condition, but this is not a valid reason to affirm that the ASED criterion failed. For the other tested Me predictions fit excellently the real values.

The other criteria were performed with the following results. Observing fig. 3.17 there are no surprises. As usual, the GMTS criterion is the best fitting the experimental trend, followed by the MTS. The G criterion proposes lower values compared with the real trend, while the SED criterion is the opposite, the values are higher and wrong. With regards to the direction of propagation of the crack in fig. 3.18 the four criteria are quite in good accordance, also with what is predicted by Abaqus both for MTS and MERR directions. An experimental comparison is not possible since data were not available.

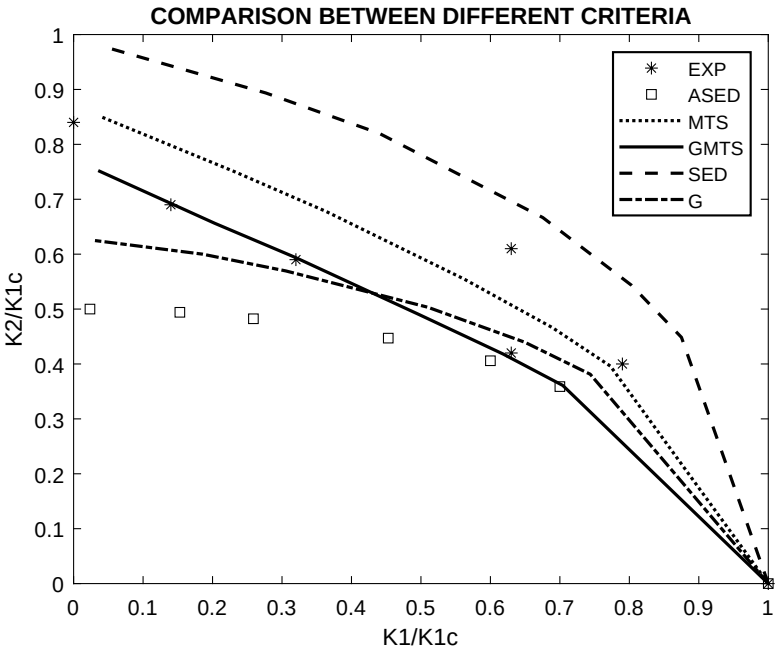

Figure 3.17: Dehbid marble: normalized stress intensity factors comparison. Experimental data were taken from Ref. [22]

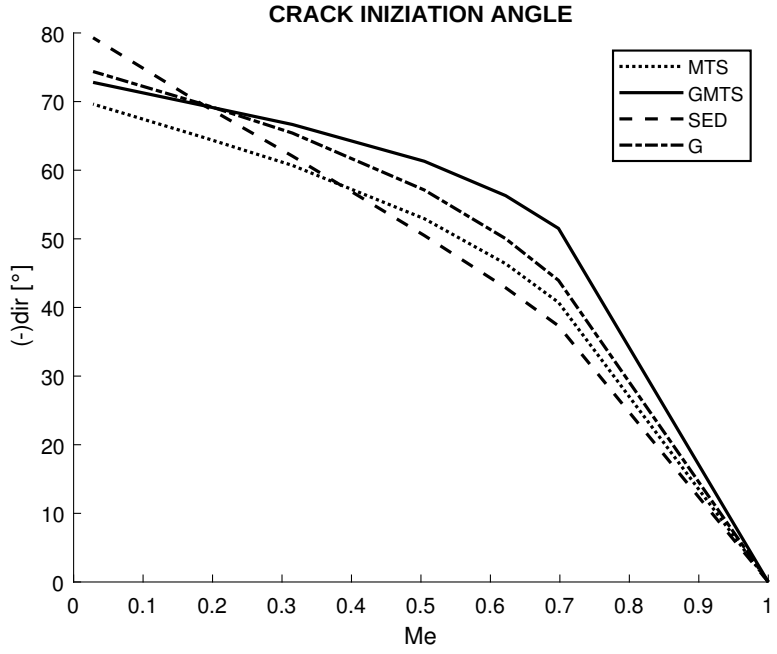

Figure 3.18: Dehbid marble: initiation angles comparison

3.1.5 Indiana Limestone

This is a rock from America, studied by Ingraffea in [23]. The material properties considered comes from *A Standard Rock Suite for Rapid Excavation Research*, Krech, Henderson and Hjelmstad [24]. In that book, different rocks are analyzed and the properties are recorded for three different samples of each one. To perform the ASED criterion, the average values were used.

L=381 mm
w=127 mm
t=63.5 mm
ν=0.27
E=30130 MPa
K_{Ic}=0.87 MPa$\sqrt{m}$
σ_t=5.23 MPa

In this case the control volume radius is $R_c = 7.9\,mm$. The experimental results available for the study are not the expected ones: both for K_{1f}, K_{2f} and the failure loads it is not possible to observe a real trend, on the contrary of the other materials.

The reason why the plot in 3.21 is so different from the other materials is because

EXPERIMENTAL RESULTS [23]					
Me	K_1 $psi\sqrt{in}$	K_2 $psi\sqrt{in}$	K_1 $MPa\sqrt{mm}$	K_2 $MPa\sqrt{mm}$	P_f N
0.0250	28.92	736.34	1.01	25.77	14694
0.0396	45.35	727.90	1.59	25.48	14525
0.0394	43.09	696.11	1.51	24.36	13891
0.0386	41.04	676.03	1.44	23.66	13490
0.2925	390.04	788.36	13.65	27.59	15732
0.3183	493.47	903.41	17.27	31.62	18028
0.4132	389.80	513.86	13.64	17.99	10254
0.4307	423.24	527.11	14.81	18.45	10518
0.4152	425.48	557.23	14.89	19.50	11119
0.4430	480.59	575.40	16.82	20.14	11482
0.6034	553.55	397.67	19.37	13.92	7936
0.5840	665.21	509.34	23.28	17.83	10164
0.5525	619.03	524.60	21.67	18.36	10468
0.5340	585.87	526.41	20.51	18.42	10505
1.0000	785	0	27.475	0	4716

Table 3.5: Indiana limestone: experimental results

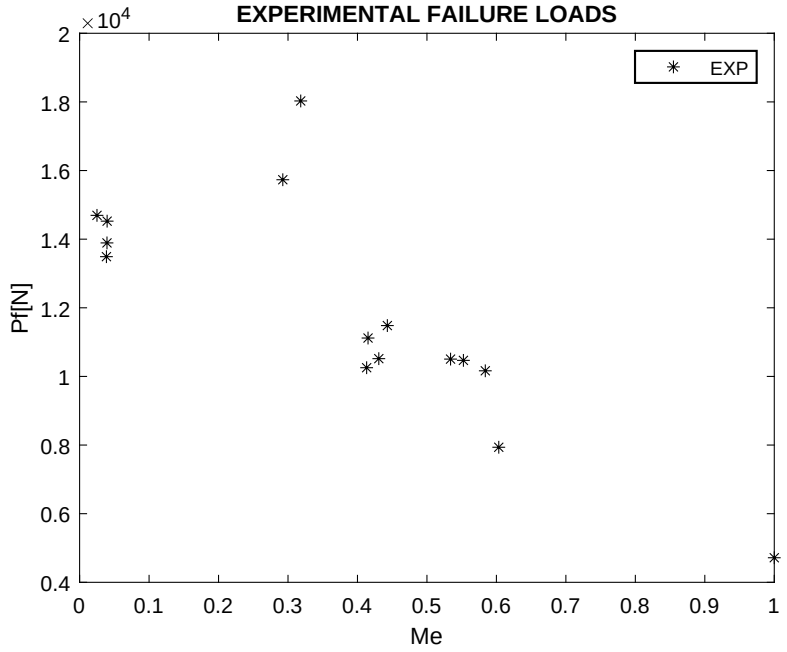

Figure 3.19: Indiana limestone: experimental failure loads. Exp data were taken from Ref. [23]

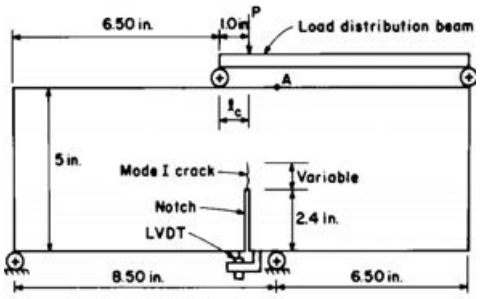

Figure 3.20: Indiana limestone: mixed-mode configuration used for experimental tests [23]

of the author's choices. To the aim of this study, the specimens considered are pre-cracked and in mixed-mode loading conditions, the crack propagates from the pre-crack tip. Ingraffea tested also non-pre-cracked specimens and specimens where the crack starts not precisely from the notch tip due to a previous load trial under pure mode I. It is comprehensible that proposing a comparison between ASED predictions and real values is more difficult. However, the FE model was prepared with the scheme in fig. 3.20 (inches were then converted in mm, simply to have a better sensibility in the dimensions). To perform mixed mode conditions the distance l_c shown in fig.3.20 assumes these values: $l_c = 0.9375,\ 0.625,\ 0.5,\ 0.25$ [in].

ASED predictions give, as first results, the failure loads trend presented in fig. 3.21. The failure load decreases approaching pure mode II. This is not realistic. One possible explanation is in the loading scheme: the load application point at the left of the crack tip is probably too much close to the crack itself. It means that the influence of pure mode I is still too important in the mixed-modes tested and for this reason, the failure loads

ASED Pf	
Me	P_f
	N
1	4921
0.5437	14178
0.3688	13028
0.2706	12376
0.0225	10709
0.0243	10383

Table 3.6: Indiana limestone: ASED predictions for failure loads

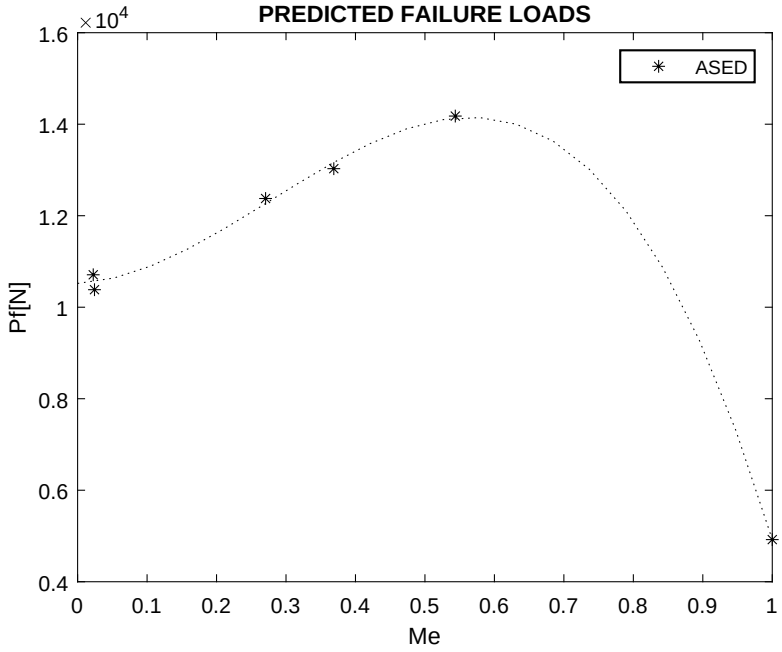

Figure 3.21: Indiana limestone: ASED predictions for failure loads

turn out to be smaller (because with pure mode I it is easier to propagate a pre-existing crack). Indeed the lower Me obtained is not rounded to 0, which means that pure mode II can not be simulated appropriately. In the paper [11], it is explained that if $l_c/W < 0.5$, the pure mode II won't be simulated. For this reason, the authors suggest maintaining $l_c/W > 1.5$. In the studied cases, this condition is never respected. Even Ingraffea himself, in [23], observed how difficult was to evaluate correctly pure mode II and mixed-mode. In confirmation of this idea, the *ELSE* contour plot was checked. The *peanut shape* in fig. 3.22 is almost unrecognizable, and it is a typical effect of an unsuitable choice of l_c for FE simulations. To complete the study, here below it is showed in the same plot the predicted trend of failure loads and the real values (3.23a). As a mere excercise, the theoretical criteria are performed and the results are presented in plots 3.23b and 3.23c. These plots have no value in terms of validation of the criteria.

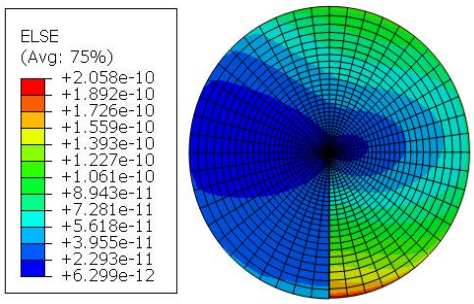

Figure 3.22: Indiana limestone: ELSE contour plot in the model, for $l_c = 0$

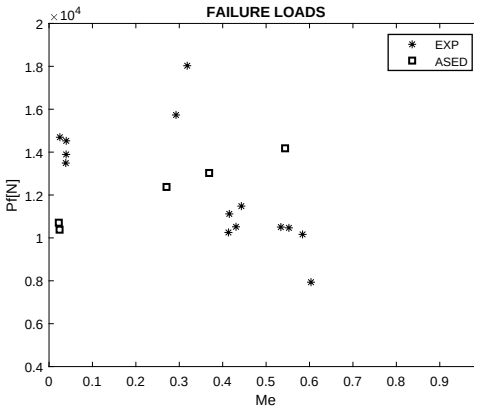

(a) Failure loads comparison [23]

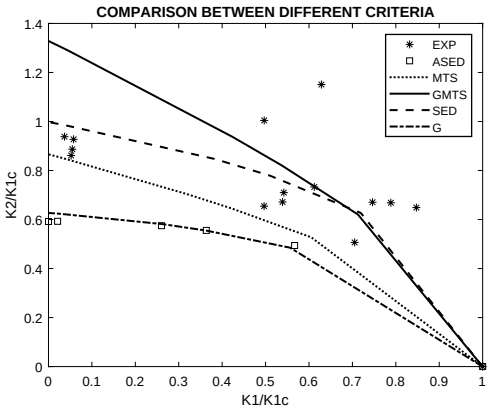

(b) Normalized stress intensity factors comparison [23]

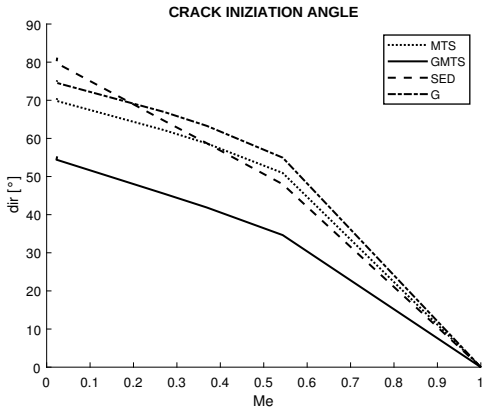

(c) Initiation angles comparison

Figure 3.23: Indiana limestone: theoretical criteria results.

3.1.6 Westerly Granite

The last rock was studied by Ingraffea with Indiana Limestone in the same papers and it is called Westerly granite. The properties of this rock and the specimen tested are presented here:

L=381 mm
w=127 mm
t=63.5 mm
ν=0.21
E=19300 MPa
K_{Ic}=2.019 MPa$\sqrt{m}$
σ_t=9.52 MPa
R_c=14.3 mm

For this rock, the same considerations made for Indiana limestone are valid. The specimen used for experimental tests was the same (3.20). Both the failure loads and the normalized stress intensity factors do not present a real trend, because different tests were carried out in different conditions (pre-cracked or non-pre-cracked specimens, etc.)
Hereafter the ASED predictions are presented in fig. 3.25. It is undeniable that these are not valid predictions, and the plot with the comparison between theoretical criteria and real results confirm it.

EXPERIMENTAL RESULTS [23]					
Me	K_1 $psi\sqrt{in}$	K_2 $psi\sqrt{in}$	K_1 $MPa\sqrt{mm}$	K_2 $MPa\sqrt{mm}$	P_f N
0.0252	73.68	1861.63	2.58	65.16	37149
0.0241	75.08	1980.54	2.63	69.32	39522
0.3812	939.33	1376.77	32.88	48.19	27473
0.5365	1052.31	938.04	36.83	32.83	18719
0.4193	1053.62	1361.67	36.88	47.66	27172
0.4374	1168.82	1424.61	40.91	49.86	28428
0.4965	1188.34	1201.60	41.59	42.06	23978
0.4400	1206.14	1457.98	42.21	51.03	29094
0.5742	1289.57	1019.31	45.14	35.68	20340
0.5116	1292.25	1245.99	45.23	43.61	24864
0.5771	1419.90	1111.95	49.70	38.92	22189
1	1824	0	63.84	0	10958

Table 3.7: Westerly granite: experimental results

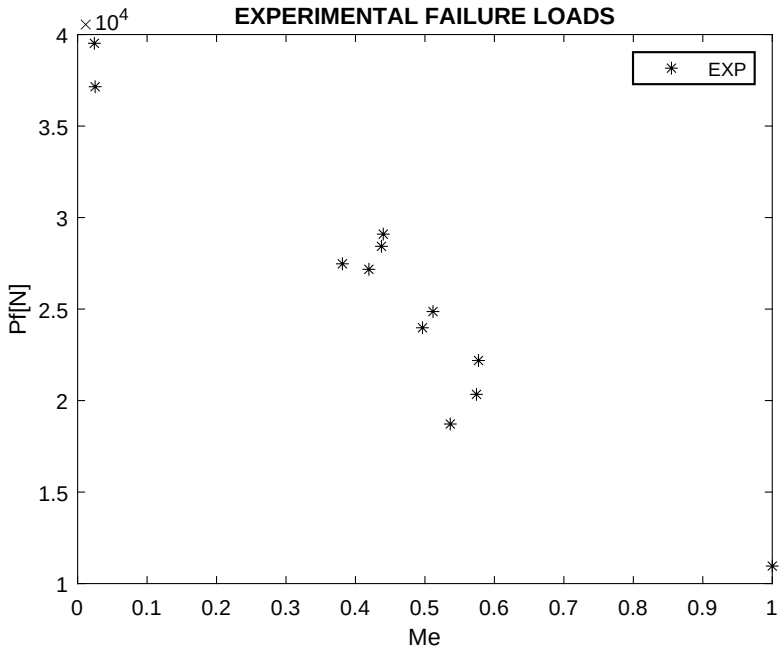

Figure 3.24: Westerly granite: experimental failure loads. Experimental data were taken from Ref. [23]

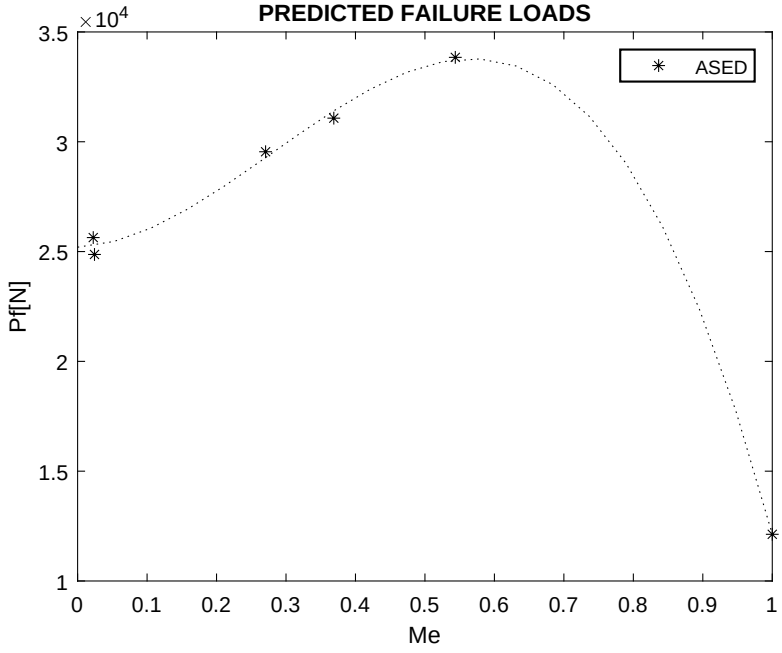

Figure 3.25: Westerly granite: ASED predictions for failure loads

ASED Pf	
Me	P_f
	N
1	12126
0.5437	33843
0.3688	31075
0.2706	29545
0.0225	25637
0.0243	24868

Table 3.8: Westerly granite: ASED predictions for failure loads

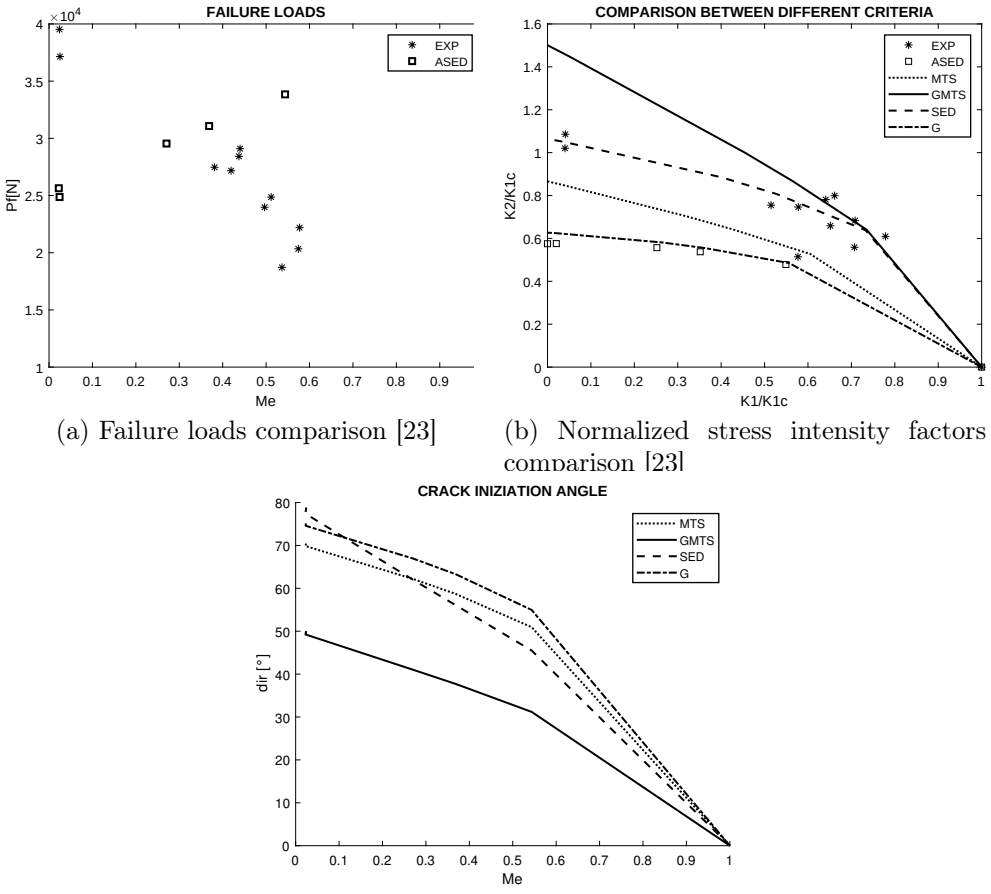

(a) Failure loads comparison [23]

(b) Normalized stress intensity factors comparison [23]

(c) Initiation angles comparison

Figure 3.26: Westerly granite: theoretical criteria results.

3.2 Polymers

3.2.1 An Overview

The second category of materials studied is Polymers. Only polymers that present a brittle fracture at room temperature are used. No elastomer or ductile polymers were considered. In detail, the materials are two types of PMMA, a rigid polyurethane foam, and a type of resin epoxy.
PMMA's complete name is Polymethyl methacrylate, commonly known as Plexiglass, which belongs to the thermoplastic class. Two types of PMMA were tested because it was the object of several studies and therefore data are abundant in the literature.
For what concerns the polyurethane foam, the properties and the fracture behavior of this material depend on the density of the foam. It was quite difficult to predict failure loads with the ASED criterion.
The last material studied is a common epoxy, for which the predictions were not promising. The experimental data available for the epoxy were obtained with the hypothesis of plane stress field even if the specimen was quite thick. This was a wrong approach to the purpose of applying the ASED criterion. Furthermore, epoxy was also tested when blended with multiwalled nanotubes of graphene. The material obtained is a composite, that is hardly homogeneous or isotropic. An attempt was made to apply the theoretical criteria on this composite, with poor results, therefore they have not been reported in the section.

3.2.2 PMMA-1^{st} type

The first material studied was PMMA. The experimental tests used as reference were presented in [25].
The dimensions and properties of the FE model are the following:

L=110 mm
w=20 mm
t=5 mm
ν=0.4
E=2000 MPa
K_{Ic}=1.87 MPa$\sqrt{m}$
σ_t=80 MPa

In the paper abovementioned [25] the Young modulus and the tensile strength were not specified. Looking for these properties in other papers, some average values were taken. For Poisson's ratio it was thought convenient to take a standard value for polymers that is 0.4. Some of the articles used are reported in the references [26] [27] [28] [29].

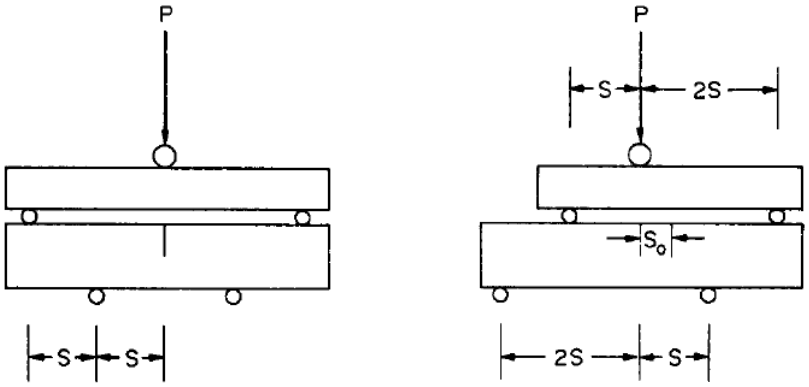

(a) (b)

Figure 3.27: PMMA-1st: configurations used for experimental tests in Ref. [25]

The crack length is $a = 10\,mm$, hence $a/W = 0.5$. With these properties the radius of the control volume was calculated as $R_c = 0.11\,mm$. The loading configuration used for the AFPB tests is presented in fig. 3.27. In the following two tables, experimental results for AFPB tests and ASED predictions are presented.

The comparison, presented in fig. 3.28 is encouraging. The ASED criterion fits properly

ASED PREDICTIONS			
Me	K_1 $MPa\sqrt{m}$	K_2 $MPa\sqrt{mm}$	P_f N
1	1.8598	0	191
0.9	1.7487	-0.3864	457
0.7	1.3580	-0.7431	729
0.5	0.9891	-0.9213	914
0.4	0.6426	-1.0210	1021
0.2	0.3307	-1.0708	1078
0.0	0.0191	-1.0882	1101

Table 3.9: PMMA-1st: ASED predictions

the experimental trend, without overestimating the failure loads, which is more precautional. The comparison between the other four criteria is presented in the next figures. Both for stress intensity factors and initiation directions the results are the expected ones. It was also possible the comparison with the real propagation angles because they were registered. The MTS and GMTS criteria are the best in fitting the experimental trend. It is interesting to notice that the ASED criterion is almost overlapped with the G criterion. In conclusion, the comparison between reality and theoretical criteria is convincing.
As previously done for Takkab granite, it is interesting to investigate the plastic zone near the crack tip for polymers, this type of PMMA was chosen. According to Schmidt,

EXPERIMENTAL RESULTS [25]				
Me	K_1 $MPa\sqrt{m}$	K_2 $MPa\sqrt{m}$	P_f N	dir $^\circ$
1	1.912	0	352	0
1	1.75	0	259	0
1	1.845	0	306	0
1	1.969	0	281	0
0.831	1.782	0.484	506	30.8
0.835	1.576	0.417	767	27.4
0.703	1.564	0.789	874	44.2
0.681	1.443	0.791	852	40.00
0.510	1.053	1.02	1142	62.50
0.513	1.060	1.017	1063	60.00
0.333	0.773	1.339	1439	61.50
0.334	0.761	1.317	1547	67.50
0.188	0.384	1.265	1446	70.20
0.194	0.420	1.336	1429	70.00
0.063	0.153	1.53	1226	70.80
0	0.000	1.769	2082	69.20

Table 3.10: PMMA-1st: experimental results

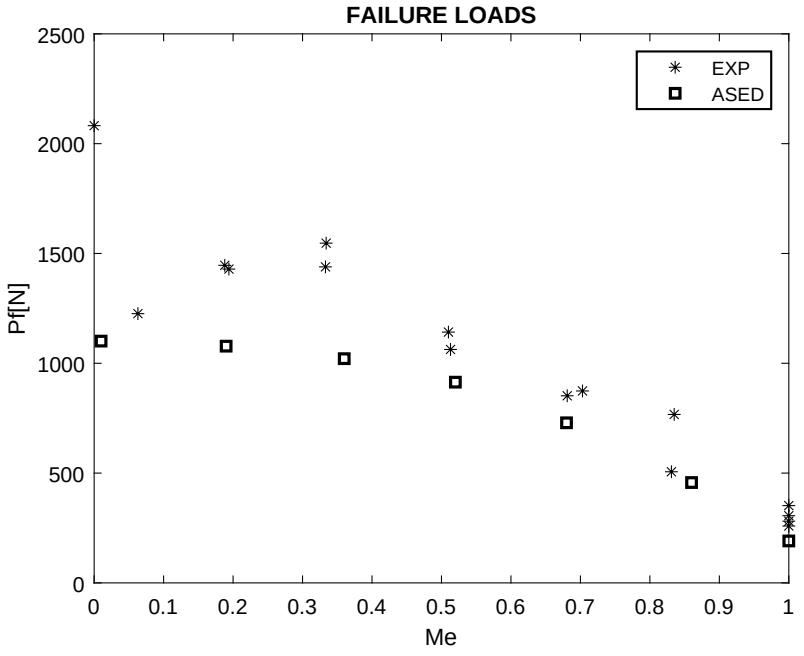

Figure 3.28: PMMA-1st: failure loads comparison. Experimental data were taken from Ref. [25]

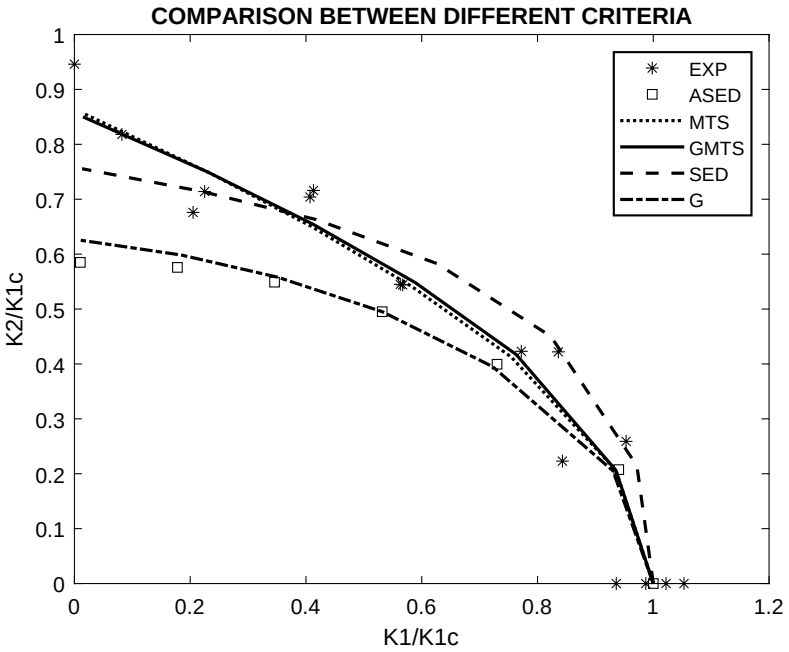

Figure 3.29: PMMA-1st: normalized stress intensity factors comparison. Experimental data were taken from Ref. [25]

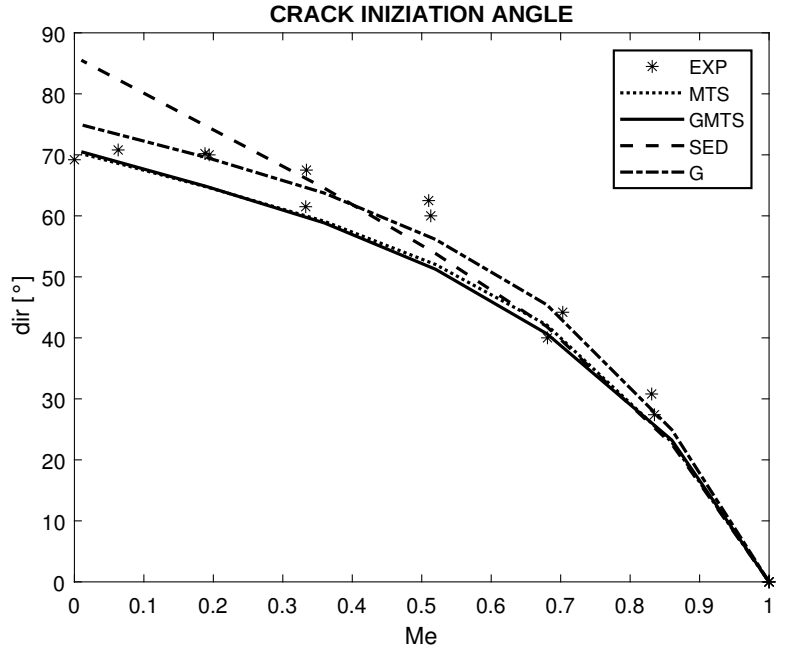

Figure 3.30: PMMA-1st: initiation angles comparison. Experimental data were taken from Ref. [25]

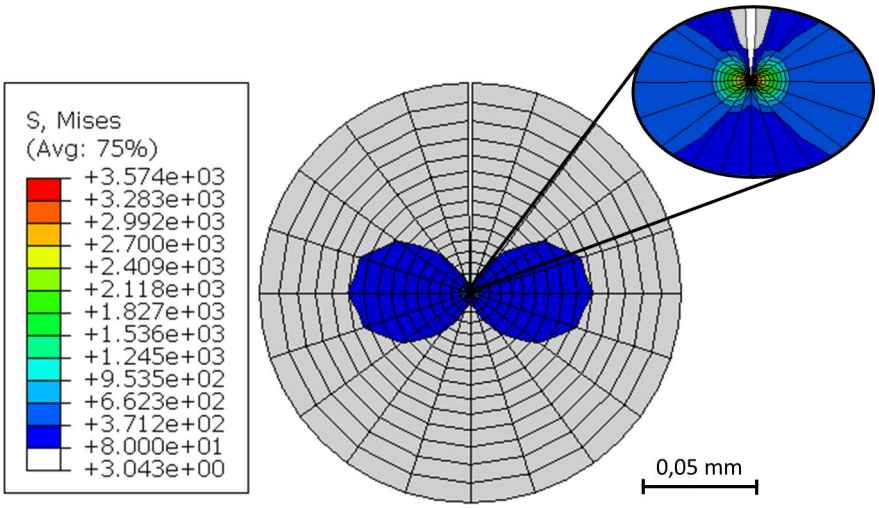

Figure 3.31: PMMA-1st: plastic zone contour plot, mode I

the r_c calculated to apply the GMTS criterion is $0.09\,mm$, quite small compared to the plastic radius obtained for the granite. The tensile strength considered is about $80\,MPa$. The contour plots showing the Von Mises ideal stress are presented in fig. 3.32. Only the areas where the stress is above the tensile strength are highlighted. The peanut shape presents the expected characteristics. It is perpendicular to the crack for pure mode I and parallels to it for pure mode II. His dimension increases while approaching mode II. The value of the radius is around $0.067\,mm$, which is a bit different from the Schmidt prediction. Anyway, they are quite similar. In fig. 3.31, there is a zoom of what happens at a distance of around $1\,\mu m$ from the tip. The stress increases to extremely high values.

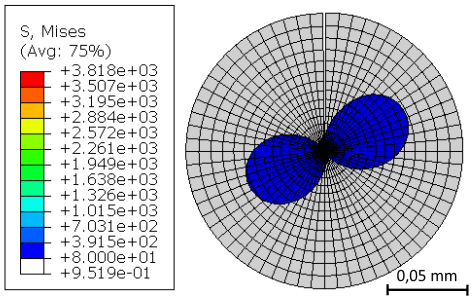

(a) Me=0.86

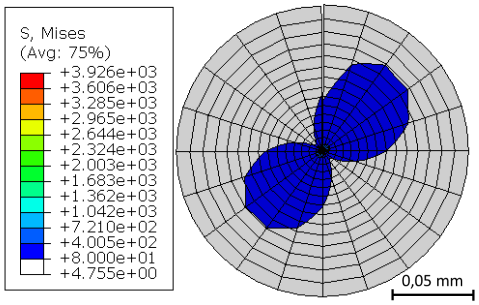

(b) Me=0,68

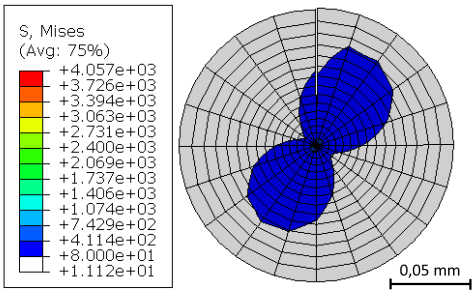

(c) Me=0,52

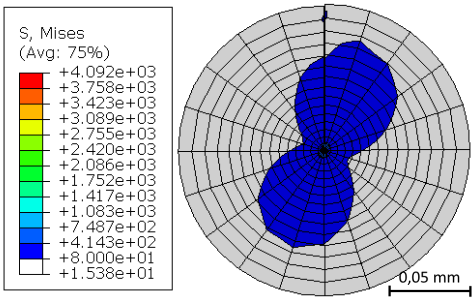

(d) Me=0,36

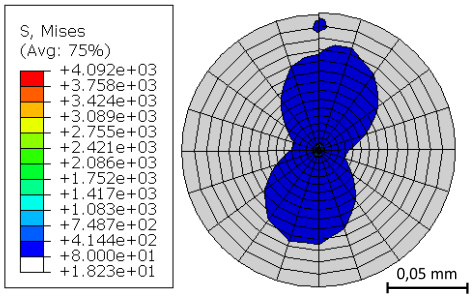

(e) Me=0,19

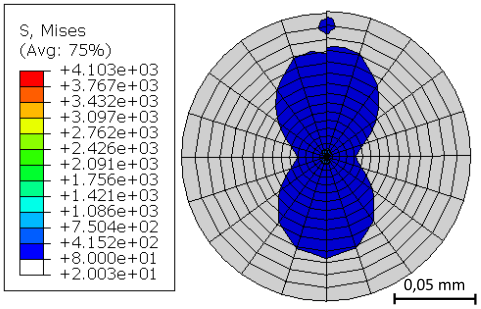

(f) Me=0,01

Figure 3.32: PMMA-1st: plastic zone contour plots

3.2.3 PMMA-2^{nd} type

Another set of data for PMMA specimens was available in the article [30], by Bhattacharjee, and Knott. The same mechanical properties of the previous study were used, but the specimen and the loading configuration are slightly different. Furthermore, through the experimental tests, a smaller K_{Ic} was registered. This is explained by the authors because K_{Ic} seems to depend on the cross-head speed of the test machine. This is possible but the application of the ASED criterion is based on the assumption that the fracture toughness is a material property. Using the same properties of the previous type of PMMA but changing the toughness will probably lead to mistakes.

L=110 mm
w=20 mm
t=6 mm
ν=0.4
E=2000 MPa
K_{Ic}=1.03 MPa$\sqrt{m}$
σ_t=80 MPa

The first difference in the configurations (fig. 3.33) is that the crack is on the lower side. Besides, they executed mode I loading configuration with an SFPB test, while, with the 1^{st} PMMA, they used a 3PB test. This could also affect the fracture toughness, but the value here considered, $K_{Ic} = 1.03\,MPa\sqrt{m}$ is still unusual.

With these data $R_c = 0.033\,mm$. It is remarkably a smaller radius compared to the first

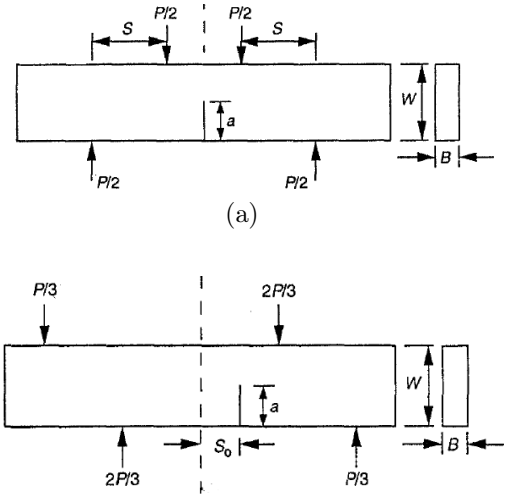

Figure 3.33: PMMA 2^{nd}: configurations used for experimental tests in Ref. [30]

type of PMMA. Results for the comparison between failure loads predicted by the ASED

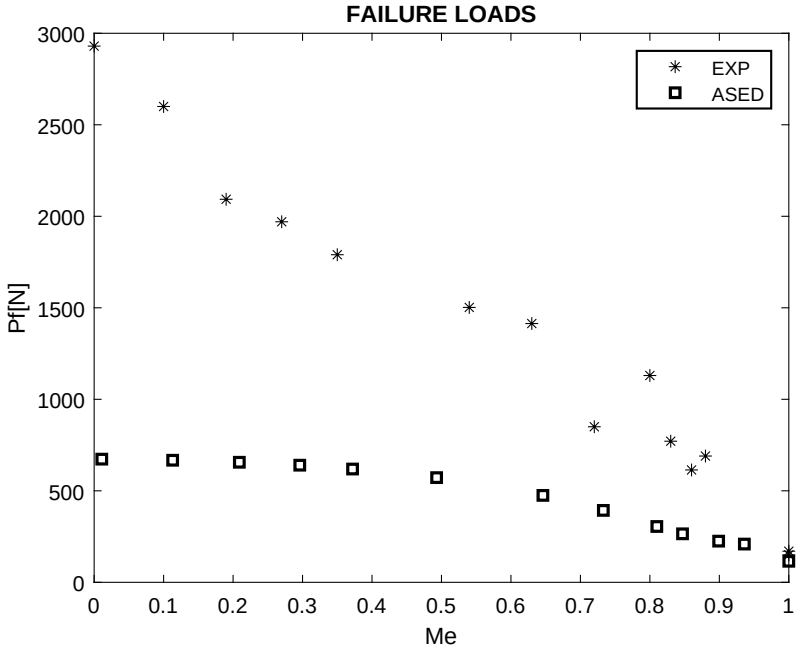

Figure 3.34: PMMA-2nd: failure loads comparison. Experimental data were taken from Ref. [30]

and the experimental ones are summarized in the following tables and figures.

It is a terrific result. By the way, every parameter was double-checked without detecting any mistakes. Even performing the other criteria, the plots are not satisfactory at all. The experimental trend is totally outside the scatter zone where the criteria's curves are. The problem regards only fig. 3.35, not the initiation angles. The comparison for directions looks like it was expected to be, which means that there are not a problem with the configuration used.

EXPERIMENTAL RESULTS [30]				
Me	K_1	K_2	P_f	dir
	$MPa\sqrt{m}$	$MPa\sqrt{m}$	N	$^\circ$
1	0.963	0	150	0
1	1.092	0	170	0
0.88	2.562	0.498	690	24
0.86	1.881	0.415	614	30
0.83	1.989	0.545	771	41
0.80	2.363	0.776	1130	47
0.72	1.279	0.601	850	48
0.63	1.514	0.989	1414	55.00
0.54	0.907	0.797	1502	62.00
0.35	0.782	1.292	1790	63.00
0.27	0.604	1.331	1970	65.00
0.19	0.423	1.389	2093	70.00
0.10	0.250	1.634	2600	72.00
0	0.000	1.936	2930	72.50

Table 3.11: PMMA-2nd: experimental results

ASED PREDICTIONS			
Me	K_1	K_2	P_f
	$MPa\sqrt{m}$	$MPa\sqrt{mm}$	N
1	0.59	0.00	200
1.0	1.02	0.00	115
0.9	1.00	0.10	209
0.9	0.98	0.16	225
0.8	0.94	0.23	265
0.8	0.90	0.28	305
0.7	0.81	0.36	393
0.6	0.70	0.43	475
0.5	0.51	0.52	572.35
0.4	0.37	0.56	619.43
0.3	0.29	0.57	639.56
0.2	0.20	0.59	655.90
0.1	0.11	0.60	667.40
0.0	0.01	0.60	673.20

Table 3.12: PMMA-2nd: ASED predictions

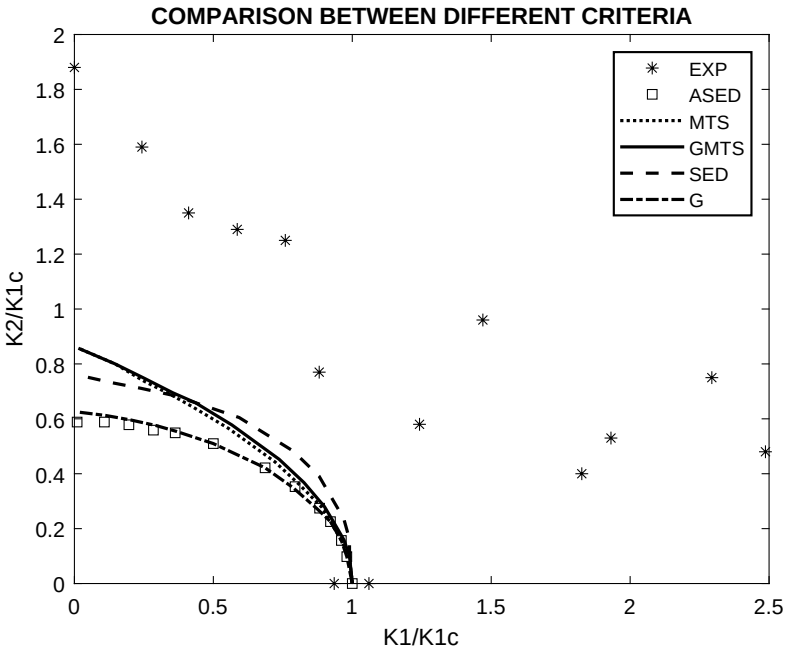

Figure 3.35: PMMA-2^{nd}: normalized stress intensity factors comparison. Experimental data were taken from Ref. [30]

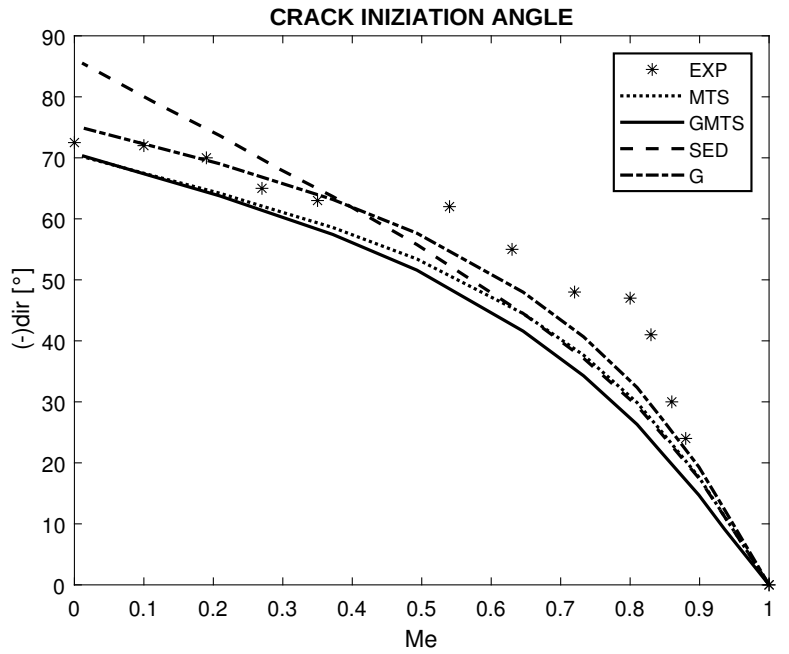

Figure 3.36: PMMA-2^{nd}: initiation angles comparison. Experimental data were taken from Ref. [30]

3.2.4 Epoxy Resin

The last polymer studied is an epoxy resin, the epoxy resin ML-506 (Bisphenol F), which AFPB test results are presented in [17]. In that paper, not only pure epoxy was analyzed: AFPB tests were carried out on specimens made of epoxy with a small percentage of fibers. The fibers are multiwalled nanotubes of graphene. ASED was performed also on these composites with bad results. The hypothesis behind the method were not respected. Therefore the results are not included in this section. Pure epoxy properties and specimen's dimensions are presented hereafter.

L=110 mm
w=20 mm
t=10 mm
ν=0.3
E=3150 MPa
K_{Ic}=1.62 MPa$\sqrt{m}$
σ_t=68.35 MPa
a=10 mm
R_c=0.15 mm

The configuration is shown in fig. 3.37. The comparison is shown in fig. 3.38 and

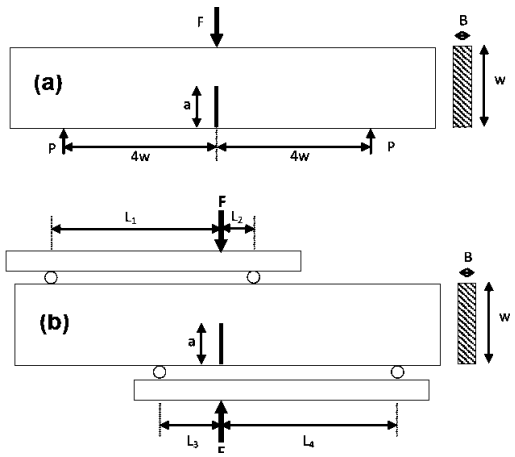

Figure 3.37: Epoxy: configurations used for experimental tests in Ref. [17]

tab. 3.13 is quite good. As usual, the ASED predictions are worse near mode II, but, on the whole, the discrepancy is under control. For what concerns the MTS, GMTS, SED,

FAILURE LOADS							
	ASED			EXP [17]			
Me	K_1 $MPa\sqrt{m}$	K_2 $MPa\sqrt{m}$	P_f N	K_1 $MPa\sqrt{m}$	K_2 $MPa\sqrt{m}$	P_f N	$\Delta\%$
1.00	1.62	0.00	216	1.62	0.012	215	-0.23
0.70	1.25	0.64	941	1.41	0.72	1050	10.37
0.50	0.83	0.87	1181	1.02	1.022	1408	16.10
0.29	0.51	0.97	1240	0.65	1.31	1804	31.30
0.01	0.09	1.02	1822	0.012	1.49	2727	33.16

Table 3.13: Epoxy: predicted and real failure loads

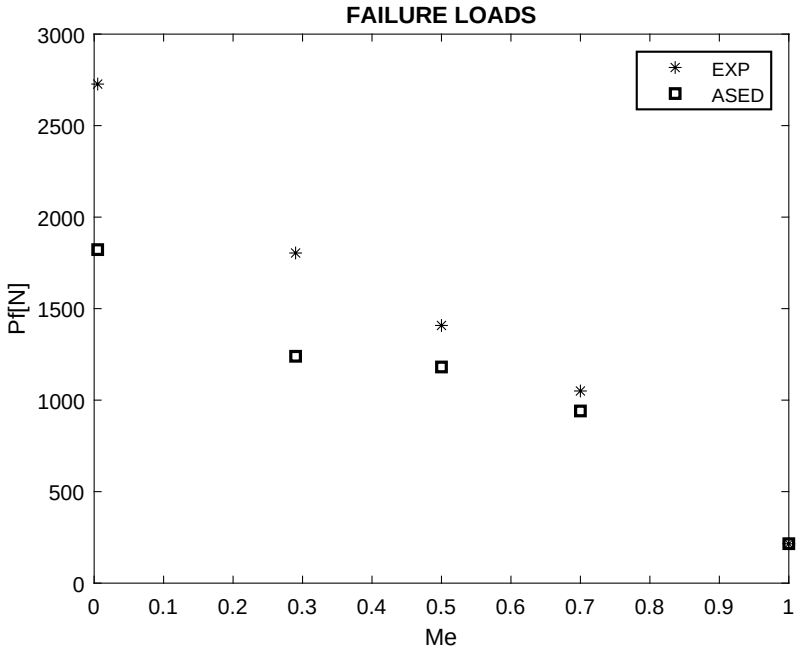

Figure 3.38: Epoxy: failure loads comparison. Experimental data were taken from Ref. [17]

and G-criterion, they were performed with the following results: looking at fig. 3.39, the SED criterion is the one that fits better the experimental trend. The MTS is closed to the GMTS curve but they are unexpectedly not the closest to the real values. The G criterion is, as usual, predicting lower results. With regards to the initiation angles, the four criteria are quite close, but the real values of the angles were not registered, hence it is not possible the comparison with the reality.

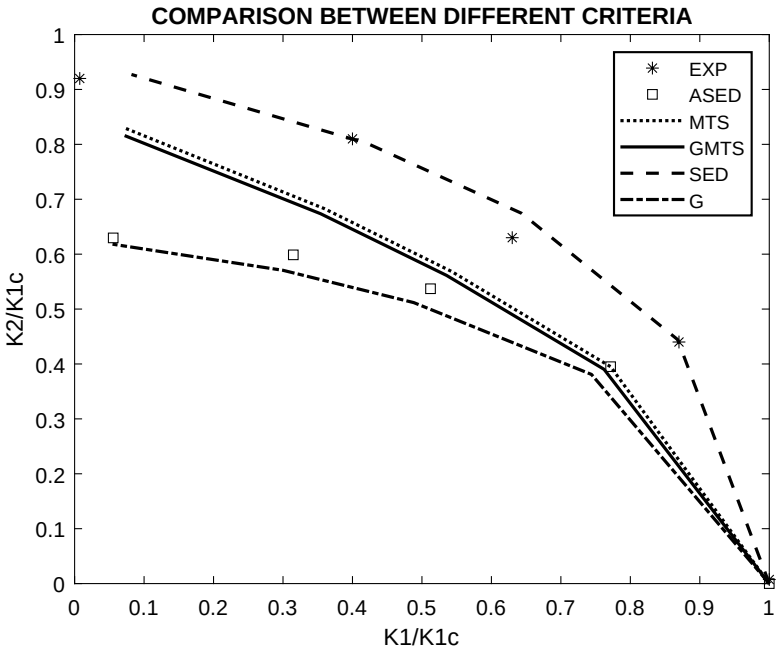

Figure 3.39: Epoxy: normalized stress intensity factors comparison. Experimental data were taken from Ref. [17]

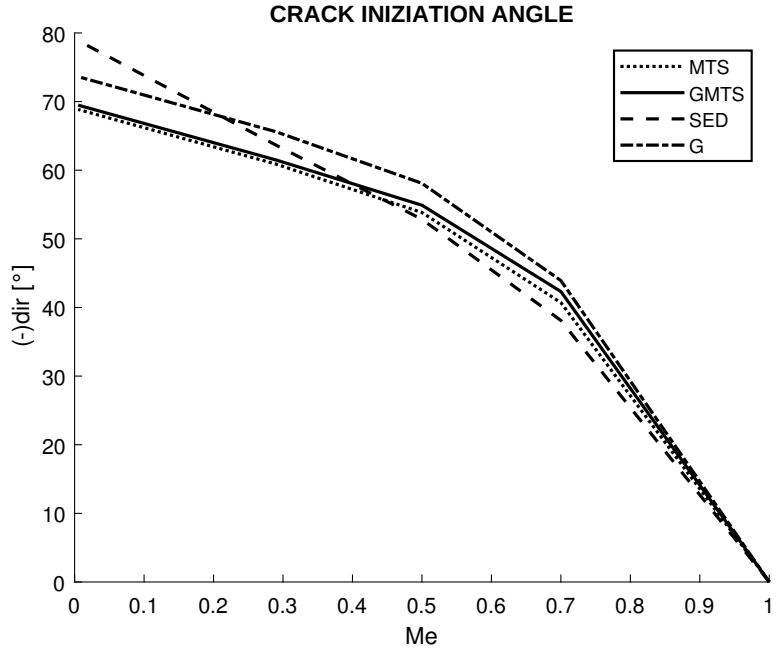

Figure 3.40: Epoxy: initiation angles comparison

3.2.5 PUR-rigid foam of polyurethane

The next material is a rigid foam of polyurethane. Mechanical properties, loading configuration, dimensions of the specimens, and experimental results come from the articles [31] [32], by Costantinescu, Marsavina, Linul. With this material, the ASED criterion does not work properly. The main reason is related to the type of material. It is a foam, therefore it is hardly considered a homogeneous material.

L=140 mm
w=25 mm
t=12.5 mm
ν=0.4
E=281 MPa
K_{Ic}=0.341 MPa$\sqrt{m}$
σ_t=3.86 MPa
a=12.5 mm

For what it is written in the articles, PUR foams were tested with three different values for the density, 300, 145, 100 kg/m^3, with three different cross-head speeds (from which depends also K_{Ic}) and with three different configurations: the values of the lengths called b_1 and b_2 can change and for this study $b_1 = 45\,mm$ and $b_2 = 55\,mm$ were chosen. Experimental tests were performed several times for each mixed-mode.

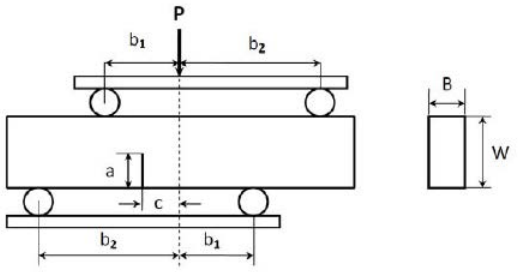

Figure 3.41: PUR: mixed-mode configuration used for the tests in Ref. [31]

Results are shown in fig. 3.42. In the plot, all the experimental attempts are visible for each Me. ASED predictions better fit the lower experimental values. This plot is tricky, it does not enable us to believe that ASED works with this material but at the same time, the comparison is quite satisfactory. In the paper mentioned above, the results weren't that satisfactory too. The authors explained how difficult was to manage the material

EXPERIMENTAL RESULTS [31]			
Me	K_1	K_2	P_f
	$MPa\sqrt{m}$	$MPa\sqrt{m}$	N
1.00	0.327735	0.000853	51
1.00	0.346456	0.000921	54
1.00	0.352696	0.000921	55
0.84	0.328895	0.08317	958
0.84	0.345297	0.087739	1010
0.84	0.35389	0.089581	1031
0.84	0.367189	0.095957	1105
0.67	0.253465	0.146289	1684
0.67	0.27696	0.159008	1831
0.67	0.316857	0.18264	2103
0.67	0.329372	0.190824	2197
0.48	0.178786	0.189528	2182
0.50	0.235188	0.237609	2736
0.50	0.251658	0.253909	2924
0.49	0.27205	0.276585	3185
0.23	0.085284	0.220934	2544
0.23	0.086068	0.223628	2575
0.23	0.112155	0.293362	3378
0.22	0.110655	0.308741	3555
0.02	0.009343	0.339227	3906
0.02	0.008593	0.343728	3958
0.02	0.012481	0.341955	3937
0.02	0.012583	0.36545	4208

Table 3.14: PUR: experimental results

ASED PREDICTIONS			
Me	K_1	K_2	P_f
	$MPa\sqrt{m}$	$MPa\sqrt{mm}$	N
1	0.32	0.00	60
0.76	0.25	0.10	1173
0.68	0.22	0.12	1394
0.55	0.17	0.14	1651
0.37	0.10	0.16	1841
0.16	0.04	0.17	1931
0	0.00	0.17	1950

Table 3.15: PMMA-2^{nd}: ASED predictions

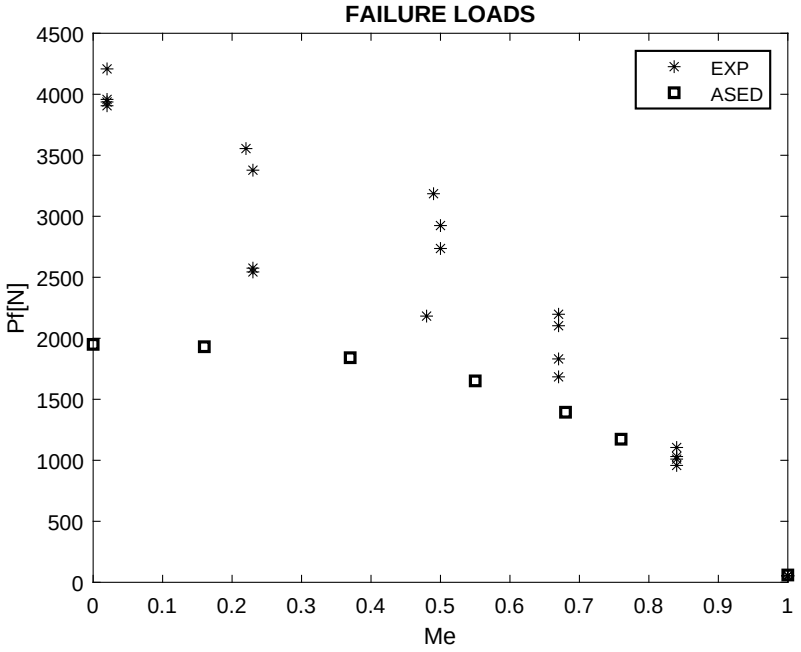

Figure 3.42: PUR: failure loads comparison. Experimental data were taken from Ref. [31]

during the tests. As it is clear from fig. 3.42, there is a large span between prediction and reality. For pure mode I the prediction is almost perfect. For the mixed-modes near mode I the fitting is not so gross and the predicted loads are lower than the real ones, and this is good from a precautional point of view. Near mode II predictions are completely wrong. The comparison for the other criteria for the stress intensity factors and propagation angle is the following:

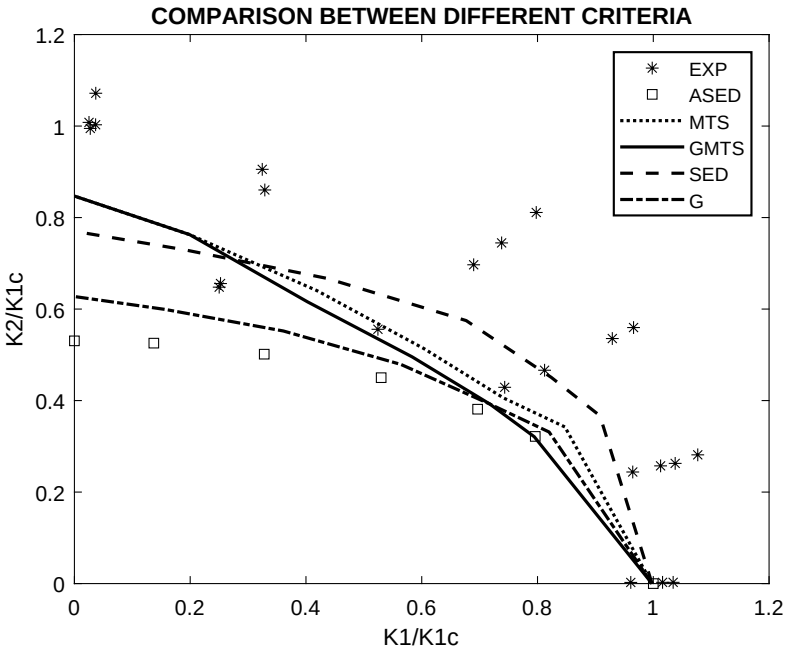

Figure 3.43: PUR: normalized stress intensity factors comparison. Experimental data were taken from Ref. [31]

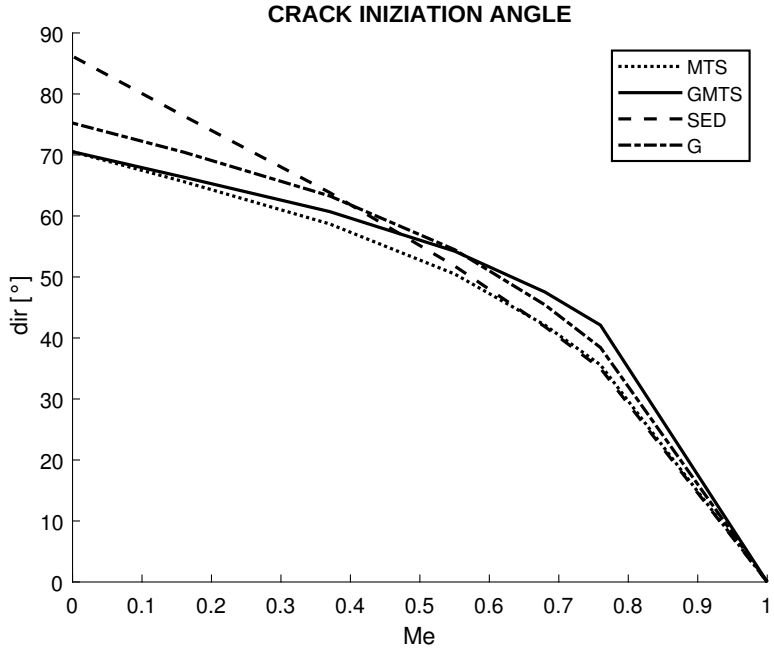

Figure 3.44: PUR: initiation angles comparison

3.3 Ceramics

3.3.1 An Overview

The third material category studied is the class of Ceramics. Three different materials were tested: the first one is Alumina, analyzed thanks to the data related to two experimental works, presented by different authors. Then Soda Lime Glass is tested. It is commonly known as 'window glass'. The last material is a type of Zirconia, *Ce-TZP*.
The literature research phase was quite hard. There are some kinds of ceramics like Zirconia or Alumina that are considered 'super materials', because they are not metals but they present characteristics, like strength, that are sometimes better compared with metals. For this reason, the fracture of ceramics is investigated thoroughly, and ceramics studies are abundant in the literature. But it was easier to find reports about different specimens, like Brazilian Disks. Besides, the material properties were not always provided. This was a problem especially for the tensile strength because the tensile test is not suitable for ceramics, but to apply the ASED criterion it is needed.
In general, it is possible to conclude that with every material the ASED criterion works fine. This is probably related to the brittle behavior of ceramics, which hardly present ductile aspects. Among the four classes of materials, this is probably the one that gave better results.

3.3.2 Alumina-1^{st} type

For this material there were several articles and experimental tests reports available in the literature. The first paper taken in consideration is by Suresh et al. [33]. The authors present the results of the AFPB fracture tests carried out on alumina specimens in two different sizes, that will be called 'longer specimen' and 'shorter specimen'.
The material is a standard commercial alumina (Al_2O_3). Alumina's mechanical properties are presented below.

$$\nu = 0.23$$
$$\text{E} = 350000 \text{ MPa}$$
$$K_{Ic} = 3.32 \text{ MPa}\sqrt{m}$$

To apply the ASED criterion, the fracture toughness K_{Ic}, the Young modulus E and the tensile strength σ_t are needed. For this example σ_t is missing because in [33] was not reported. To look for this value in the literature could be hard because it depends on an amount of factors, hence it is not expected to find a proper value. Moreover, tensile strength is obtained through a tensile test. But with ceramics it is not common to lead a

tensile test till fracture because they are fragile materials, they do not present a ductile behavior at all. More frequently tests like three-point bending are carried out, and for this reason it is more likely that the articles provide the parameter called flexural strength. Actually, in an ideal case, flexural strength and tensile strength should be quite similar. The difference between flexural strength and tensile strength increases in proportion with the amount of impurities in the specimen. Flexural fracture is less easier to occur in this eventuality, beacuse a smaller portion of material is exposed to the maximum stress.
This was a brief introduction to the problematic choice of a proper σ_t to use to prepare the FE model and to apply the theoretical criteria.

LONGER SPECIMEN
As first attempt a value of $\sigma_t = 69\,MPa$ was used. It is a standard value found in the literature for a generic type of Alumina. With all the properties needed it is possible to calculate the radius: $Rc = 0.72\,mm$.
The specimens are common rectangular SEN bars, which dimensions are:

L=78.7 mm
w=10.2 mm
t=4.8 mm

The crack length is $a = 4.2\,mm$, and $a/W = 0.4$. A scheme of the specimen and the loading configuration is shown below. This is the model simulated in Abaqus, with the

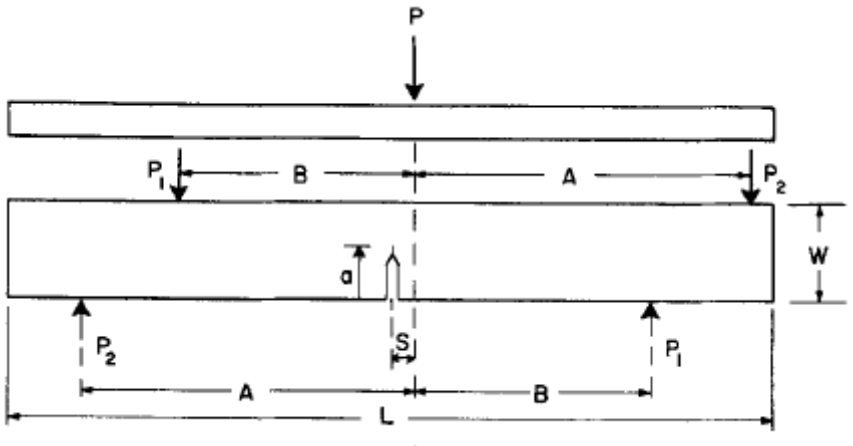

Figure 3.45: Alumina 1^{st}: mixed-mode configuration used for experimental tests in Ref. [33]

loading distances that are $A = 34.3\,mm$ and $B = 24.1\,mm$. The load applied is $1\,N$, distributed correctly in two concentrated loads to have the bending moment equal to zero in the symmetry plane. Moving the crack, it is possible to simulate different mixed-modes.

When the crack is in the symmetry plane, pure mode II is simulated. To perform pure mode I, it is sufficient to change the loading span to obtain a SFPB configuration.
In table 3.16, the comparison between experimental results and ASED predictions is presented. Actually, in the paper only the trend of K_1 over K_2 was available. To get

FAILURE LOADS							
	ASED			EXP [33]			
Me	K_1 $MPa\sqrt{m}$	K_2 $MPa\sqrt{m}$	P_f N	K_1 $MPa\sqrt{m}$	K_2 $MPa\sqrt{m}$	P_f N	$\Delta\%$
1	3.54	0.00	392	3.45	0	383	-2.42
0.70	2.76	-1.40	2824	2.36	1.29	2721	-3.80
0.66	2.56	-1.54	3120	2.54	1.67	3522	11.41
0.59	2.29	-1.70	3444	2.14	1.75	3691	6.70
0.47	1.76	-1.93	3921	1.53	1.94	4092	4.16
0.31	1.13	-2.11	4286	1.01	2.55	5378	20.31
0.18	0.63	-2.19	4453	0.36	2.34	4935	9.78
0.06	0.22	-2.23	4516	0	3.07	6475	30.26

Table 3.16: Alumina-1st: predicted and real failure loads

the failure loads, equations (3.3) and (3.4) were used. These equations are presented in the paper and the geometry factors F_1 and F_2 are needed. In the paper, there are table and graphs providing those factors, and these were used in this work. In (3.3) and (3.4) failure load is not directly inserted but it is obviously related to σ and τ, the stress field components.

$$K_1 = \sigma\sqrt{\pi a}F_1\Big(\frac{a}{W}\Big) = 6\tau\frac{S}{W}\sqrt{\pi a}F_1\Big(\frac{a}{W}\Big) \tag{3.3}$$

$$K_2 = \tau\sqrt{\pi a}F_2\Big(\frac{a}{W}\Big) \tag{3.4}$$

As told before, to simulate different mixed-modes it is necessary to move the crack towards the left of the specimen by a distance called S. This distance, if not provided by the authors and testers, can be calculated:

$$S = \frac{F_2}{F_1}\frac{K1}{K2}W \tag{3.5}$$

It is clear that the method produce some errors especially for mode II. By the way, being the value of σ_t chosen with no accurancy, these are not bad results. They are easier to understand in the picture 3.46. The predicted curve follows in a quite good way the real one. Observing fig. 3.47 it can be noted that the MTS and GMTS fit better

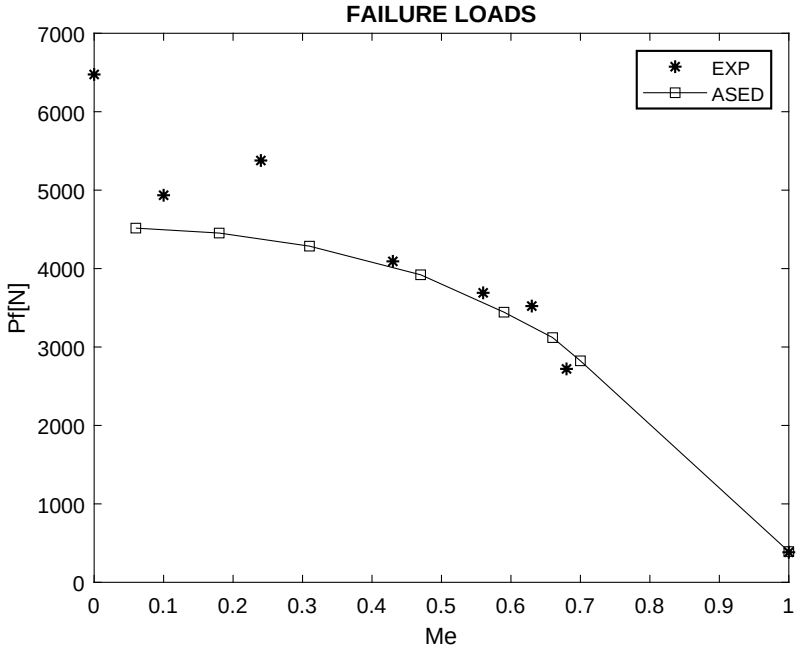

Figure 3.46: Alumina-1st: failure loads comparison. Experimental data were taken from [33]

the experimental trend, that is actually really close to the ASED predictions. For what concerns the directions, unfortunately during the test were not registered the initiation angles of the cracks. For this reason it is possible the comparison between the prediction of the four criteria, but it is not possible to say which is the most reliable. They are all pretty close to each others, especially for the smaller values of Me.

Just to try, another attempt was made using the flexural strength instead of the tensile strength. The main reason is that the flexural strength is provided in paper [33], while the tensile strength was found in the literature, it is a proper value, but it is unlikely the correct one. The flexural strength is $\sigma_{3pb} = 331\ MPa$. Using this value it os obtained $Rc = 0.03\ mm$, but the ASED predictions are not satisfactory with this control volume. The table 3.17 presents the comparison between experimental results and ASED prediction for this case.

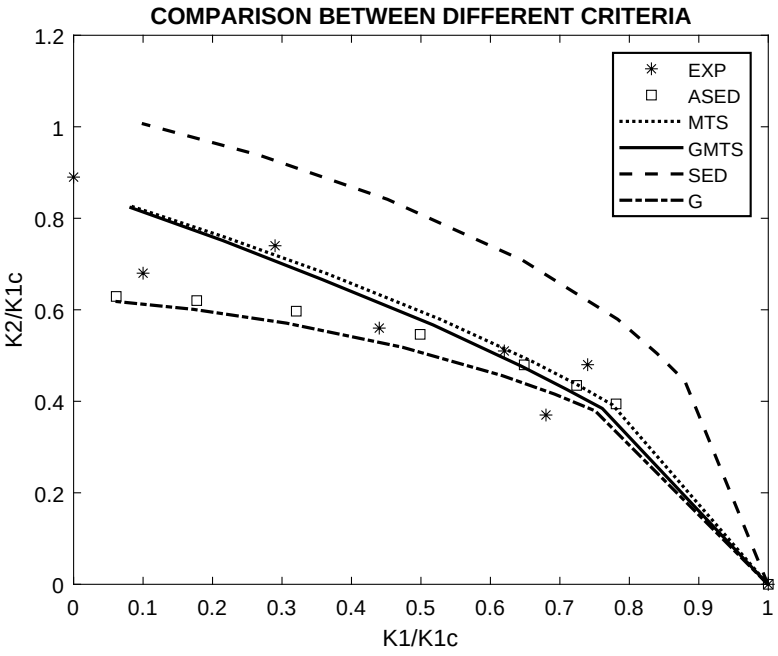

Figure 3.47: Alumina-1st: normalized stress intensity factors comparison. Experimental data were taken from [33]

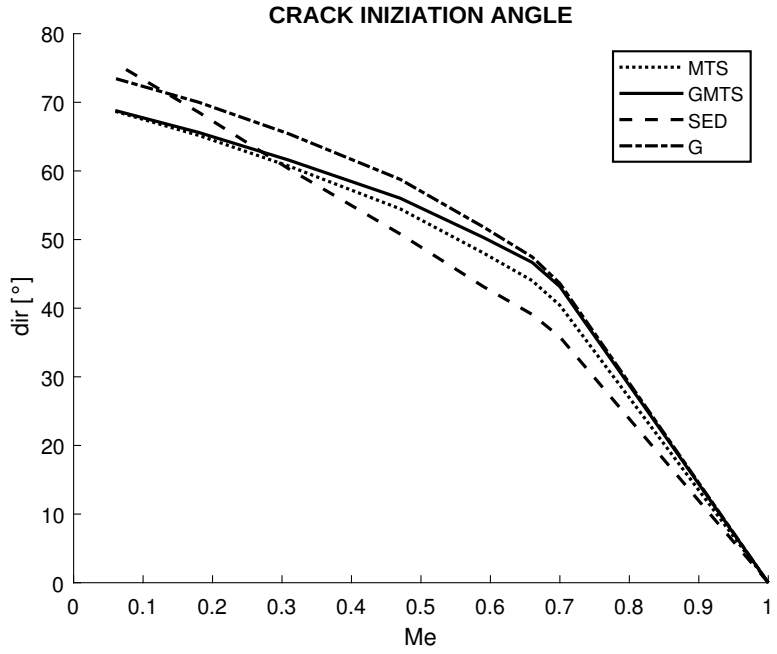

Figure 3.48: Alumina-1st: initiation angles comparison

	$ASED$	EXP	
Me	Pf N	Pf N	$\Delta\%$
1	284	383	25.83
0.70	2102	2721	22.75
0.66	2330	3522	33.83
0.59	2590	3691	29.83
0.47	2985	4092	27.05
0.31	3296	5378	38.71
0.18	3442	4935	30.25
0.06	3498	6475	45.97

Table 3.17: Alumina-1st: predicted and real failure loads using the flexural strength

SHORTER SPECIMEN

For this new simulation the material is the same, already presented previously, but the dimensions of the specimen change:

L=50.8 mm

w=9.9 mm

t=4.8 mm

The crack length is $a = 4.2\,mm$, and $a/W = 0.4$. In the loading configuration now $A = 19.8\ mm$ and $B = 9.9\ mm$. As already exposed, for Alumina tensile strength was not indicated and it was an hard task to decide what value was the proper one. As for the longer specimen, the tensile strngth was considered as $\sigma_t = 69\,MPa$. The comparison for the failure loads is shown in tab. 3.18 and fig. 3.49.

FAILURE LOADS							
	ASED			EXP [33]			
Me	K_1 $MPa\sqrt{m}$	K_2 $MPa\sqrt{m}$	P_f N	K_1 $MPa\sqrt{m}$	K_2 $MPa\sqrt{m}$	P_f N	$\Delta\%$
1	3.26	0.00	343	3.11	0.00	328	-4.58
0.65	2.33	-1.45	1417	2.69	1.81	1941	27.00
0.53	1.88	-1.70	1671	1.97	2.01	2156	22.49
0.35	1.17	-1.93	1930	1.09	2.23	2392	19.29
0.06	0.20	-2.07	2093	0.00	3.25	3486	39.96

Table 3.18: Alumina-1st, shorter specimen: predicted and real failure loads

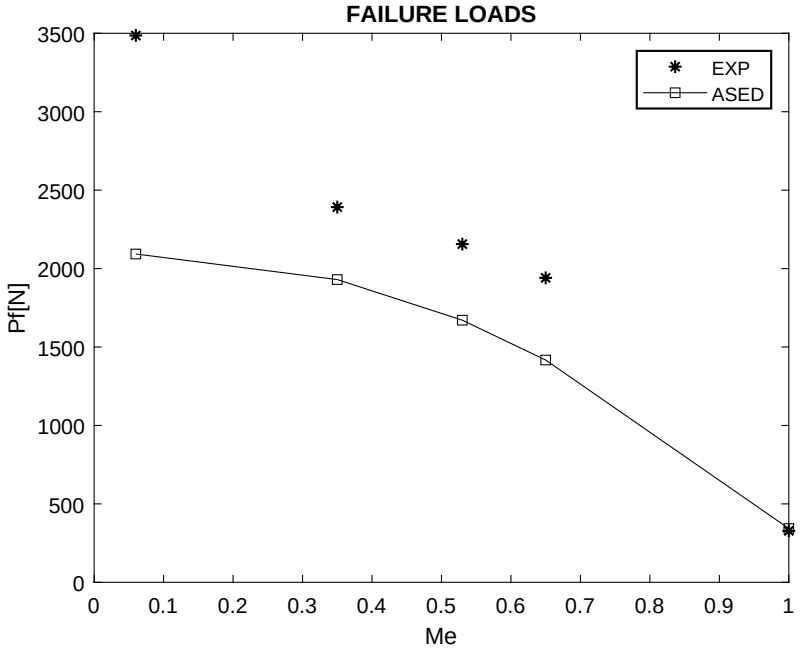

Figure 3.49: Alumina-1st, shorter specimen: failure loads comparison. Experimental data were taken from [33]

Also the other theoretical criteria were applied, with satisfactory results. The comparison are shown in fig. 3.50 and 3.51.

Simply to see the difference, another attempt of study of these specimens was made with the flexural strength $\sigma_{3pb} = 331\,mm$ instead of the tensile strength. Once again the comparison for the failure loads is worse then the previous case. With this value $Rc = 0.027\,mm$.

	$ASED$	EXP	
Me	Pf N	Pf N	$\Delta\%$
1	280	328	14.89
0.64	1184	1941	38.99
0.53	1412	2156	34.52
0.35	1651	2392	30.97
0.06	1804	3486	48.24

Table 3.19: Alumina-1st, shorter specimen: predicted and real failure loads using the flexural strength

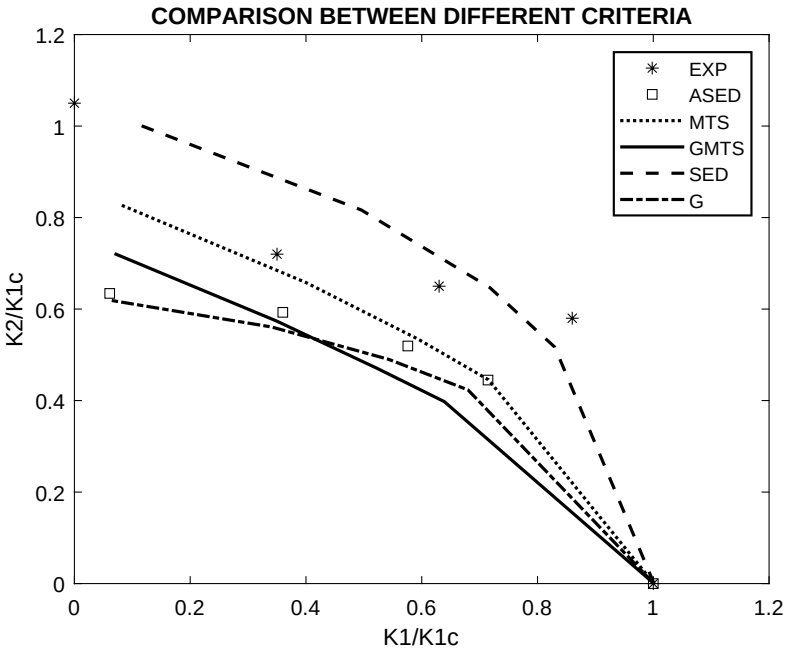

Figure 3.50: Alumina-1st, shorter specimen: normalized stress intensity factors comparison. Experimental data were taken from [33]

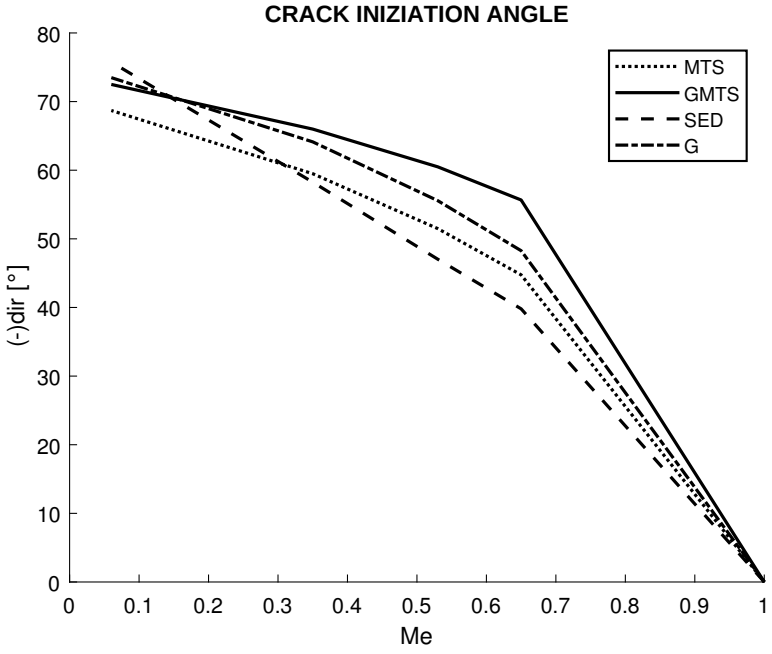

Figure 3.51: Alumina-1st, shorter specimen: initiation angles comparison

3.3.3 Alumina-2^{nd} type

The data used for the second type of Alumina tested comes from another paper, [34]. In this paper the AFPB test's results for Alumina and Soda Lime Glass are presented. The properties declared for the Alumina used are presented below. It is a polycrystalline material, with large grain size $(5-201, \mu m)$. The loading configuration is the same shown in fig. 3.45

L=32 mm
w=3.2 mm
t=3 mm
ν=0.23
E=348000 MPa
K_{Ic}=4.4 MPa$\sqrt{m}$
σ_{3pb}=261 MPa

The crack length is $a = 1.6\ mm$ and $a/W = 0.5$. The loading distances are provided, using the same name of the previous material, they are respectively $A = 10\ mm$ and $B = 5\ mm$. To calculate Rc this time it was used directly the value of the flexural strength, presented in the paper. It is obtained $Rc = 0.09\ mm$.
Experimental data were also provided in [34], but evidently the author had more than one test for the same configuration. To present data in a easier way and to make more comprehensible the comparison with the predictions, average values for each mixed-modes configuration were calculated. The results for the comparison between experimental failure loads and ASED predictions are in tab. 3.20. They are also plotted in fig. 3.52.
This time the ASED predictions fit perfectly the experimental trend. This allow us to

FAILURE LOADS							
	ASED			EXP [34]			
Me	K_1 $MPa\sqrt{m}$	K_2 $MPa\sqrt{m}$	P_f N	K_1 $MPa\sqrt{m}$	K_2 $MPa\sqrt{m}$	P_f N	$\Delta\%$
1.00	4.53	0.00	86	4.40	0.00	85	1.72
0.83	4.20	-1.12	319	3.87	1.06	320	-0.31
0.50	2.53	-2.51	731	2.07	2.07	636	12.92
0.35	1.70	-2.81	818	1.50	2.68	812	0.65
0.13	0.61	-3.00	875	0.70	2.73	826	5.64
0.00	0.00	-3.03	883	0.00	2.77	839	5.03

Table 3.20: Alumina-2^{nd}: predicted and real failure loads

think that this time it is really worthly to use the flexural strength instead of the tensile

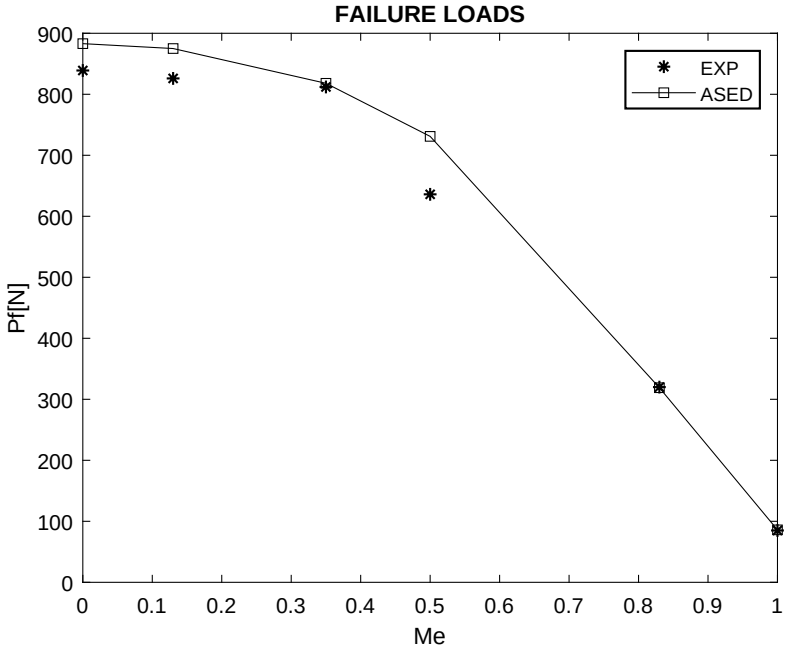

Figure 3.52: Alumina-2^{nd}: failure loads comparison. Experimental data were taken from Ref. [34]

strength, even if with the previous alumina, this solution did not work. A possible explanation is in the way the flexural test was carried out. It is possible that the flexural strength is really similar to the tensile strength, even if obtained through a different test. The other theoretical criteria were performed with predictions of the ASED one. Results are presented in fig. 3.53 and 3.54. Referring to fig. 3.53, it can be noticed that also in this case the MTS and GMTS criteria are the closest to the real and the predicted trend of the normalized SIFs. But near pure mode II, that means on the left area of the figure, the G criterion seems the best. Instead, the SED criterion is definitly far from the scatter zone of the results.

As said before, it was assumed that the flexural strength proposed in the paper [34] is quite similar to the tensile strength. Being a brittle material, in the stress-strain curve, it is not recognized the yielding stress. Therefore it is assumed that the plastic zone around the tip presents a stress value higher than the tensile strength, which should be around $261\,MPa$. To verify this hypothesis, the plastic zone around the tip is plotted. As usual, the radius of such zone increase approaching mode II. But the most important thing is that for mode I $r_c = 0.04\,mm$. This is quite the same value predicted with Schmidt to apply the GMTS criterion. The prediction was $r_c = 0.045\,mm$. The conclusion is that the choice of using flexural strength is valid.

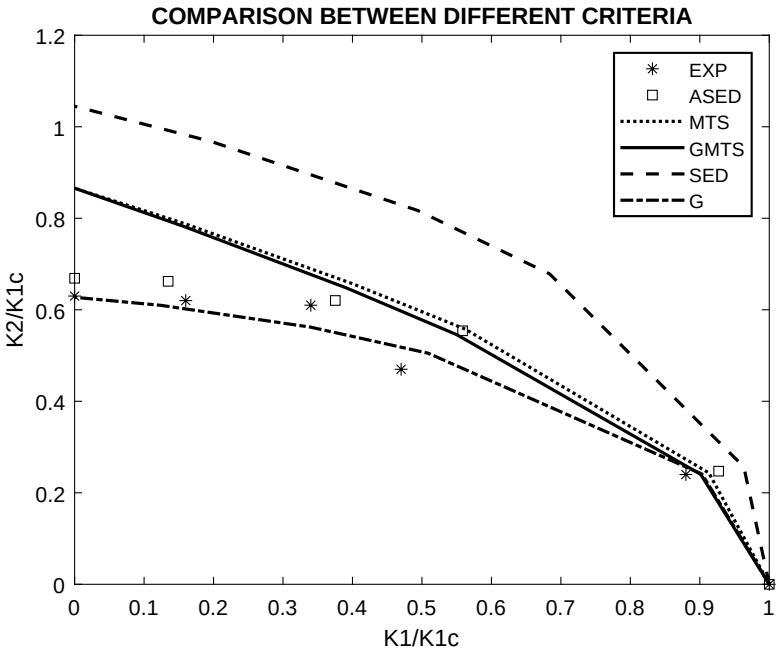

Figure 3.53: Alumina-2nd: normalized stress intensity factors comparison. Experimental data were taken from Ref. [34]

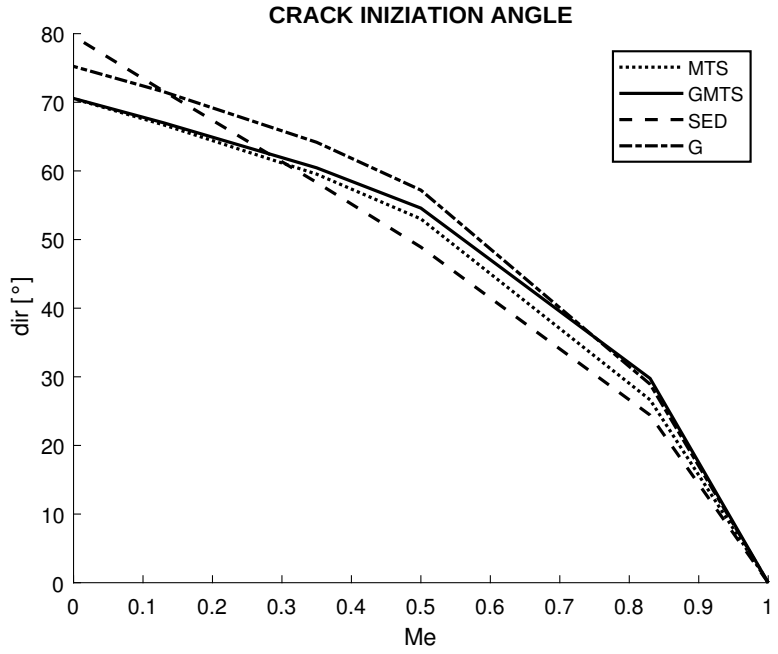

Figure 3.54: Alumina-2nd: initiation angles comparison

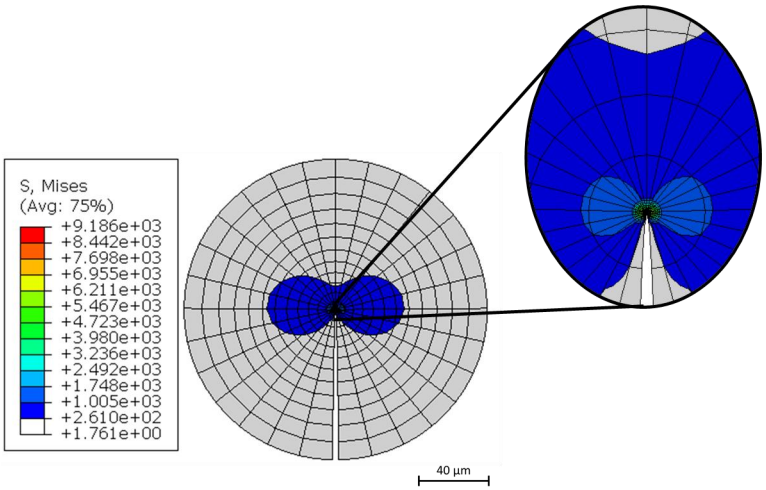

(a) Me=1

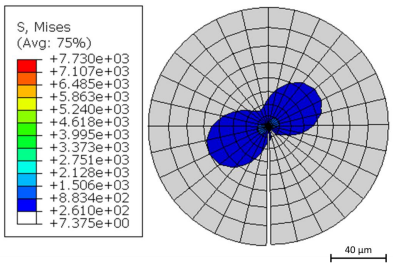

(b) Me=0.83

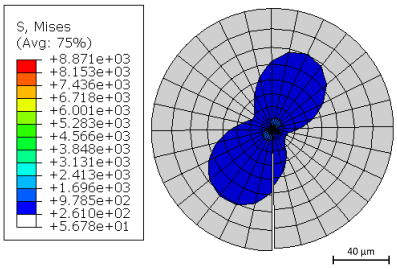

(c) Me=0.50

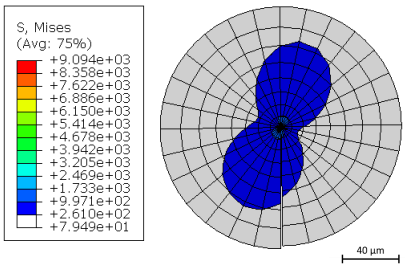

(d) Me=0.35

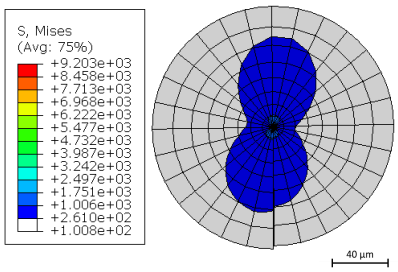

(e) Me=0.13

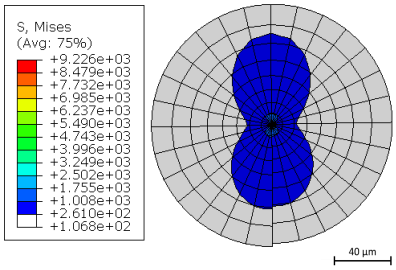

(f) Me=0

Figure 3.55: Alumina-2^{nd}: plastic zone contour plots

3.3.4 Soda Lime Glass

In the same paper of the previous material [34], another material is analyzed. Soda lime glass was chosen as an example of an homogenous and isotropic material. The properties are the following.

L=37 mm
w=4 mm
t=4 mm
ν=0.23
E=73300 MPa
K_{Ic}=0.62 MPa$\sqrt{m}$
σ_{3pb}=76.9 MPa

The crack length is $a = 2\ mm$ and $a/W = 0.5$. The loading distances are $A = 15\ mm$ and $B = 5\ mm$. Using the flexural strength to calculate the radius it is obtained $Rc = 0.019\ mm$. Next tables show, as in the previous case, experimental results compared with the ASED predictions for the failure loads. The plot of the comparison is also attached. Also with this material ASED predictions fit really well the trend of the

FAILURE LOADS							
	ASED			EXP [34]			
Me	K_1 $MPa\sqrt{m}$	K_2 $MPa\sqrt{m}$	P_f N	K_1 $MPa\sqrt{m}$	K_2 $MPa\sqrt{m}$	P_f N	$\Delta\%$
1.00	0.62	0.00	19.46	0.62	0.00	22.31	-14.61
0.84	0.58	-0.15	37.49	0.52	0.14	41.03	-9.44
0.49	0.34	-0.35	88.97	0.25	0.25	74.60	16.16
0.37	0.25	-0.38	97.79	0.16	0.28	83.92	14.19
0.20	0.13	-0.41	104.64	0.08	0.29	87.65	16.24
0.00	0.00	-0.42	107.47	0.00	0.33	98.84	8.03

Table 3.21: Soda Lime Glass: predicted and real failure loads

experimental points. This seems another confirmation that with the flexural strength the proper R_c could be obtained.
With the predicted failure loads and the model in Abaqus is possible to predict also the SIFs to apply the other energetic and stress-based criteria. Experimental data for the crack initialitation angle weren't available but the comparison was led in anycase. This time the criterion that is closer to the experimental curve is the G criterion. The second is the GMTS that follows in a better way the shape of the curve, but gives higher value.

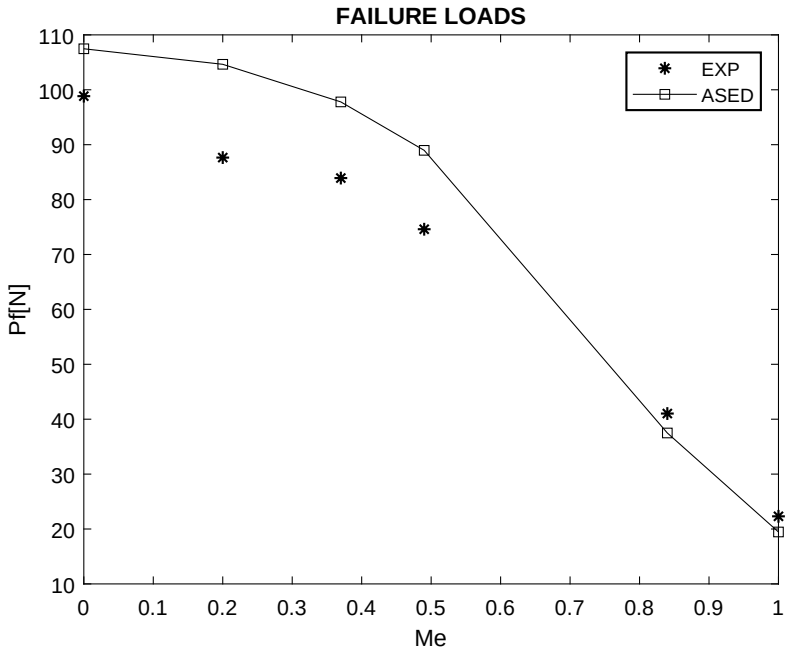

Figure 3.56: Soda Lime Glass: failure loads comparison. Experimental data were taken from Ref. [34]

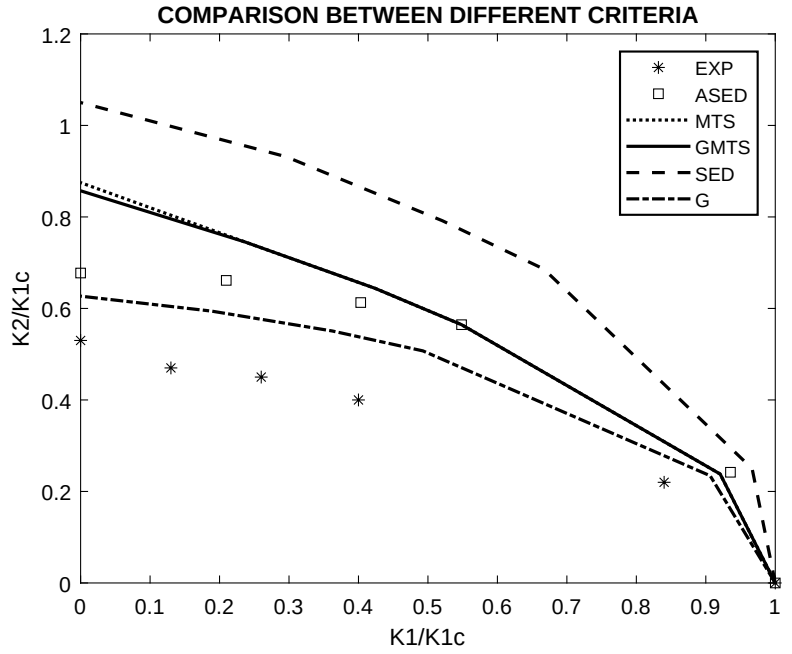

Figure 3.57: Soda Lime Glass: normalized stress intensity factors comparison. Experimental data were taken from Ref. [34]

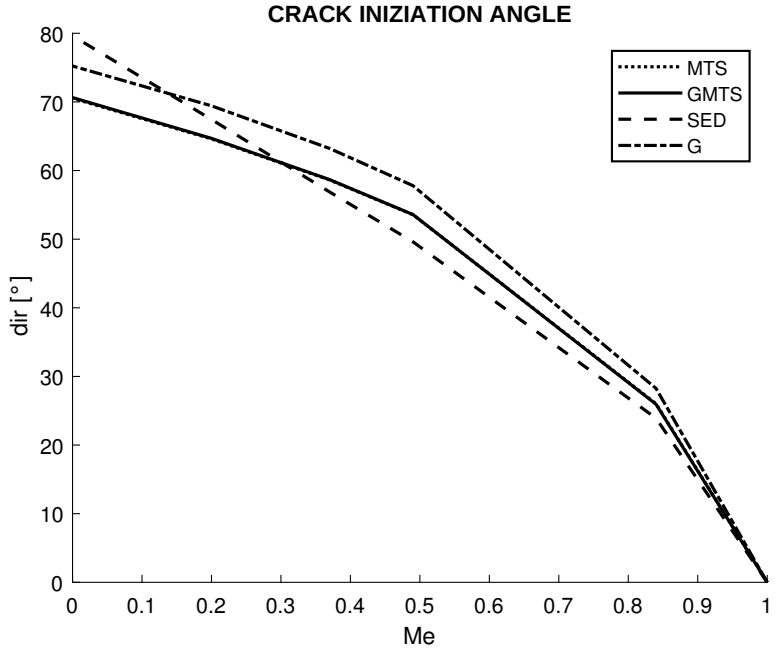

Figure 3.58: Soda Lime Glass: initiation angles comparison

3.3.5 Zirconia

A dataset of experimental results for Zirconia was available in the paper by Tikare and Choi [35]. As usual, AFPB was the technique used to track failure loads, with different mixed-modes, of $Ce - TZP$, tetragonal zirconia blended with Cerio. Material properties were not found in the paper, except for the toughness. Looking for the properties in the literature adds uncertainity to the investigation. Probably, with known properties of the tested material, the ASED predictions could be more precise.
The properties used and the specimens dimensions.

L=40 mm
w=3 mm
t=4 mm
ν=0.31
E=200000 MPa
K_{Ic}=8.2 MPa$\sqrt{m}$
σ_{3pb}=700 MPa

The loading configuration is similar to the one of the previous materials and the loading ditances are:

A=15 mm
B=5 mm

FAILURE LOADS							
	ASED			EXP [35]			
Me	K_1 $MPa\sqrt{m}$	K_2 $MPa\sqrt{m}$	P_f N	K_1 $MPa\sqrt{m}$	K_2 $MPa\sqrt{m}$	P_f N	$\Delta\%$
1	8.69	0.000	388	8.26	0	383	1.40
0.83	7.96	2.22	1912	7.87	2.61	1916	-0.18
0.74	7.17	3.09	2687	7.14	3.79	2782	-3.51
0.64	6.06	3.91	3410	6.25	5.03	3692	-8.28
0.58	5.47	4.23	3696	5.62	5.69	4177	-13.01
0.42	3.80	4.89	4279	3.87	6.3	4624	-8.07
0.30	2.68	5.17	4527	2.53	7.31	5366	-18.52
0.16	1.39	5.36	4699	0.96	8.03	5894	-25.43
0.00	0.00	5.43	4763	0	8.64	7833	-64.46

Table 3.22: Zirconia: predicted and real failure loads

a=0.75 mm

a\W=0.25

Experimental results were presented in in a plot with K_{1f} over K_{2f}. Taking the coordinates of each point, failure loads can be extracted using equations found in [35]. For pure mode I a SFPB specimens was used, and the theory of Murakami [2] for the geometry factors and failure loads was applied.

As it is shown in fig. 3.59 for some values of the ratio Me predictions fit really well the experimental points. But especially for pure mode II the difference is huge. The hope is that it is a problem related to the wrong choice of properties. There is also to add that to extrapolate failure loads from SIFs which values are presented in a plot is a big source of imprecision. Anyway, the MTS , GMTS, SED and G criteria were tested with the results shown in the pictures.

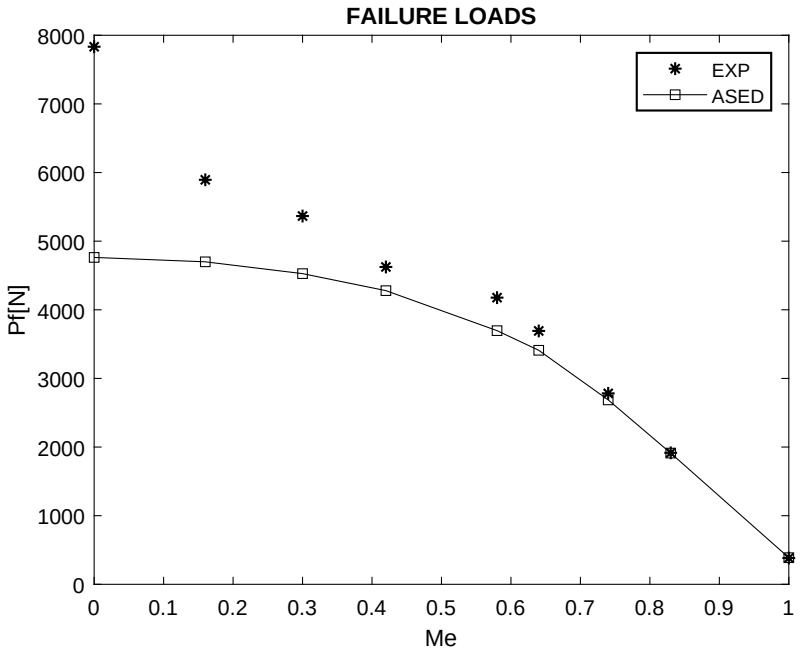

Figure 3.59: Zirconia: failure loads comparison. Experimental data were taken from Ref. [35]

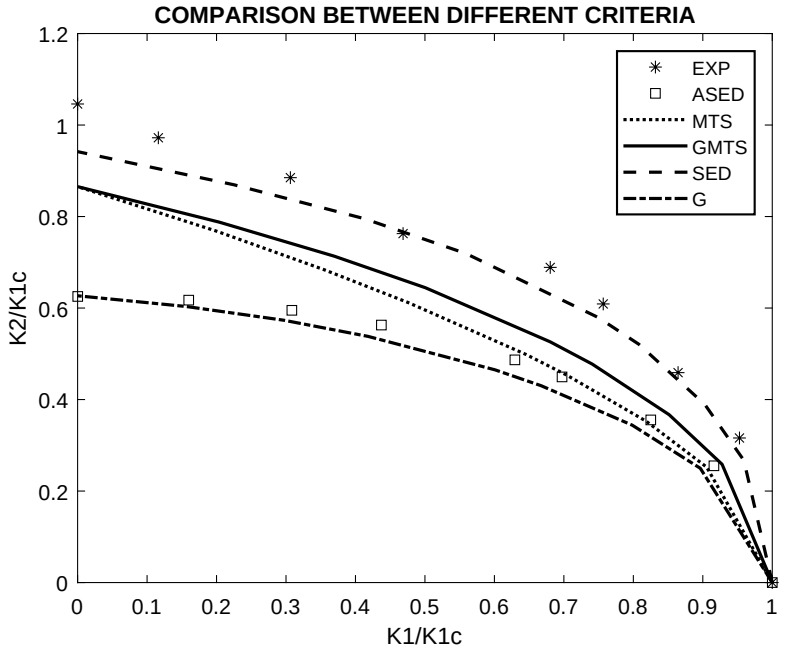

Figure 3.60: Zirconia: normalized stress intensity factors comparison. Experimental data were taken from Ref. [35]

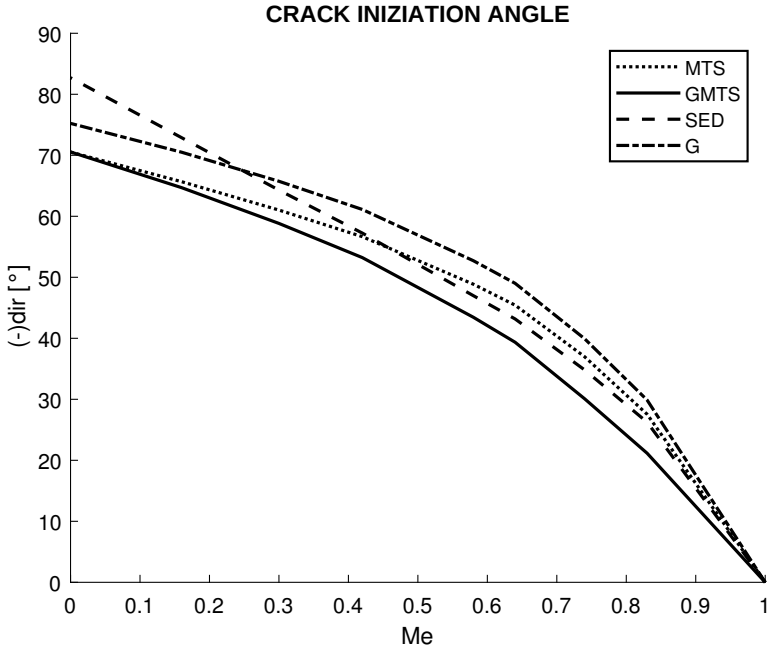

Figure 3.61: Zirconia: initiation angles comparison

It is strange that this time experimental trend for normalied SIFs is almost perfectly fitted by the SED criterion. Actually, also in the paper the fact that the best criterion is this one is observed, but no explanations are produced.

3.4 Steels

3.4.1 An Overview

For the last class of materials, a large range of steels was tested. They are in order, En3B, 1Cr-Mo-0.3V with large grain size and small grain size, C-Mn weld, HY100, HY130.
As explained largely in the previous sections, the ASED criterion works fine only with materials that present brittle fracture. This type of fracture is characterized by the absence of plastic deformation before the failure occurs. The cracks are unstable and they propagate even without a sensible increase of the applied stress. A typical mechanism of rupture for brittle materials is called cleavage, and it consists of the rupture of the atomic bonds along crystallographic planes. This affects also the aspect of the fracture surface on a cracked specimen: the surface is smooth and shiny. Typical examples of materials that fail in a brittle way are ceramics.
The opposite model of a fracture is the ductile fracture, which is typical of steels and metals in general. The ductile fracture is characterized by an important plastic deformation previous to the rupture. In a tensile test, for example, it is possible to see the necking of the material. This type of fracture absorbs a large quantity of energy compared to the brittle one. Even the fracture surface is different because it usually shows the dimples, the prints of the grain that are detached from the specimen during the fracture.
To apply the ASED criterion, it is necessary to calculate the critical value of the strain

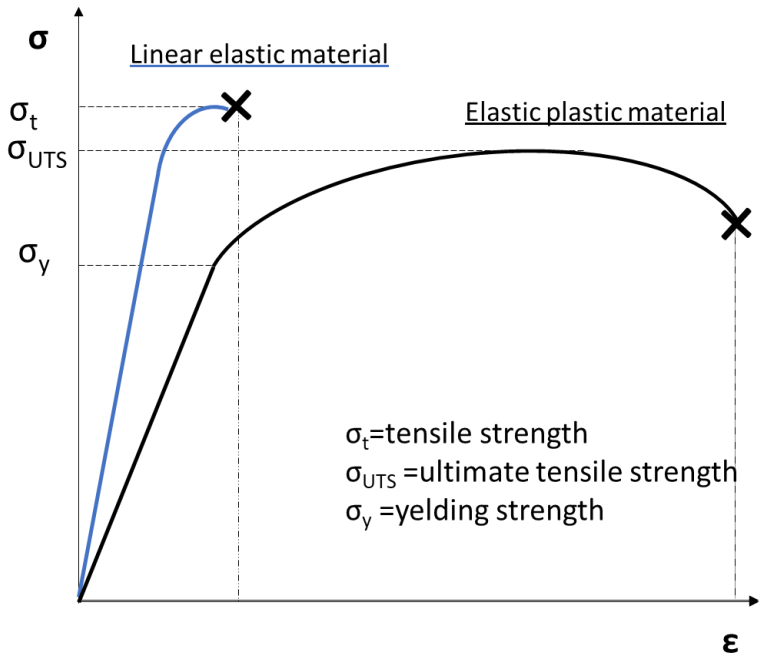

Figure 3.62: Stress-strain curves for ductile and brittle materials

energy density.

$$W_c = \frac{\sigma_t}{2E} \tag{3.6}$$

where σ_t is the tensile strength of the material. From the plot 3.62 it is clear that for a brittle material it is immediate to obtained W_c, but not for a ductile one.

Therefore, in the following sections, it is possible to study steels with the ASED criterion thanks to a peculiar phenomenon typical of the metals, called ductile to brittle transition. A ductile material becomes brittle if the temperature reaches an extremely low value that is called transition temperature. Testing the materials at low temperatures is the only way to apply the ASED criterion with good results. For this reason, the first four types of steel are tested at $-196°C$. If the steel is tested at room temperature, the ASED

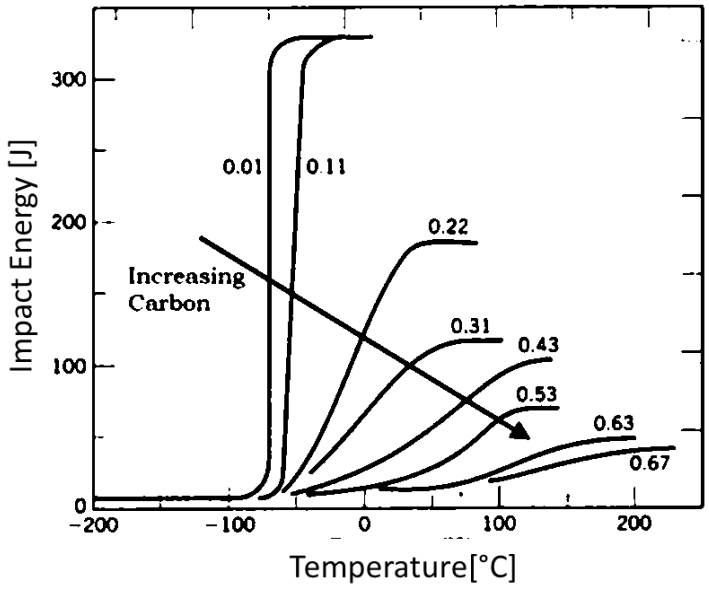

Figure 3.63: Ductile to brittle temperature for steels

criterion gives bad results, or it is not even applicable. There is another possibility. To menage a ductile material it is possible to apply the Equivalent Material Concept (EMC), which consists of creating a fake material that behaves like the original one but with an ideally brittle attitude. More details about this method will be proposed in the following sections.

3.4.2 En3b

General Information

For the next materials (En3b, 1Cr-Mo-0.3V, C-Mn weld) the experimental results and the information about the specimens are presented in the article [36], by Maccagno and Knotts. All the materials are tested with Asymmetric Four-Point Bend specimen which dimensions are:

L=100 mm
w=20 mm
t=10 mm
a/W=0.5

The tests are performed for different values of β the equivalent crack angle, that is an indicator of the mixed-mode:

$$\beta = arctg\left(\frac{K_1}{K_2}\right) \tag{3.7}$$

The values used are β=90°, 75°, 60°, 45°, 30°, 15°, 0°, where $\beta = 90°$ is pure mode I and $\beta = 0°$ is pure mode II. To promote the continuity with the previous materials, the angle β is not used as an indicator of the mixed-mode, but it is used to find the mixed-mode coefficient Me, as usual.

The most important information to have about these tests is that they were led at a temperature of $-196°C$ in order to promote the brittle fracture for cleavage. As a matter of fact, steels usually have a transition from ductile to brittle when they are in a cool environment, beyond the transition temperature.

In fig. 3.64 the specimens used and the loading configuration are sketched.

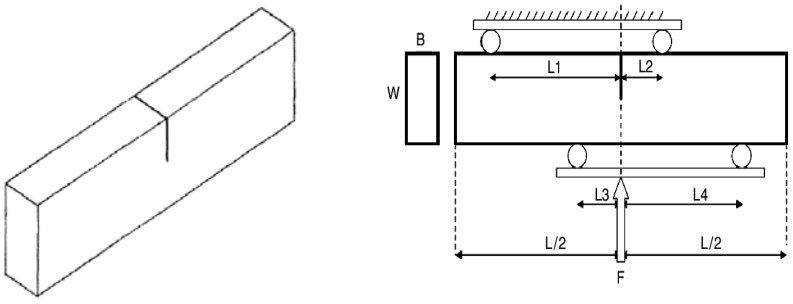

(a) (b)

Figure 3.64: Steels: specimens and loading configuration scheme used in Ref. [36]

The first material studied belonging to the class of steel is the steel denominated En3b.

Material Composition									
Material	C	Mn	Si	S	P	Ni	Cr	Mo	V
En3b	0.11	0.3	0.07	0.01	0.02	0.14	0.08	0.02	-

Table 3.23: En3b: material composition

It is a mild steel that undergoes a heat treatment (heated to $1200°C$ for 4 hours) and then cooled slowly till room temperature. The composition is shown in table 3.23.

The material properties are:

$$\nu{=}0.3$$
$$\text{E}{=}200000 \text{ MPa}$$
$$K_{Ic}{=}24.9 \text{ MPa}\sqrt{m}$$
$$\sigma_y{=}700 \text{ Mpa}$$
$$\sigma_t{=}700 \text{ Mpa}$$

With these values, calculating R_c with the standard equation for plane strain cases gives $R_c = 0.34\,mm$.

At this temperature ($-196°C$) $\sigma_y = \sigma_t$, and this is the proof that the ductile to brittle transition has occurred.

The expectation is, for this reason, that the ASED criterion works very well.

The experimental results for this material are reported in the table 3.24. It is important to notice that the tests were not carried out as scheduled: for $Me = 0.190$, not even close to mode II, the failure load reaches $50000\,N$. With a load of such an intensity, it is not possible to ignore plastic phenomena, especially on the load application points that will undergo a plastic deformation with the possibility of cracking. Therefore it was not possible to carry out further tests.

In the next tables, the ASED predictions are shown. To compare them with the experimental results and calculate the discrepancy in percentage points, average values of the experimental failure loads are calculated.

Results are even more clear in fig. 3.65. The comparison is satisfactory: as expected, the ASED criterion works perfectly with the steel because of the low temperature.

Also, the other criteria are performed with this data to obtain the predictions of the initiation angle of the crack. The results of these comparisons are presented in the following plots 3.66 and 3.67. In these pictures, good accordance between criteria and experimental results is shown. The best criterion in fitting the real trend of the normalized stress intensity factors is the SED criterion. This is quite news because usually the MTS and the GMTS criteria are the best. The SED criterion is good also with the initiation angle, but in this case, all the criteria are quite close to each other.

EXPERIMENTAL RESULTS [36]				
Me	K_1 $MPa\sqrt{m}$	K_2 $MPa\sqrt{m}$	P_f N	dir $^\circ$
1	22.6	0	5700	0
1	25	0	6100	0
1	27.1	0	6600	0
0.827	23.3	6.5	14300	25.2
0.826	21.7	6.1	13000	30
0.666	20.9	12.1	29900	40.2
0.663	21.7	12.7	28100	41.5
0.500	16.8	16.8	38400	49.00
0.530	16.8	15.3	31900	50.00
0.332	12.8	22.3	51400	52.00
0.333	12.8	22.2	50700	51.00
0.316	11.2	20.7	36500	54.50
0.344	16.7	27.8	44200	53.80
0.228	7.5	20	38800	61.50
0.190	7.8	25.3	50000	63.20
/	/	/	/	/
/	/	/	/	/

Table 3.24: En3b: experimental results

ASED PREDICTIONS			
Me	K_1 $MPa\sqrt{m}$	K_2 $MPa\sqrt{mm}$	P_f N
1	25.13	0.00	6282
0.85	23.46	5.76	14650
0.96	18.69	1.10	25282
0.52	13.80	13.12	31972
0.35	8.86	14.70	36111
0.19	4.81	15.43	38103
0	0.28	15.72	39050

Table 3.25: En3b: ASED predictions

FAILURE LOADS			
	ASED	EXP [36]	
Me	P_f N	P_f N	$\Delta\%$
1	6282	6133	-2.43
0.85	14650	13650	-7.32
0.67	25282	29000	12.82
0.52	31972	35150	9.04
0.35	36111	45700	20.98
0.19	38103	/	/
0.01	39050	/	/

Table 3.26: En3b: predicted and real failure loads

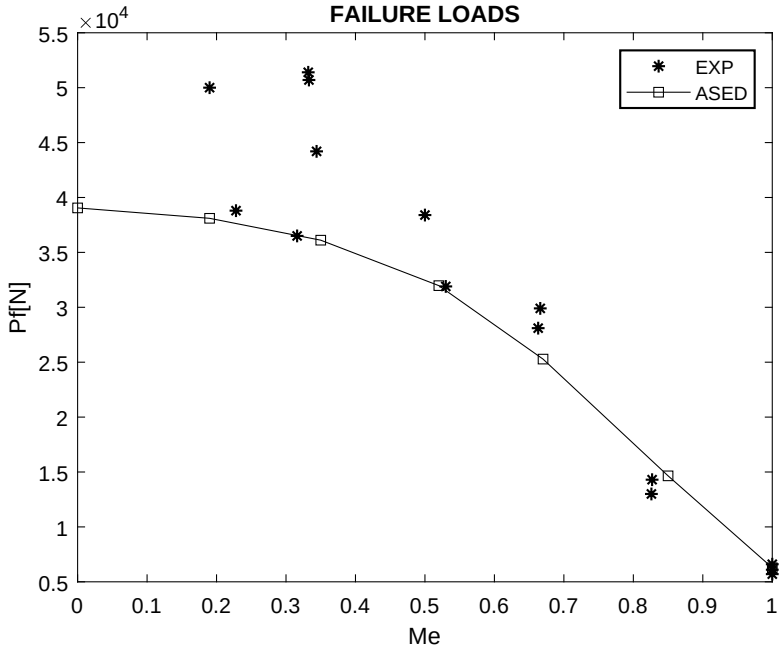

Figure 3.65: En3b: failure loads comparison. Experimental data were taken from Ref. [36]

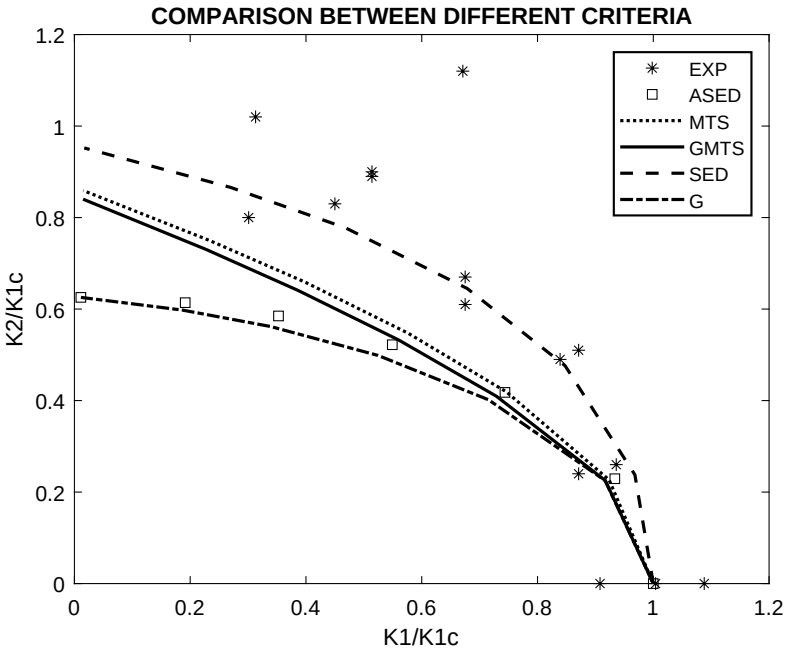

Figure 3.66: En3b: normalized stress intensity factors comparison. Experimental data were taken from Ref. [36]

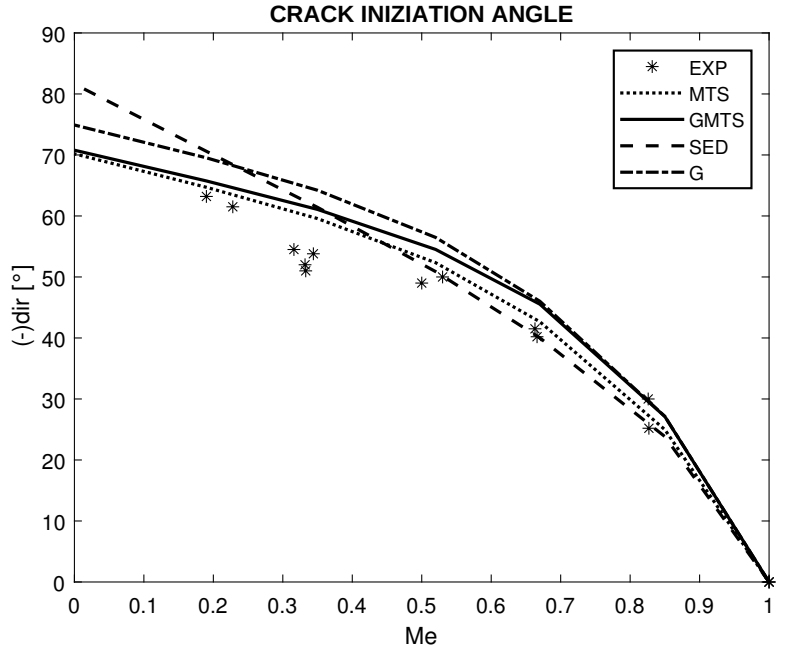

Figure 3.67: En3b: initiation angles comparison. Experimental data were taken from Ref. [36]

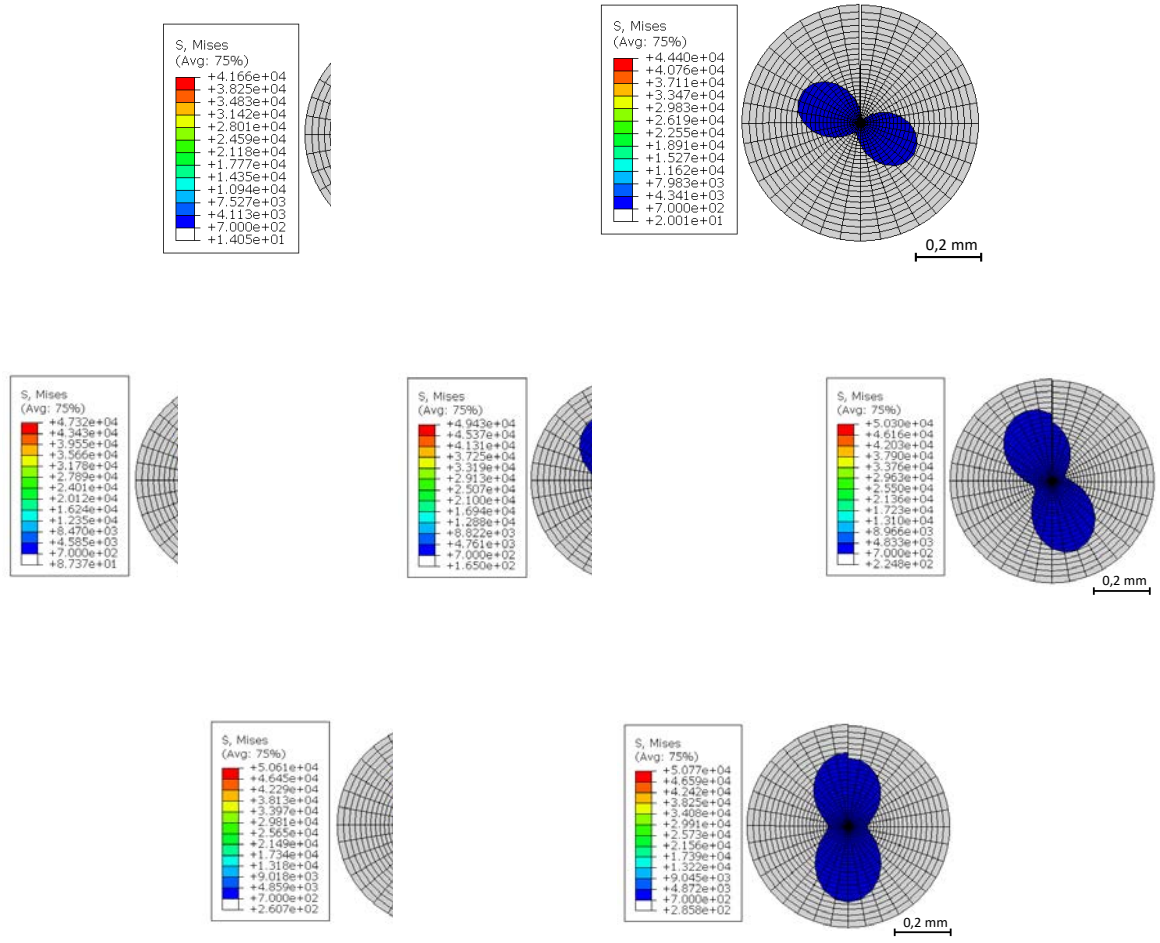

(f) Me= (g) Me=0

Figure 3.68: En3b: plastic zone contour plots

For En3b the plastic radius is investigated. To perform the GMTS criterion, the critical radius is obtained with the Schmidt relation as $0.02\,mm$. The contour plot of the Von Mises stress shows good accordance with this value. For mode I the peanut shape has a maximum radius of around $0.16\,mm$

3.4.3 1Cr-Mo-0.3V-Large Grain Size

The second steel tested is presented with two different microstructures, the first with a large grain size and the second with small grain size. The one with a large grain size undergoes a stress relief process at $650°C$ for hours before testing. The averaged grain size is 400 μm. The composition is:

Material Composition									
Material	C	Mn	Si	S	P	Ni	Cr	Mo	V
1Cr-Mo-0.3V	0.15	0.6	0.21	0.03	0.02	0.24	1	0.95	0.32

Table 3.27: 1Cr-Mo-0.3V-Large Grain Size: material composition

The material properties are:

ν=0.3
E=200000 MPa
K_{Ic}=23.85 MPa$\sqrt{m}$
σ_y=650 Mpa
σ_t=710 Mpa

With these values $R_c = 0.36\,mm$ is obtained.
In tab. 3.28, the experimental results of the AFPB tests are presented. Then, in 3.29 and 3.30, the ASED predictions and the comparison is shown.

As shown in fig. 3.69, the fitting is good, except for pure mode II, but it is quite typical for the ASED criterion. Probably the plastic deformation is interfering too much with the fracture, even if the temperature is low since the failure loads are high.
Even the MTS, the GMTS, the SED, and the G criterion are applied with success. The results are presented in the following plots.
Predictions for the angle are in good accordance with the reality, especially for the MTS and the GMTS criteria. The comparison for the normalized stress intensity factors is less interesting due to the strange trend of the experimental points.

EXPERIMENTAL RESULTS [36]				
Me	K_1 $MPa\sqrt{m}$	K_2 $MPa\sqrt{m}$	P_f N	dir $^\circ$
1	21.8	0	5500	0
1	25.9	0	6400	0
0.833	23.5	6.3	13700	26
0.838	18.4	4.8	10600	29
0.688	19.9	10.6	18900	50.5
0.531	19.1	17.3	31300	48.5
0.334	11	19	41900	64
0.335	10.7	18.4	40700	56.00
0.137	6.5	29.8	59400	62.00
0.222	9.3	25.6	41700	60.00
0.060	2.9	30.9	57700	67.50
0.058	2.7	29.5	58900	67.00

Table 3.28: 1Cr-Mo-0.3V-Large Grain Size: experimental results

ASED PREDICTIONS			
Me	K_1 $MPa\sqrt{m}$	K_2 $MPa\sqrt{mm}$	P_f N
1	24.03	0.00	6012
0.85	22.43	5.50	14019
0.67	17.87	10.03	24185
0.52	13.19	12.54	30577
0.35	8.47	14.05	34530
0.19	4.59	14.74	36432
0	0.27	15.02	37336

Table 3.29: 1Cr-Mo-0.3V-Large Grain Size: ASED predictions

FAILURE LOADS			
	ASED	EXP [36]	
Me	P_f N	P_f N	$\Delta\%$
1.00	6012	5950	-1.04
0.85	14019	12150	-15.38
0.67	24185	18900	-27.96
0.52	30577	31300	2.31
0.35	34530	41300	16.39
0.19	36432	50550	27.93
0.01	37336	58300	35.96

Table 3.30: 1Cr-Mo-0.3V-Large Grain Size: predicted and real failure loads

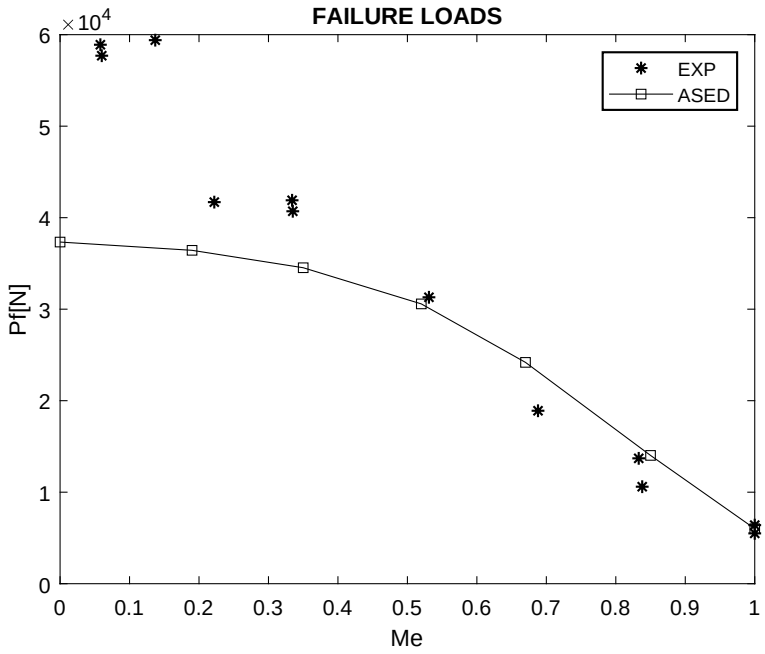

Figure 3.69: 1Cr-Mo-0.3V-Large Grain Size: failure loads comparison. Experimental data were taken from Ref. [36]

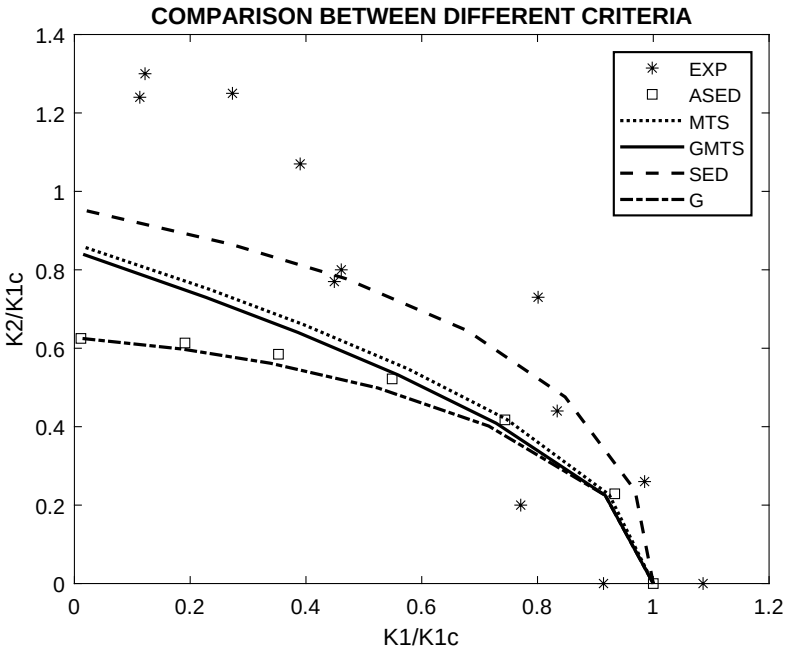

Figure 3.70: 1Cr-Mo-0.3V-Large Grain Size: normalized stress intensity factors comparison. Experimental data were taken from Ref. [36]

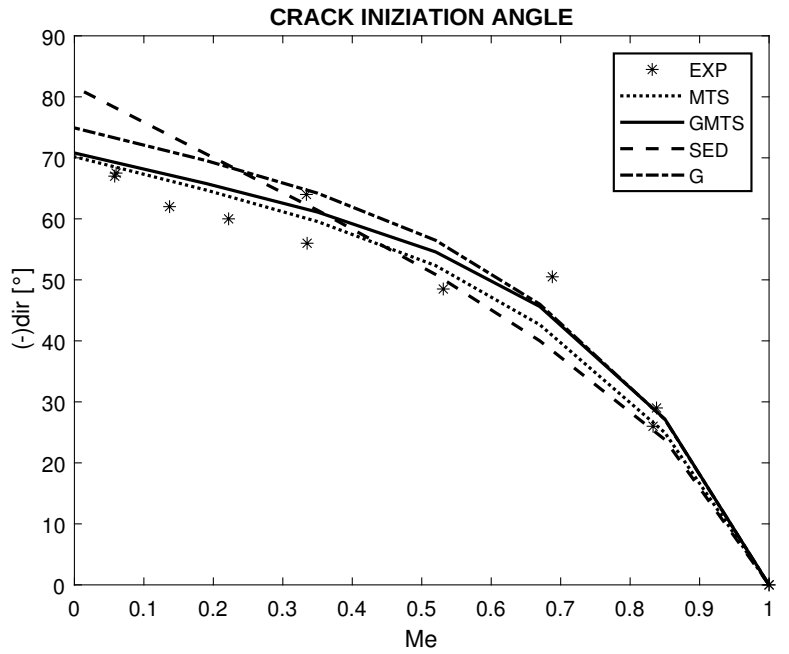

Figure 3.71: 1Cr-Mo-0.3V-Large Grain Size: initiation angles comparison. Experimental data were taken from Ref. [36]

3.4.4 1Cr-Mo-0.3V-Small Grain Size

The same steel presented before, 1Cr Mo 0.3V, is now analyzed with a smaller grain size, which is about 50 μm.
If the chemical composition does not change, it is not possible to say the same for the mechanical properties, that depends on the microstructure.

ν=0.3
E=200000 MPa
K_{Ic}=24 MPa$\sqrt{m}$
σ_y=570 Mpa
σ_t=570 Mpa

With these properties $R_c = 0.48\, mm$.
Experimental results, ASED predictions and the comparisons arehown in the following tables. 3.31, 3.32 and 3.33.

EXPERIMENTAL RESULTS [36]				
Me	K_1 $MPa\sqrt{m}$	K_2 $MPa\sqrt{m}$	P_f N	dir $^\circ$
1	23.6	0	5800	0
1	24.4	0	6200	0
0.837	25.6	6.7	13800	27.2
0.652	22	13.4	31900	44.5
0.661	21.9	12.9	30600	37.5
0.518	14.4	13.6	30400	47.5
0.527	14.7	13.5	30200	49
0.258	8.2	19.1	42700	55.20
0.065	3.3	32.1	49500	65.00

Table 3.31: 1Cr-Mo-0.3V-Small Grain Size: experimental results

For what concerns the ASED criterion, the predictions are as usual worst near pure mode II, but still good. They are even better than the previous case, which was the same steel with larger grain size.
About the other criteria, the same observations done for the previous case are valid: with the normalized stress intensity factors, the experimental trend is included between the SED predictions and the MTS and GMTS trend. For the initiation angles, the best is the MTS and the GMTS criterion.

ASED PREDICTIONS			
Me	K_1	K_2	P_f
	$MPa\sqrt{m}$	$MPa\sqrt{mm}$	N
1	24.57	0.00	6155
0.85	22.84	5.60	14303
0.67	18.16	10.19	24623
0.52	13.38	12.72	31087
0.35	8.59	14.24	35074
0.19	4.66	14.93	36988
0	0.27	15.22	37900

Table 3.32: 1Cr-Mo-0.3V-Small Grain Size: ASED predictions

FAILURE LOADS			
	ASED	EXP [36]	
Me	P_f	P_f	$\Delta\%$
	N	N	
1.00	6155	6000	-2.59
0.85	14303	13800	-3.64
0.67	24623	31250	21.21
0.52	31087	30300	-2.60
0.35	35074	42700	17.86
0.19	36988	/	/
0.01	37900	49500	23.43

Table 3.33: 1Cr-Mo-0.3V-Small Grain Size: predicted and real failure loads

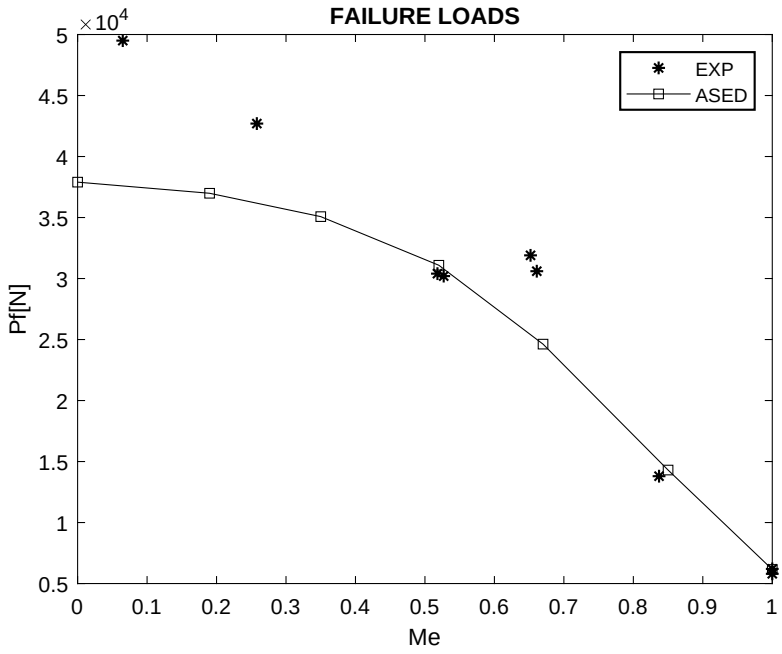

Figure 3.72: 1Cr-Mo-0.3V-Small Grain Size: failure loads comparison. Experimental data were taken from Ref. [36]

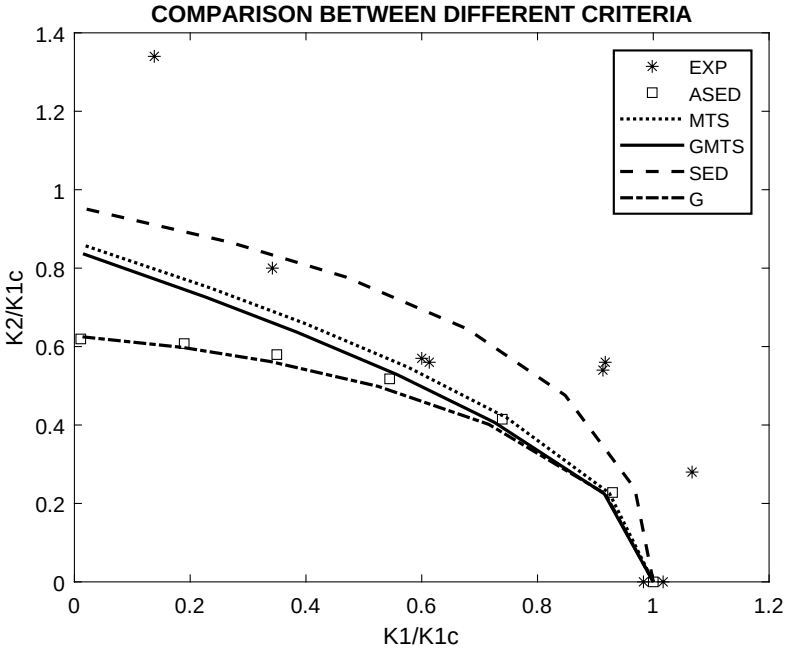

Figure 3.73: 1Cr-Mo-0.3V-Small Grain Size: normalized stress intensity factors comparison. Experimental data were taken from Ref. [36]

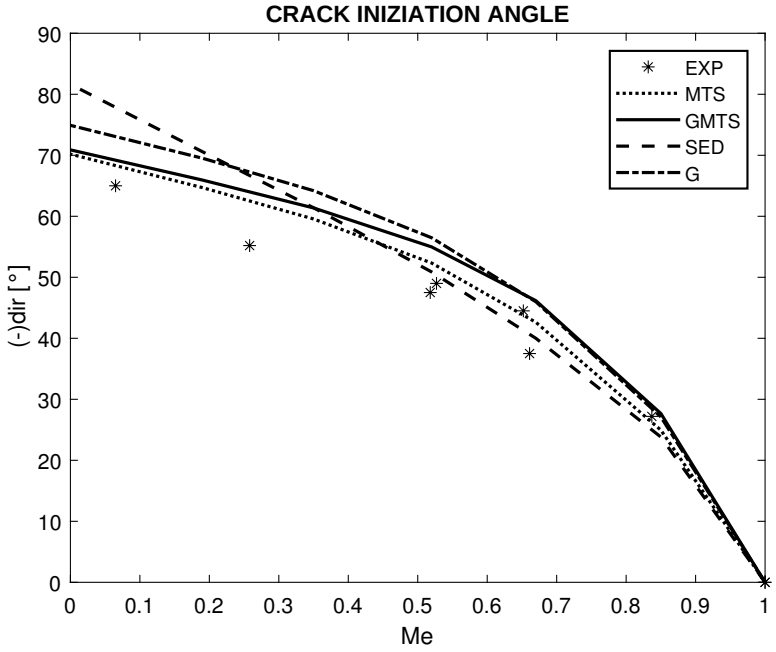

Figure 3.74: 1Cr-Mo-0.3V-Small Grain Size: initiation angles comparison. Experimental data were taken from Ref. [36]

3.4.5 C Mn-weld

The material composition is in the following table:

Material Composition									
Material	C	Mn	Si	S	P	Ni	Cr	Mo	V
C Mn-weld	0.06	1.56	0.41	0.038	0.021	-	-	-	0.-

Table 3.34: C Mn-weld: material composition

The material properties are:

$$\nu{=}0.3$$
$$\text{E}{=}200000 \text{ MPa}$$
$$K_{Ic}{=}21.55 \text{ MPa}\sqrt{m}$$
$$\sigma_y{=}850 \text{ Mpa}$$
$$\sigma_t{=}850 \text{ Mpa}$$

With these values, calculating R_c with the standard equation for plane strain cases gives $R_c = 0.17\,mm$.

Because of the welding, the microstructure is altered. When dealing with welded specimens, to get a valuable result it is important to control the pre-crack tip position and the equiaxiality of the grain in the re-heated zone. For this material, not all the mixed-mode combinations were tested. Probably the microstructure affected the tests equivalent to

β=15°, 0°. From the tensile test, the authors of the paper did not register a great difference between the behavior of this steel at room temperature and $-196°C$. In Abaqus

EXPERIMENTAL RESULTS [36]				
Me	K_1	K_2	P_f	dir
	$MPa\sqrt{m}$	$MPa\sqrt{m}$	N	°
1	20.4	0	5200	0
1	22.7	0	6200	0
0.838	20.8	5.4	13800	22.8
0.830	28.9	7.9	20200	24.2
0.670	23.5	13.4	31800	42
0.671	23.9	13.6	35900	41.5
0.540	19.6	17.3	45500	49
0.532	22.7	20.5	54000	49.50
0.333	16.9	29.3	71900	59.00
/	/	/	110700	61.00

Table 3.35: C Mn-weld: experimental results

also the configuration for β=15°, 0° were tested, even if it is not possible the comparison with the experimental values of the failure loads.

The application of other criteria lead to these graphs. The comparison is not good at all

ASED PREDICTIONS			
Me	K_1	K_2	P_f
	$MPa\sqrt{m}$	$MPa\sqrt{mm}$	N
1	21.38	0.00	5249
0.85	19.96	4.91	12246
0.67	15.97	8.98	21220
0.52	11.82	11.26	26904
0.34	7.61	12.64	30441
0.19	4.13	13.27	32146
0	0.24	13.53	32955

Table 3.36: C Mn-weld: ASED predictions

for stress intensity factors.

FAILURE LOADS			
	ASED	EXP [36]	
Me	P_f	P_f	$\Delta\%$
	N	N	
1.00	5249	5700	7.91
0.85	12246	17000	27.97
0.67	21220	33850	37.31
0.52	26904	49750	45.92
0.34	30441	91300	66.66
0.19	32146	/	/
0.01	32955	/	/

Table 3.37: C Mn-weld: predicted and real failure loads

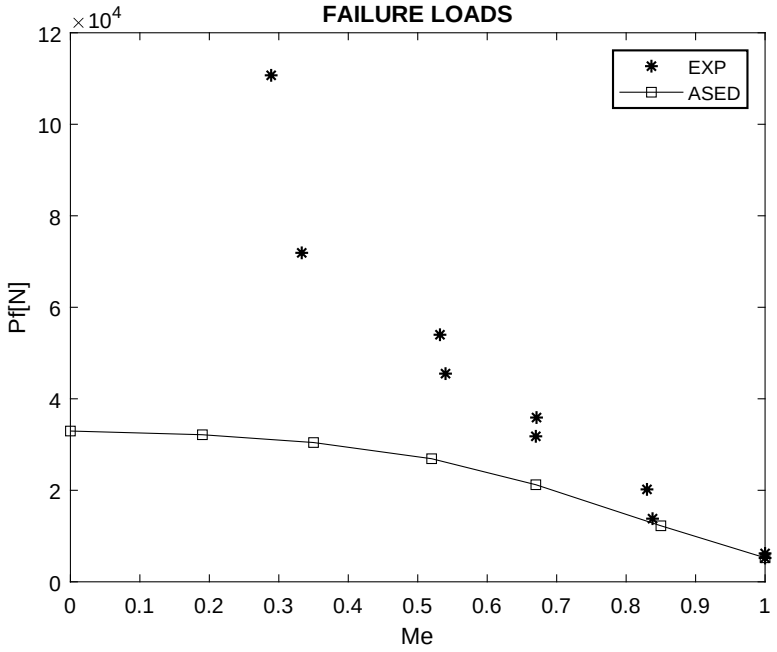

Figure 3.75: C Mn-weld: failure loads comparison. Experimental data were taken from Ref. [36]

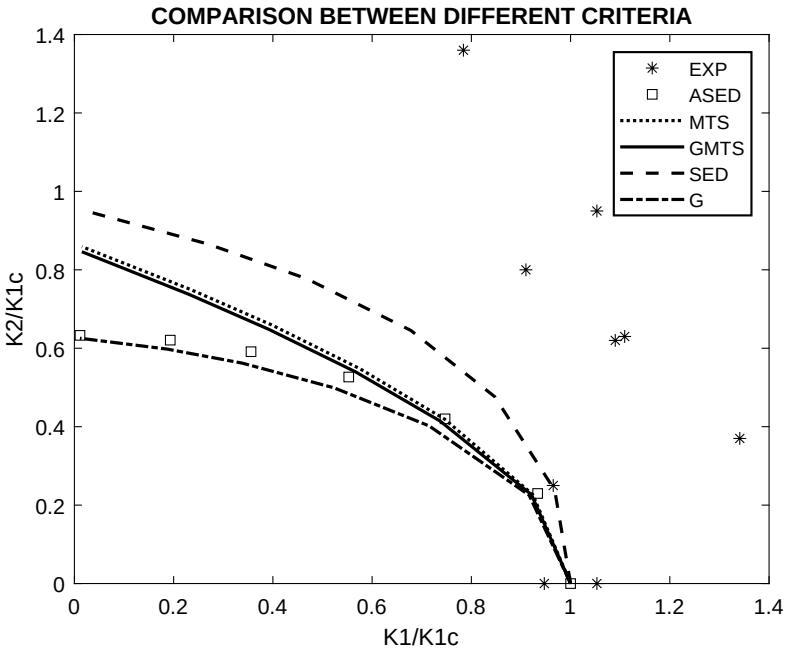

Figure 3.76: C Mn-weld: normalized stress intensity factors comparison. Experimental data were taken from Ref. [36]

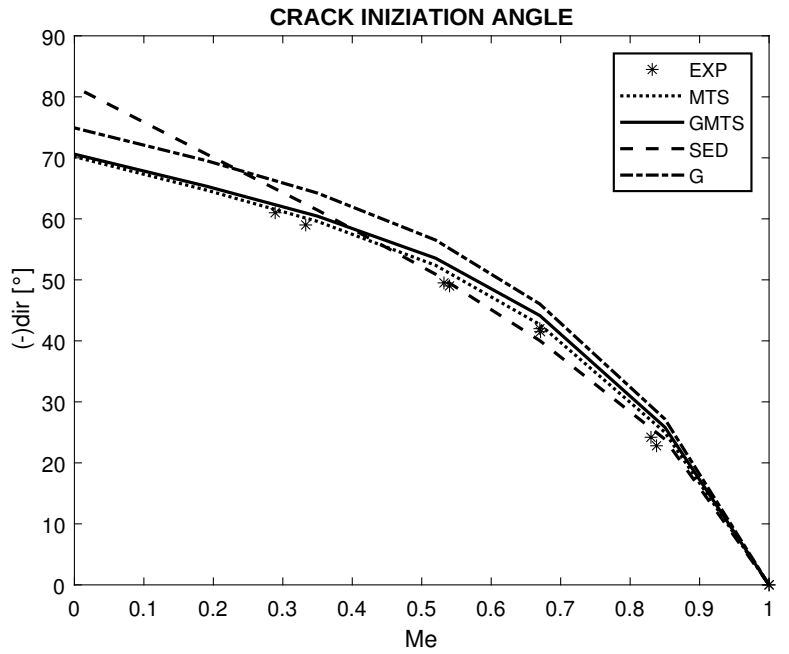

Figure 3.77: C Mn-weld: initiation angles comparison. Experimental data were taken from Ref. [36]

3.4.6 HY 130

This is a high yield steel that was heat-treated at 980°C for 2 hours, quenched in oil, and then tempered at 350°C for 1 hour. Composition and properties are the following:

Material Composition									
Material	C	Mn	Si	S	P	Ni	Cr	Mo	V
HY 130	0.14	0.76	0.22	0.007	0.008	4.90	0.56	0.53	0.05

Table 3.38: HY 130: material composition

The material properties are:

ν=0.3

E=200000 MPa

K_{Ic}=41.4 MPa$\sqrt{m}$

σ_y=1200 Mpa

σ_t=1450 Mpa

With these properties $R_c = 0.32\,mm$.

Unfortunately the authors of [36] registered a non-linear trend of the load versus time

EXPERIMENTAL RESULTS [36]				
Me	K_1 $MPa\sqrt{m}$	K_2 $MPa\sqrt{m}$	P_f N	dir °
1	41.7	0	10600	0
1	41.1	0	10100	0
0.837	35.1	9.2	20000	26.8
0.836	35.2	9.3	22900	25.2
0.670	31.9	18.2	42000	43.2
0.668	28.5	16.4	46200	42.8
0.48	/	/	76200	53.8
0.50	/	/	69900	53.80
0.33	/	/	148500	60.20
0.34	/	/	154700	59.00
0.19	/	/	196300	69.50

Table 3.39: HY 130: experimental results

curve obtained while carrying out the experimental tests for mixed-mode combinations corresponding to $\beta > 45°$. Even if there is not a complete table of experimental results to compare with, FE simulations were carried out for all the scheduled value of β. As it was foreseeable, the discrepancy between real and predicted failure loads is huge for

ASED PREDICTIONS			
Me	K_1	K_2	P_f
	$MPa\sqrt{m}$	$MPa\sqrt{mm}$	N
1	41.78	0.00	10435
0.85	38.99	9.57	24334
0.67	31.08	17.45	42012
0.52	22.95	21.83	53141
0.35	14.75	24.46	60031
0.19	8.00	25.67	63347
0	0.47	26.16	64923

Table 3.40: HY 130: ASED predictions

FAILURE LOADS			
	ASED	EXP [36]	
Me	P_f	P_f	$\Delta\%$
	N	N	
1.00	10435	10350	-0.82
0.85	24334	21450	-13.44
0.67	42012	44100	4.74
0.52	53141	73050	27.25
0.35	60031	151600	60.40
0.19	63347	196300	67.73
0.01	64923	/	/

Table 3.41: HY 130: predicted and real failure loads

$\beta > 45°$, probably for the non-linear effect. Predictions were as usual accurate for mode I and near it.

Even if there are few experimental points, fig. 3.79 shows good accordance between reality and all the criteria, especially the G criterion. Instead, regarding the propagation angle prediction, the better criterion is the GMTS (experimental tests were carried out for $\beta > 45°$ besides the non-linearity effects just to observe the direction along which the crack grows, that is the reason why there are more experimental points in fig. 3.80 than in fig. 3.79.

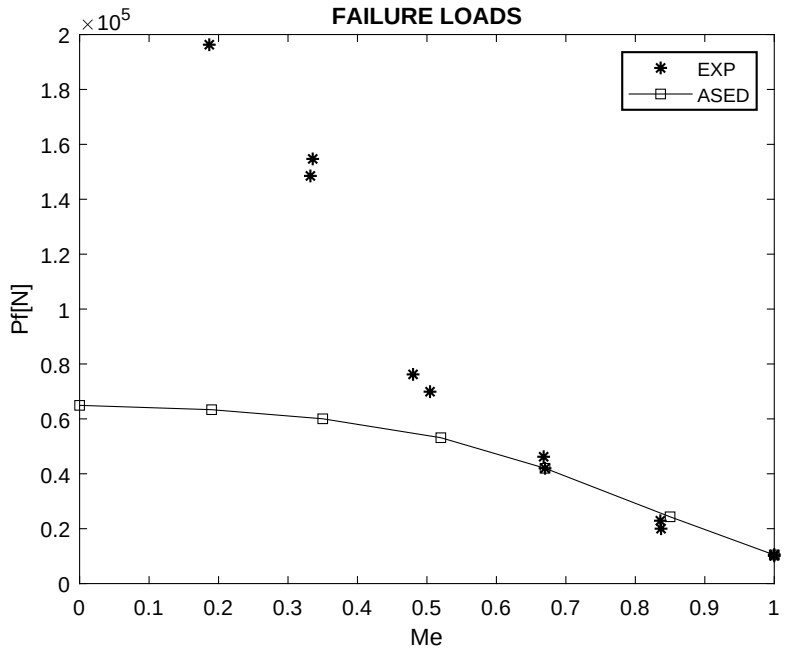

Figure 3.78: HY 130: failure loads comparison. Experimental data were taken from Ref. [36]

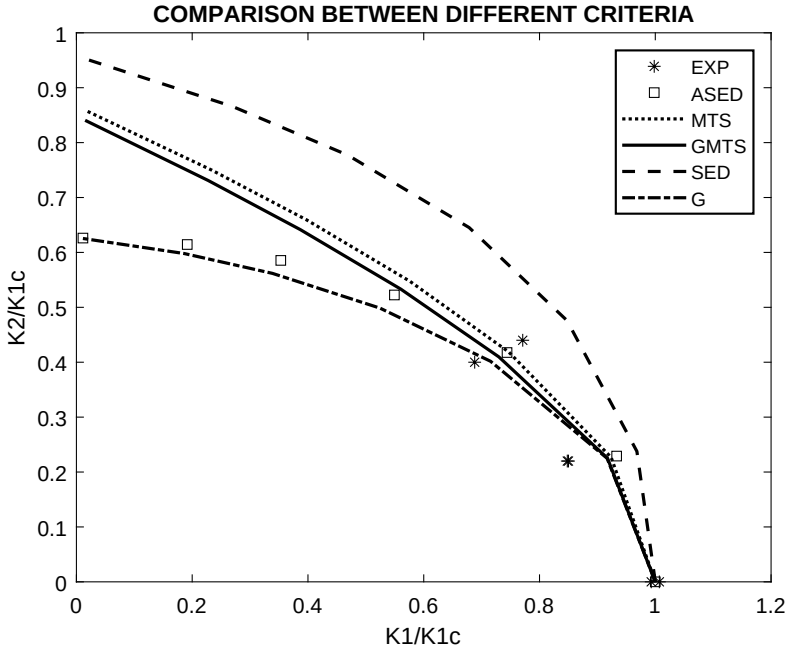

Figure 3.79: HY 130: normalized stress intensity factors comparison. Experimental data were taken from Ref. [36]

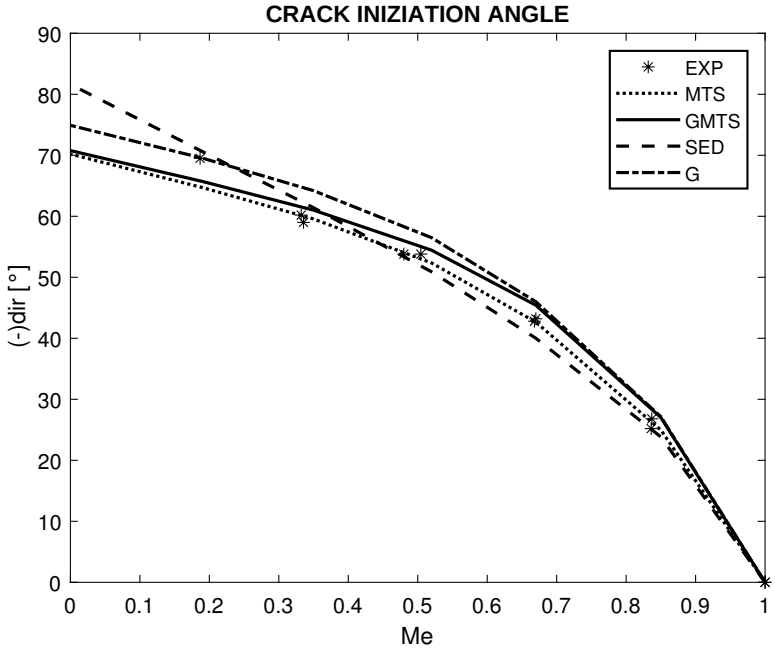

Figure 3.80: HY 130 initiation angles comparison. Experimental data were taken from Ref. [36]

3.4.7 The ASED Criterion Application at Room Temperature

This section presents some indications of how to deal with ductile materials. Two steels are tested at room temperature. This means that they present ductile behavior. The first one is HY 100 and the second one is HY 130. As it was expected, the ASED criterion and the other criteria either, do not work properly. In this situation it is possible to apply the EMC concept, to deal with an equivalent brittle material [18] [37] [38]. This attempt is carried on, but with these specimens, it is not possible to show the power of the EMC concept. Further details will be presented later.

HY 100 at 22°C

In the paper [39], by Bhattacharjee and Knott, asymmetric four-point bending tests were carried out on specimens of HY 100 steel, at room temperature. It is expected that the ASED criterion is not going to work.

The specimens underwent a heat treatment at 950°C for 2 hours to get an austenitic microstructure, and they are then quenched in water and tempered at 450°C for 2 hours. The composition of this high yield steel is:

Material Composition									
Material	C	Mn	Si	S	P	Ni	Cr	Mo	V
HY 100	0.15	0.35	0.17	0.005	0.009	3.25	1.69	0.40	0.32

Table 3.42: HY 100: material composition

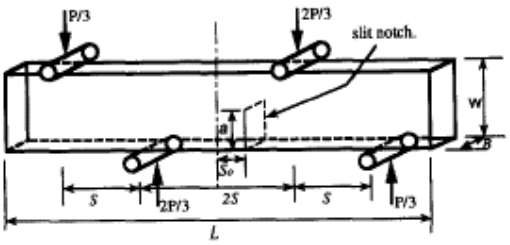

Figure 3.81: HY 100: loading configuration used in Ref. [39]

The material properties are:

ν=0.3

E=200000 MPa

K_{Ic}=137 MPa$\sqrt{m}$

σ_y=1050 Mpa

σ_t=1160 Mpa

With these properties $R_c = 4.58\,mm$. This is the larger radius ever obtained.
The fracture toughness was difficult to find, another paper was used [40]. Unfortunately, the treatments on the specimens and the composition are different, that could affect K_{Ic} and this add uncertainty to the results. Besides, not a lot of information was available in the paper regarding the test's results.
The configuration of the AFPB specimen is slightly different from the previous ones.

EXPERIMENTAL RESULTS [39]	
P_f	K_1/K_2
N	/
137500	3.15
153500	2.2
173000	1.57
178800	1.57
186500	0.94
184300	0.94
192300	0.63
201500	0.31

Table 3.43: HY 100: experimental results

In tables 3.43 and 3.44, the comparison between predicted failure loads and experimental failure loads is presented. It is astonishing how good is the ASED criteria in fitting the experimental trend.
The other theoretical criteria were applied. It was not possible to compare the experimental data. To perform the criteria was useful simply to see if they were in good

FAILURE LOADS			
	ASED	EXP	
Me	P_f N	P_f N	$\Delta\%$
1	42292	–	–
0.81	108103	137500	21.38
0.73	135546	153500	11.70
0.65	159505	175900	9.32
0.50	185575	185400	-0.09
0.37	197065	192300	-2.48
0.21	205432	201500	-1.95
0.01	209100	–	–

Table 3.44: HY 100: predicted and real failure loads

accordance or if something strange was going on. In fig. 3.83a the ASED criterion gives a trend that is particularly far from the other criteria. This is quite strange.

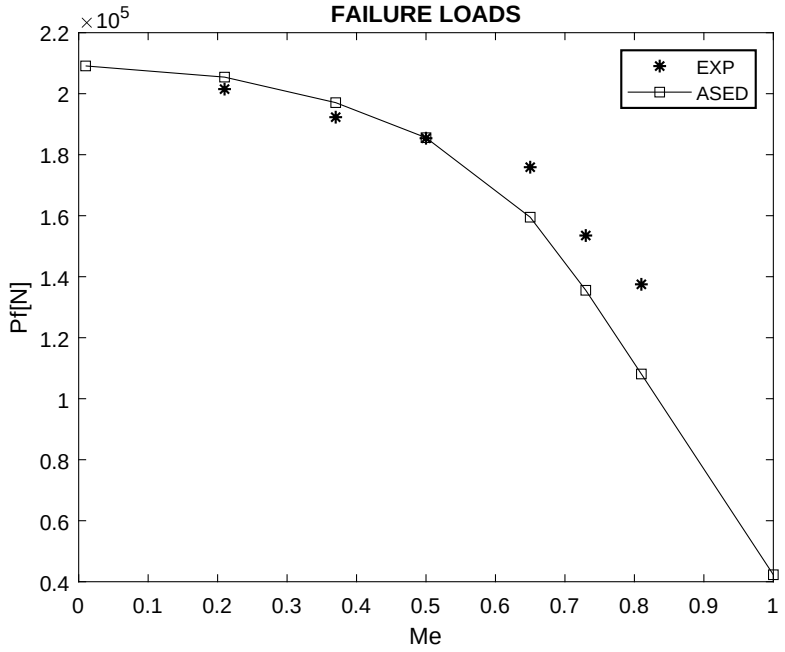

Figure 3.82: HY 100: failure loads comparison. Experimental data were taken from Ref. [39]

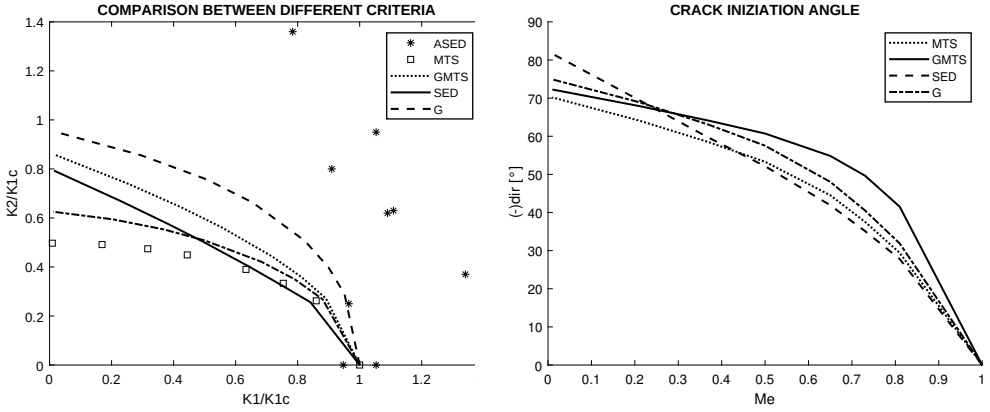

(a) (b)

Figure 3.83: HY 100: normalized stress intensity factors and initiation angles comparison. Experimental data were taken from Ref. [39]

HY 130 at 20°C

This material has already been studied, but this time the ASED criterion is applied at room temperature. The properties are:

$$\nu{=}0.3$$
$$\text{E}{=}200000 \text{ MPa}$$
$$K_{Ic}{=}210.47 \text{ MPa}\sqrt{m}$$
$$\sigma_t{=}896 \text{ Mpa}$$

With these properties, the control radius is calculated as $R_c = 14.83\,mm$. Being the specimens dimensions the same presented previously, it is impossible to perform the ASED criterion: the width of the specimens is $20\,mm$, it is not possible to sketch the circular control volume. The reason why the radius has such a magnitude compared to the brittle materials is related to the shape of the stress-strain curve. The material is ductile, the curve shows the plastic deformation zone. The area subtended by the curve is huge, at it is the strain energy. This is why to obtain $\overline{W}$ it is necessary to use a massive control volume.

The EMC application

The Equivalent Material Concept is used when dealing with ductile material on which applying the ASED criterion. The ductile material is transformed into an equivalent brittle material. The equivalence is based on the strain energy, the area subtended by the strain-stress curve. A brittle material is creating maintaining the same strain energy. The tensile strength obtained is an equivalent property and in fig. 3.84 is depicted as σ_{t-eq} and is obtained with the following equation.

$$\sigma_{t-eq} = \sqrt{\sigma_y + \frac{2EK}{n+1}\left(\left(\frac{\sigma_{UTS}}{K}\right)^{(n+1)/n} - 0.002^{n+1}\right)} \tag{3.8}$$

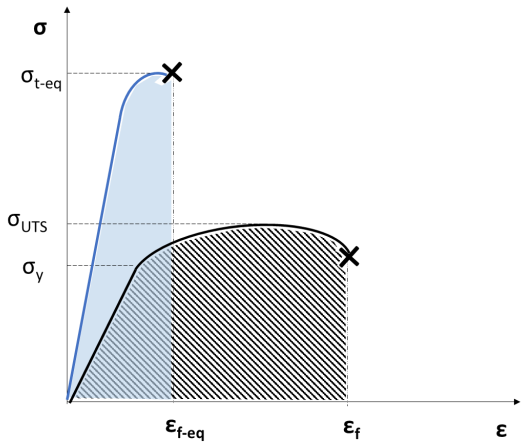

Figure 3.84: Equivalence between a ductile material and a brittle one

where σ_y is the yielding stress of the material, σ_{UTS} the ultimate tensile strength, and K and n are respectively the Hollomon constant and the Hollomon exponent. According to Hollomon, for a ductile material, the strain-stress curve corresponding to the plastic deformation is obtained as $\sigma = K\epsilon^n$. Eq. (3.8) comes from the following equivalence

$$(\overline{W})_{BRITTLE} = (\overline{W})_{DUCTILE}$$

where the two terms indicate respectively the blue area and the dashed one in fig. 3.84. For both the terms general relations have been proposed in section 1.2.

The theory of EMC is used hereafter on both the materials presented, HY 100 and HY 130. But in both cases, the ASED criterion was not appliable. Being the material ductile, the σ_{t-eq} are incredibly high and as a consequence, the radius obtained were not suitable.

HY 100:

$$\sigma_{t-eq} = 147281\,MPa$$

$$R_c = 0.000233\,mm$$

HY 130:

$$\sigma_{t-eq} = 65802.0682\,MPa$$

$$R_c = 0.002750\,mm$$

Chapter 4

ZIRCONIA AFPB TESTS RESULTS

Due to the availability of Zirconia specimens, it was possible to carry out experimental tests on this material, with an AFPB fixture available in the workshop of the university NTNU. In the following section, the whole process is described: the specimen's and material's characteristics, the procedure for the experimental tests, the simulation part in Abaqus, and the comparison between experimented failure loads and predicted failure loads.

4.1 Experimental Tests

4.1.1 The Specimen

The specimens available are Zirconia specimens of tiny dimensions. They were provided by the American *Superior Technical Ceramics Corp*, St. Albans, VT.
The particular type of Zirconia under consideration is called YTZP: Yttria Stabilized Zirconia. The addition of Yttria turns Zirconia in her tetragonal phase. The phase has a significant impact on the strength and fracture toughness of the material.
Two different variations of YTZP were studied: the first one, denominated *Zirconia 2000*, is characterized by the properties proposed in tab 4.1. The second one is called *Zirconia 4000* and the properties are in tab 4.2.

Zirconia 2000		
E	210	GPa
ν	0.3	\
σ_t	550	MPa

Table 4.1: Zirconia 2000: Material properties

The specimen used in the test is shown in fig. 4.1. Shape and dimensions are the same

Zirconia 4000		
E	210	GPa
ν	0.3	\
σ_t	690	MPa

Table 4.2: Zirconia 4000: Material properties

for both types of Zirconia. They are pre-cracked specimens, with the initial crack length called a that is half of the specimen's width. Dimensions are:

$$L = 50\,mm$$
$$w = 4\,mm$$
$$t = 3\,mm$$
$$a/W = 0.5$$

Figure 4.1: The specimen

4.1.2 The Fixture

The tests were carried out thanks to the AFPB fixture shown in fig. 4.2. The system was fixed in a *MTS Criterion, Model 42* machine, with a load cell of $5\,kN$. The fixture is composed of two rails and four rollers which diameter is $4\,mm$. The specimen is supported by the rollers, which means, ideally, that the contact is *punctual*. The rollers are placed in the fixture in designated slots. The slots are provided with mechanisms that enable movement along the rail. Therefore, the positions of the four rollers are independent. Upper rollers were fixed with rubber bands. In fig. 4.2 the Symmetric Four-Point Bend configuration is shown, which allows performing the pure mode I fracture.

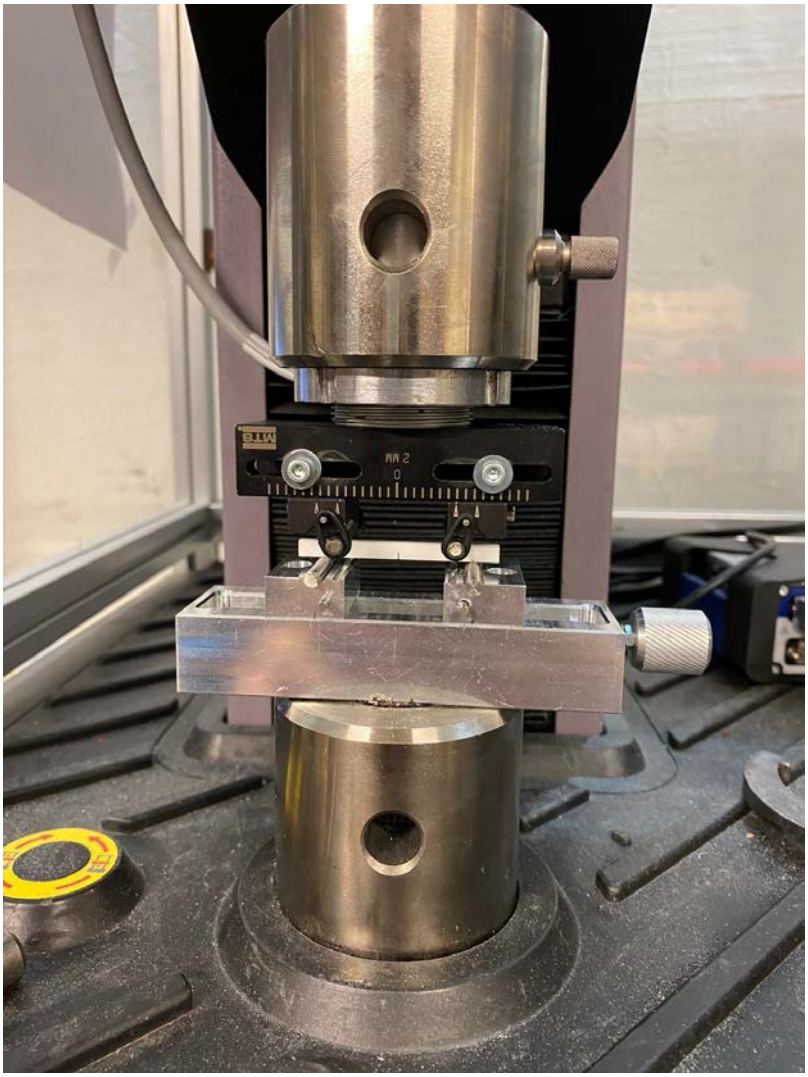

(a)

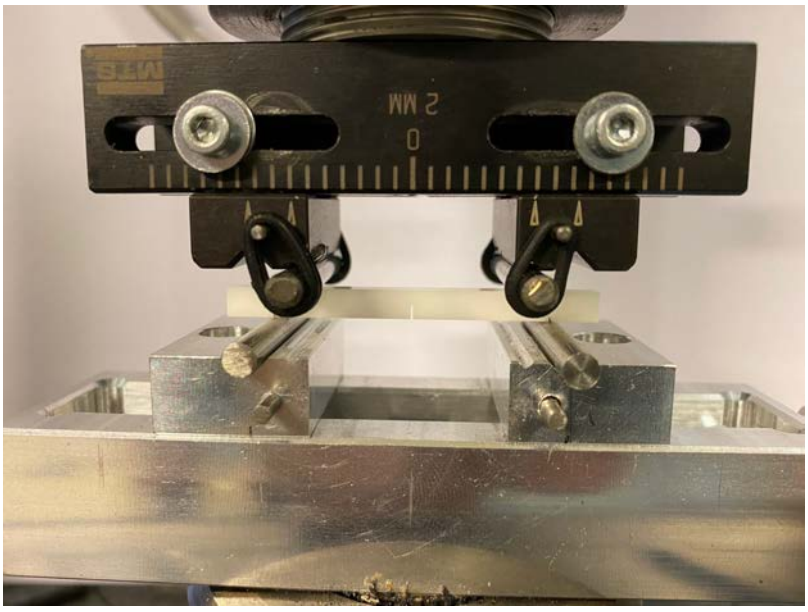

(b)

Figure 4.2: The fixture

4.1.3 The Procedure

A strict procedure was followed, in order to obtain reliable results.
First of all, it was necessary to align the fixture in her location. Both the rails must be perfectly horizontal, but they also have to be parallel to each other. To be sure of these alignments, the fixture was observed from different angulations, especially when the two halves of the fixture are close to each other. The rails centers should also be aligned. While it is easy to find the center of the upper rail because there is a ruler on it (see fig. 4.2), for the lower rail it is necessary to find the center by measuring the block with a digital calibre and marking it .
When the alignment is satisfactory, it is possible to move the rollers slots to create the right loading configuration to lead the specimen to fracture under the required mixed-mode conditions.
Also the specimen should be prepared by marking the points where the lower rollers should touch it. In this way, it is easier to place it in the fixture. It is also important to check that the specimen is in the middle of the rollers.
Before starting the tests, a warm-up of the machine is made with a piece of wood to see if the force-displacement curve presents anomalies.
The machine is equipped with a data acquisition system. From the interface of the dedicated software, it is possible to set some parameters: first, the crosshead speed is set at $0.1\,mm/min$. The tests are already quite fast.
Then, it is important to check if the initial load is zero or around zero. Indeed, the upper rollers must be almost in contact with the specimen before starting the test. They have to be close, but not touching themselves. If the initial load registered is different from zero, a brittle specimen could break before the test starts. Once the right distance is found, the displacement should be set equal to zero. At this point, it is possible to begin with the test.
For both types of Zirconia, three tests were carried out for each configuration. Five different configurations were used, in order to explore different possibilities between pure mode I and pure mode II. The configurations were chosen using a FE software and they are characterized by Me, the mixed-mode coefficient. The chosen sequence is: $Me = 1\,(pure\,mode\,I)$; $Me = 0\,(pure\,mode\,II)$; $Me = 0.25$; 0.47; 0.8.
After every test, the fragments of the specimen were collected, taking care of not touching the fracture surface, and marked.
In the following section, photographic documentation of the tests is presented.

4.1.4 Photographic Reportage

4.1.4.1. Mode I

To perform mode I, the fixture must be set in the Symmetric Four-Point bending (SFPB) configuration. A scheme of this configuration is shown in fig. 4.3.

The loading spans S_{inn} and S_{out} are chosen accurately observing what it is common to

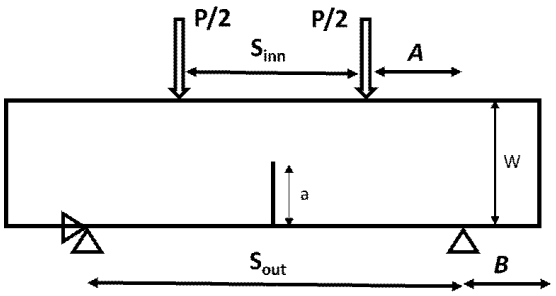

Figure 4.3: Symmetric Four-Point bending Configuration (SFPB)

do when testing specimens with this configuration in other authors' work. An appropriate value for the *outer span* is $S_{out} = 37\,mm$. The *inner span* was chosen in order to have a proper value for the parameter A, which should be long enough, otherwise, the application point of the load will be too close to the constraint, for both sides of the specimen, and this would affect the test. Being these rollers quite big compared to the specimen's dimensions, to set $B = W$, as it is common, was not enough. After some attempts, $S_{inn} = 27\,mm$ was chosen. To resume, loading distances are:

$$S_{inn} = 37\,mm$$
$$S_{out} = 27\,mm$$
$$A = 5\,mm$$
$$B = 6.5\,mm$$

A picture of the fixture in this configuration has been already proposed in fig. 4.2. In fig. 4.4 the cracked specimens of *Zirconia 2000* and *Zirconia 4000* are presented.
The crack is clearly propagated from the tip of the pre-crack which original length was a, in a perpendicular direction to the specimen's length.

4.1.4.2 Mode II

After pure mode I, the smartest thing is to perform pure mode II. That is because,

(a) zirconia 2000.

(b) Zirconia 4000.

Figure 4.4: Mode I

from this position, it is easier to change the distance $L2$ to set the fixture in the mixed-mode configurations. A scheme of the configuration is presented in fig. 4.5.

To perform pure mode II, distances should be $L_1 = L_4$ and $L_2 = L_3$. This is the classical

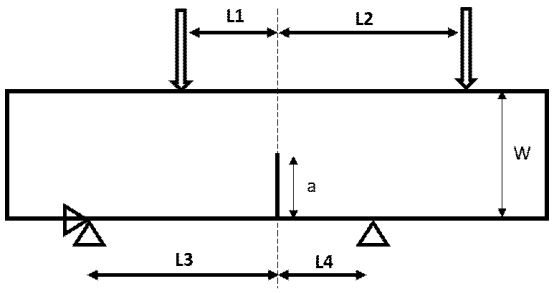

Figure 4.5: Asymmetric Four-Point bending Configuration (AFPB)

AFPB configuration. These values were chosen to guarantee $Me = 0$:

$$L_1 = 5\,mm$$
$$L_2 = 15\,mm$$
$$L_3 = 15\,mm$$
$$L_4 = 5\,mm$$

The picture of the fixture in this configuration and the broken specimens are presented hereafter. From fig. 4.7 is interesting to notice the particular path of the crack.

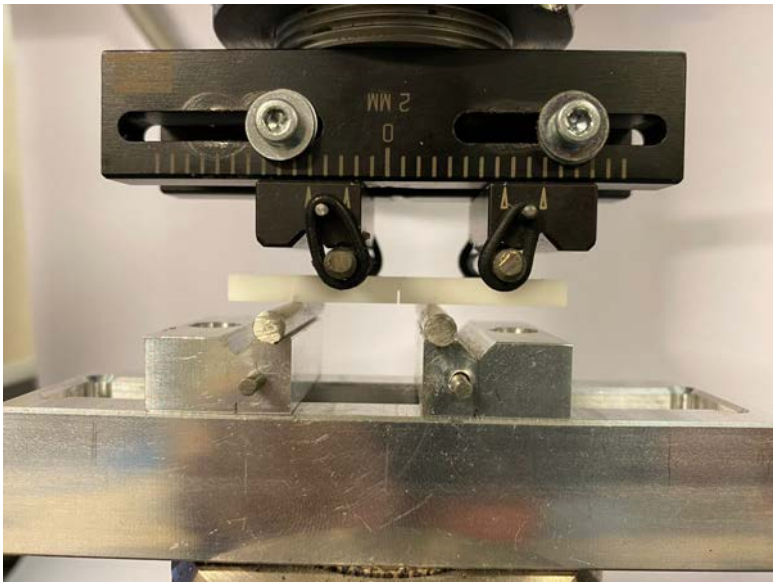

Figure 4.6: The fixture when Me=0

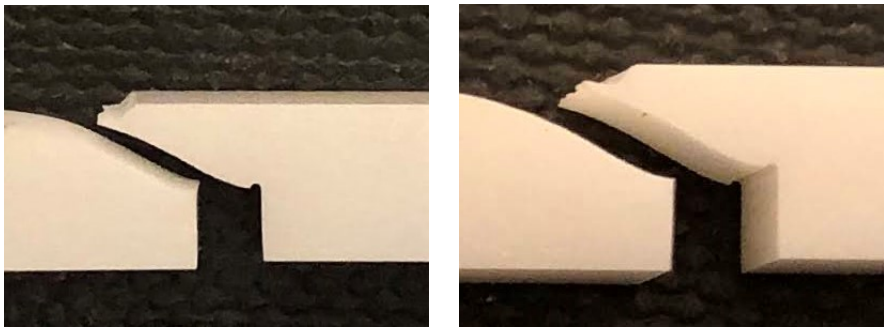

(a) Zirconia 2000. (b) Zirconia 4000.

Figure 4.7: Me=0; details of the crack

4.1.4.3 Me=0.25

To obtain mixed-mode configurations it's sufficient to change the distance $L2$. This concept is easy to understand observing fig. 4.8: decreasing $L2$ means to increase the mode I component in the mixed-mode.

The following distances were set:

$$L_1 = 5\,mm$$
$$L_2 = 13\,mm$$
$$L_3 = 15\,mm$$
$$L_4 = 5\,mm$$

The picture of the fixture in this configuration and the broken specimens are presented hereafter.

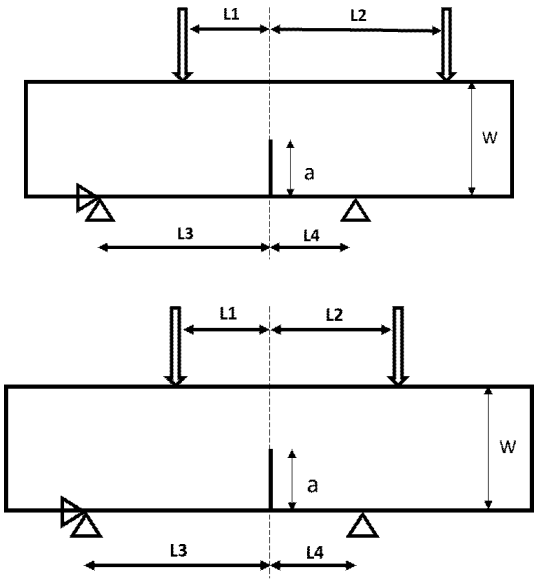

Figure 4.8: Asymetric Four-Point bending Configuration (top) and a generical mixed-mode configuration (bottom)

Figure 4.9: The fixture when Me=0.25

(a) Zirconia 2000. (b) Zirconia 4000.

Figure 4.10: Me=0.25; details of the crack

4.1.4.4 Me=0.47

The following distances were set:

$$L_1 = 5\,mm$$
$$L_2 = 12\,mm$$
$$L_3 = 15\,mm$$
$$L_4 = 5\,mm$$

The picture of the fixture in this configuration and the broken specimens are presented hereafter in fig. 4.11 and 4.12.

4.1.4.5 Me=0.80

The last mixed-mode proposed is the closest to pure mode I. The distances chosen are the following:

$$L_1 = 5\,mm$$
$$L_2 = 8\,mm$$
$$L_3 = 15\,mm$$
$$L_4 = 5\,mm$$

The picture of the fixture in this configuration and the broken specimens are presented in fig. 4.13 and 4.14.

It would be interesting to study the fracture surface with an SEM microscopy. It is the only instrument that can take pictures of the grains in the fracture surface. Zirconia is not a good conductor, and to use SEM, it would necessary to coat the specimens with a thin layer of gold.

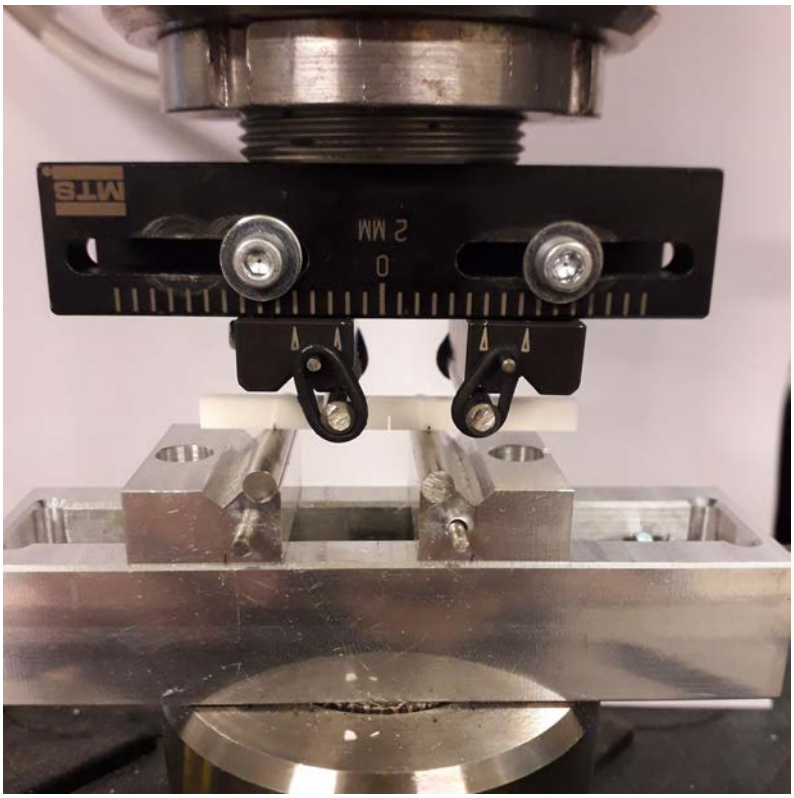

Figure 4.11: The fixture when Me=0.47

(a) Zirconia 2000. (b) Zirconia 4000.

Figure 4.12: Me=0.47; details of the crack

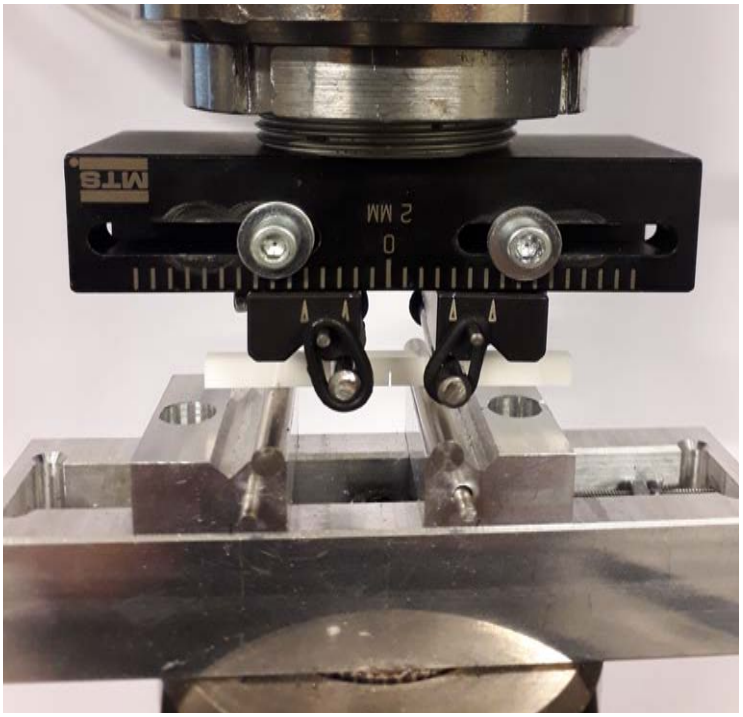

Figure 4.13: The fixture when Me=0.80

(a) Zirconia 2000.

(b) Zirconia 4000.

Figure 4.14: Me=0.80; details of the crack

4.1.5 Results and Discussion

In the following tables the failure loads, registered during the tests, are presented. As said before, three tests were carried out for every configuration. Sometimes something in the tests went wrong: Some specimens did not break at all and some others broke down when the system had already stopped registering the load-displacement curve. That means that the registered failure load is lower than the real one. These problems are highlighted with colors in the tables: red for the specimens that did not break and orange for the problematic tests.

Zirconia 2000	
Specimen	Pf $[N]$
$1-1-1$	408.5
$1-1-2$	423.5
$1-1-3$	390.54
$1-5-1$	1287.91
$1-5-2$	1630.98
$1-5-3$	4457.15
$1-4-1$	4457.48
$1-4-2$	1250.86
$1-4-3$	3422.96
$1-3-1$	3631.87
$1-3-2$	3799
$1-3-3$	3305.39
$1-2-1$	2828
$1-2-2$	4053
$1-2-3$	4163

(a)

Zirconia 4000	
Specimen	Pf $[N]$
$2-1-1$	398.31
$2-1-2$	384.45
$2-1-3$	397.67
$2-5-1$	4455.14
$2-5-2$	1643.33
$2-5-3$	1795.51
$2-4-1$	4462.47
$2-4-2$	4460.79
$2-4-3$	4054.22
$2-3-1$	3644.79
$2-3-2$	4450
$2-3-3$	4137.33
$2-2-1$	3968.29
$2-2-2$	3529.72
$2-2-3$	3956.38

(b)

Legenda
Specimen X-Y-Z
X= Zirconia's type: 1=Zirconia 2000;
2=Zirconia 4000.
Y= Loading Mode: 1=Mode I;
2=Mode II;
3=$Me = 0.25$;
4=$Me = 0.47$;
5=$Me = 0.80$.
Z=n° of the specimen, from 1 to 3 tests for each configuration.
e.g. Specimen 1-3-2: Zirconia 2000, loading mode with $Me = 0.25$, 2^{nd} test.

Table 4.3: Experimental failure loads for Zirconia 2000 and Zirconia 4000 specimens

To show the difference between a normal test and a test where something went wrong, fig. 4.15 is attached: the top-plot is the expected curve for a specimen that breaks after reaching his failure load, and it is the curve of the specimen 1-1-1. The bottom-plot is the curve of the specimen 1-5-3: this specimen did not fracture and actually the curve it is different.

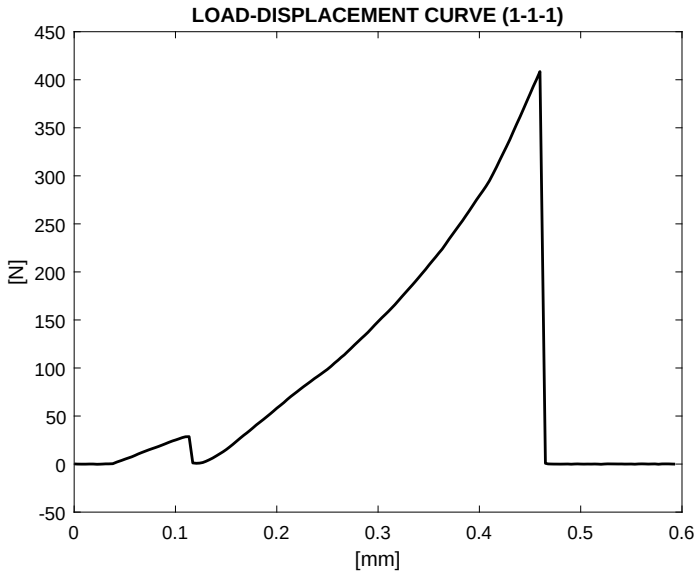

(a)

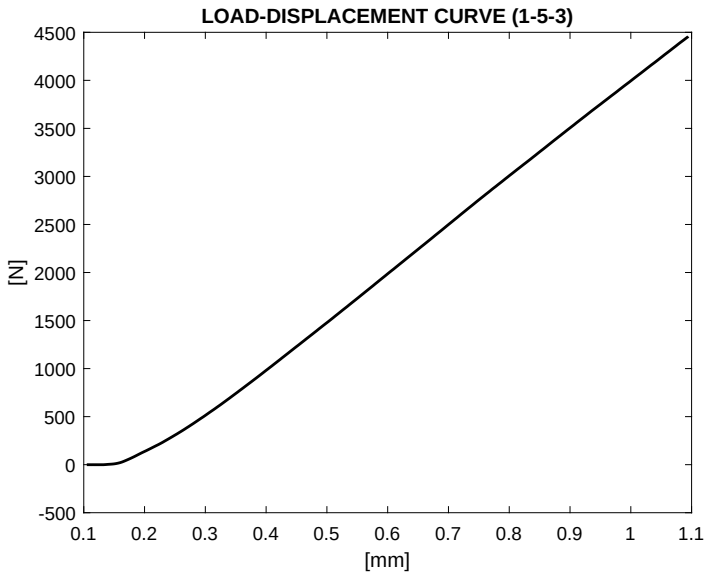

(b)

Figure 4.15: Load-displacement curves for two different specimens

4.2 ASED Predictions

4.2.1 Prediction and comparison with experimental results

The ASED criterion is applied in order to predict failure loads for the same loading configurations in which the experimental tests were carried out. Specimens' dimensions and materials properties are well known and already presented in the previous sections. Therefore, the model in the FE software Abaqus can be created. To apply ASED it is necessary to create the circular control volume. The radius R_c is a function of the material. The fracture toughness is almost the same for both types of Zirconia: $K_{Ic} = 15\,MPa\sqrt{m}$. Hence, the control radius, with the hypothesis of plane strain, are:

$$R_c = 0.20\,mm \quad \textit{(Zirconia 2000)}$$
$$R_c = 0.13\,mm \quad \textit{(Zirconia 4000)}$$

In Abaqus, the total applied load is $1\,N$. Then the force is properly split in two com-

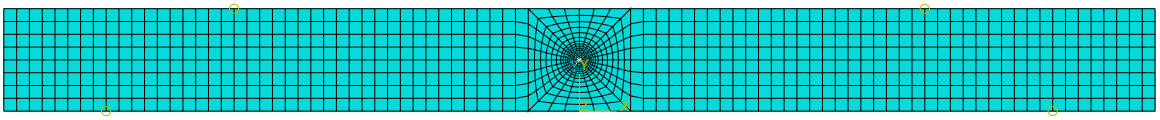

Figure 4.16: Typical mesh

ASED PREDICTED FAILURE LOADS (Zirconia 2000)								
	L_1 $[mm]$	L_2 $[mm]$	L_3 $[mm]$	L_4 $[mm]$	P_1 $[N]$	P_2 $[N]$	Me	Pf $[N]$
1	13.5	13.5	18.5	18.5	0.5	0.5	1	422
2	5	8	15	5	0.62	0.38	0.80	1339
3	5	12	15	5	0.71	0.29	0.47	2013
4	5	13	15	5	0.72	0.28	0.25	2156
5	5	15	15	5	0.75	0.25	0	2101

Table 4.4: Zirconia 2000: the ASED criterion predictions

The comparison between ASED predictions and experimental failure load is easier to understand graphically in the fig. 4.17 and 4.18.

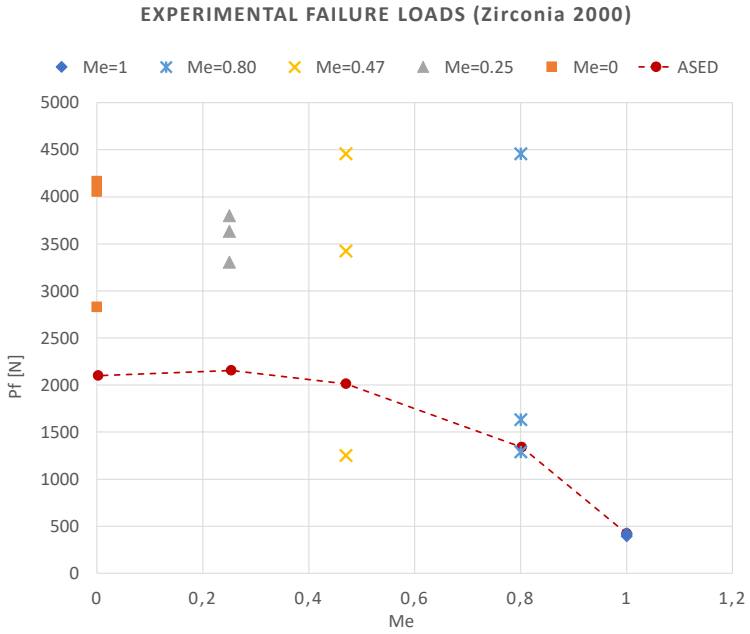

Figure 4.17: Zirconia 2000: failure loads comparison

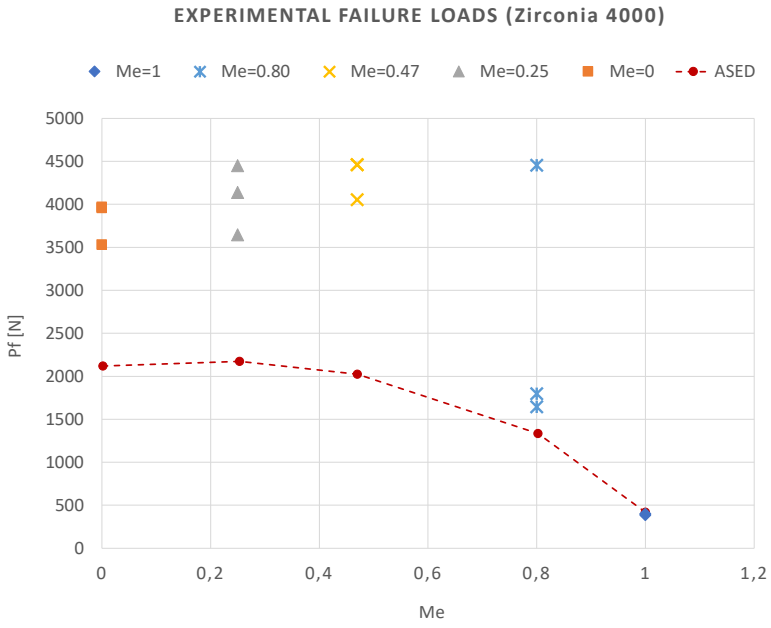

Figure 4.18: Zirconia 4000: failure loads comparison

ASED PREDICTED FAILURE LOADS (Zirconia 4000)								
	L_1 $[mm]$	L_2 $[mm]$	L_3 $[mm]$	L_4 $[mm]$	P_1 $[N]$	P_2 $[N]$	Me	Pf $[N]$
1	13.5	13.5	18.5	18.5	0.5	0.5	1	420
2	5	8	15	5	0.62	0.38	0.80	1336
3	5	12	15	5	0.71	0.29	0.47	2025
4	5	13	15	5	0.72	0.28	0.25	2174
5	5	15	15	5	0.75	0.25	0	2120

Table 4.5: Zirconia 4000: the ASED criterion predictions

Unfortunately, the comparison is not as good as expected for both cases. As usual, for mode I and the first mixed-mode ($Me = 0.80$) results are not that bad. There are some data decisively out of the scatter zone, probably something happened with those specimens and the corresponding point should not be considered.
Problems are greater when $Me = 0.47$. For the first Zirconia, the three points are completely different. Checking the experimental results in tab. 4.3a we can notice that the specimen $1 - 5 - 1$ was problematic, but even the failure load for specimen $1 - 5 - 3$ is strangely low. For *Zirconia 4000* instead, the three values found out for $Me = 0.47$ are close to each other: this is a hint towards their correctness. But they are totally different from the prediction.
In general, the same observation can be done for results of mode II and $Me = 0.25$, for both types of Zirconia: experimental results are higher than the predicted ones. The only analogy between the experimental curve and predicted curve is that in both cases for mode II the failure load is lower than for $Me = 0.25$.

Observations

The comparison concludes that, in this case of study, ASED predictions do not fit properly the experimental results. Observing the cracked specimens, it is easy to notice that there are some anomalies in the way the fracture occurred. One possibility is that the tests were not carried out correctly and for this reason, the comparison with the ASED criterion does not work.
Taking under consideration fig. 4.4, 4.7, 4.10, 4.12 and 4.14 some observations can be done.

- The specimens cracked in three pieces instead of two. The only exceptions are the mode I specimens. One possible explanation is that the upper rollers did not touch the specimen at the same time. Under the roller which first touched the specimen, the pressure could be high enough to provoke another fracture.

- Observing the specimen from the upper side, it is possible to see that sometimes the crack is developed with a strange angle that suggests the presence of torsion. If there is also a component of mode III in the mixed-mode, it is because of the placement of the specimen. It was probably not correctly aligned in the fixture.

- The specimens are tiny but it is easy to notice that the crack has a radius not close to zero. It is more similar to a U-notch then to an ideal crack. The fact that a crack can be considered ideal or a U-notch depends on the relation between the averaged grain size of the material and the radius of the notch. In any case, this aspect needs further investigation. If it is a notch the equations to apply ASED Criterion change.

- It is not so clear if the crack starts from the tip of the pre-crack or from the side. Ideally, the crack should propagate from the tip, along a direction that depends on the mixed-mode. In fig.4.4 we can see that for mode I the crack was almost *vertical*, as to say that the initiation angle was almost 0°. But for the other specimens, it is difficult to distinguish mode II from mixed-modes. They look almost all like mode II fracture propagation.

4.2.2 Theoretical criteria application

Other theoretical criteria are performed to predict the normalized values of the stress intensity factors and the initiation angles of the cracks. The criteria used are as usual the MTS, GMTS, SED, and G criteria. The inputs necessary to perform them are provided thanks to the application of the ASED criterion and to the use of the FE software. In the following plots, the results of this analysis are presented for both *Zirconia 2000* and *Zirconia 4000*.

For both types of Zirconia we can see that the closest criteria to ASED is the G criterion.

For what concerns the directions, the four criteria are in good agreement. They are also confirmed by the predictions obtained with Abaqus. It would be interesting to measure also the real angles of initiation of the cracks in the fractured specimens. For this purpose, it would be necessary at least a magnifying glass (or something more accurate) and a goniometer.

Using equations (4.1) and (4.2), it was possible to calculate the stress intensity factors using the experimental failure loads and the values for the adimensional geometry factors Y_1 and Y_2 found in fig. 4.23.

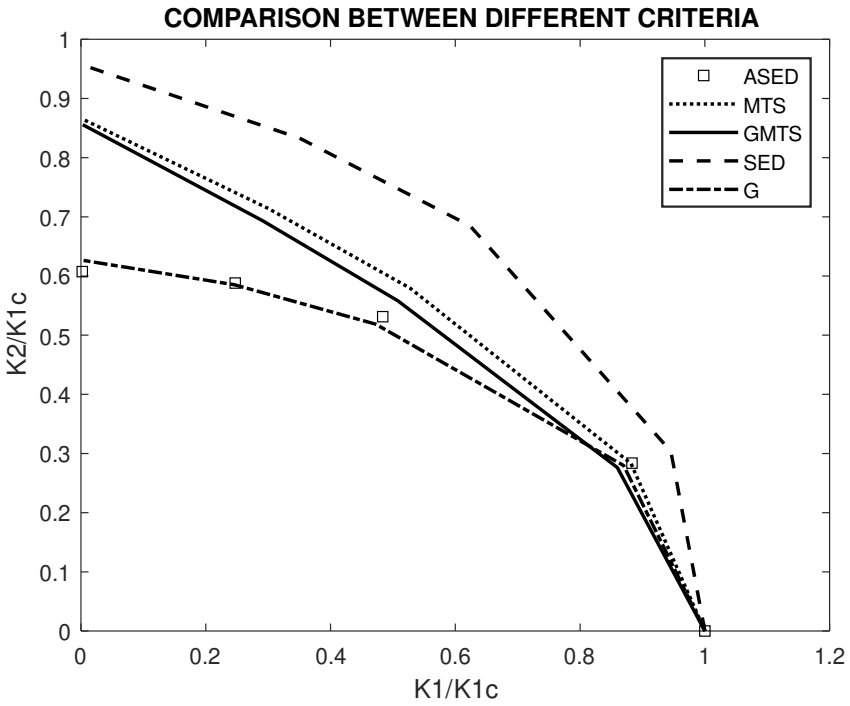

Figure 4.19: Zirconia 2000: normalized stress intensity factors comparison

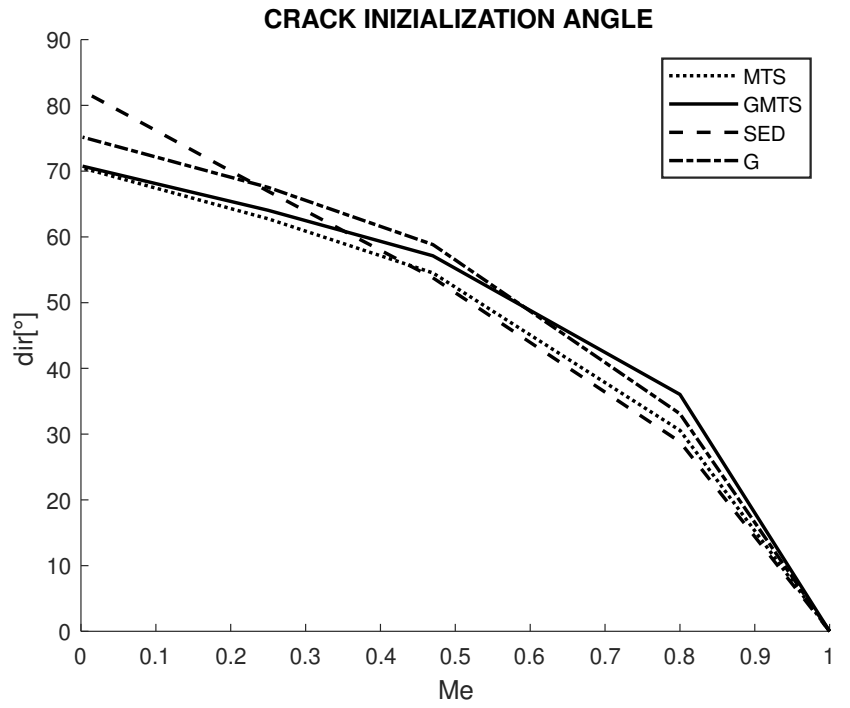

Figure 4.20: Zirconia 2000: initiation angle comparison

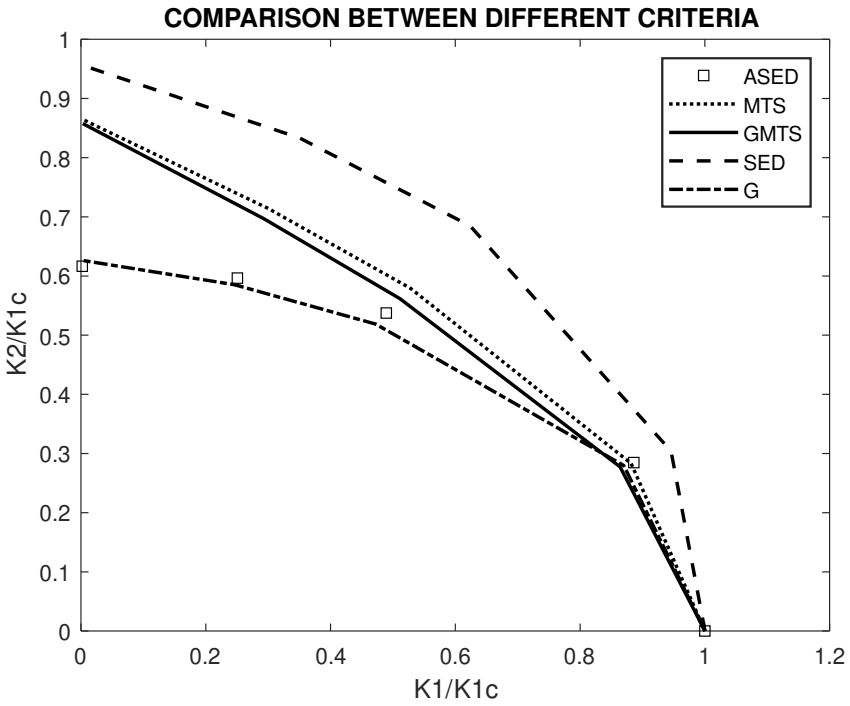

Figure 4.21: Zirconia 4000: normalized stress intensity factors comparison

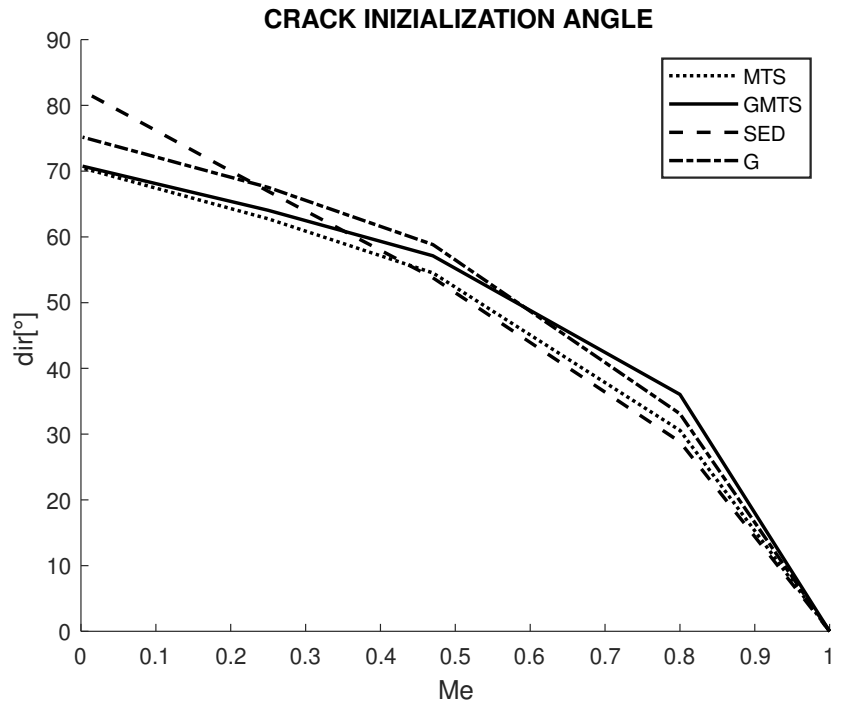

Figure 4.22: Zirconia 4000: initiation angle comparison

$$K_1 = \frac{P\sqrt{\pi a}Y_1}{BW}\left(1 - \frac{L_2}{L_4}\right) \tag{4.1}$$

$$K_2 = \frac{P\sqrt{\pi a}Y_2}{BW}\left(1 - \frac{L_2}{L_4}\right) \tag{4.2}$$

$$\tag{4.3}$$

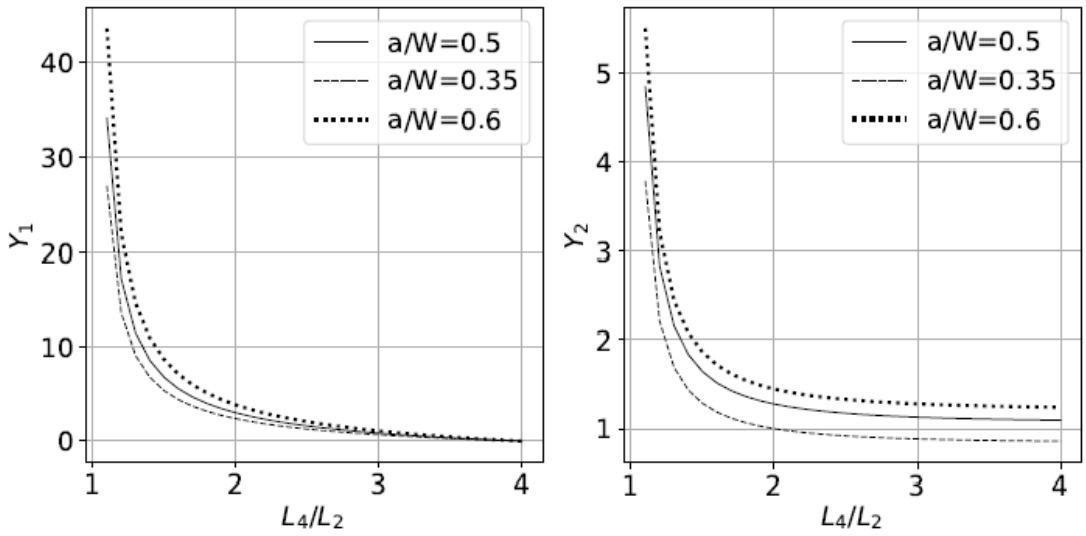

Figure 4.23: Adimensional geometry factors

Studying table 4.3a and 4.3b, it appears that some data are out of the trend. Indeed, the stress intensity factors obtained with these failure loads are out of the trend too. It was considered easier to calculate averaged values for the stress intensity factors, but the elements colored in red were not considered for the reason explained before. Even with this precaution, the experimental trend is really different from the theoretical one, as pictures 4.24 and 4.25 show. (These pictures content is the same as fig. 4.19 and 4.21, but there is also the experimental curve.)

Zirconia 2000		
Me	$K1$ $MPa\sqrt{m}$	$K2$ $MPa\sqrt{m}$
1	15.13	0
1	15.68	0
1	14.46	0
0.8	17.23	4.79
0.8	21.82	6.06
0.8	59.63	16.56
0.47	32.64	20.27
0.47	9.16	5.69
0.47	25.06	15.56
0.25	20.67	17.13
0.25	21.62	17.92
0.25	18.81	15.59
0	9.96	14.42
0	14.28	20.66
0	14.67	21.22

(a)

Zirconia 2000		
Me	$\overline{K1}$ $MPa\sqrt{m}$	$\overline{K2}$ $MPa\sqrt{m}$
1	15.09	0
0.8	19.52	5.42
0.47	28.85	17.92
0.25	20.37	16.88
0	12.97	18.76

(b)

Table 4.6: Zirconia 2000: stress intensity factors

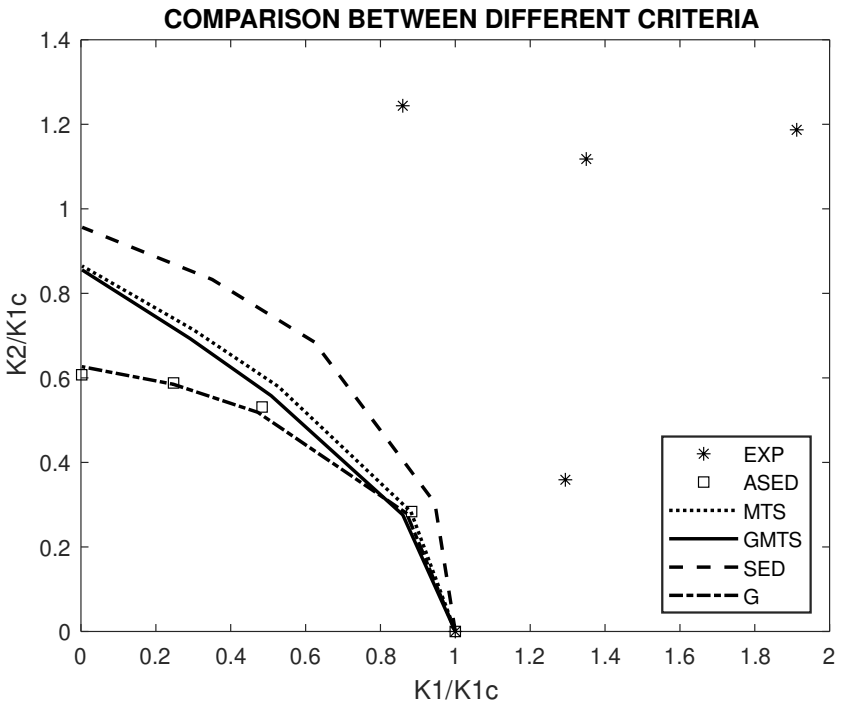

Figure 4.24: Zirconia 2000: normalized stress intensity factors with the experimental values

Zirconia 4000		
Me	$K1$ $MPa\sqrt{m}$	$K2$ $MPa\sqrt{m}$
1	14.75	0
1	14.24	0
1	14.72	0
0.8	59.6	16.56
0.8	21.98	6.11
0.8	24.02	6.67
0.47	32.67	20.29
0.47	32.66	20.28
0.47	29.68	18.44
0.25	20.74	17.19
0.25	25.33	20.99
0.25	23.55	19.51
0	13.98	19.75
0	12.44	17.57
0	13.94	19.69

(a)

Zirconia 4000		
Me	$\overline{K1}$ $MPa*$ $m^0.5$	$\overline{K2}$ $MPa*$ $m^0.5$
1	14.57	0
0.8	23	6.39
0.47	31.67	19.67
0.25	23.21	19.23
0	13.45	19

(b)

Table 4.7: Zirconia 4000: stress intensity factors

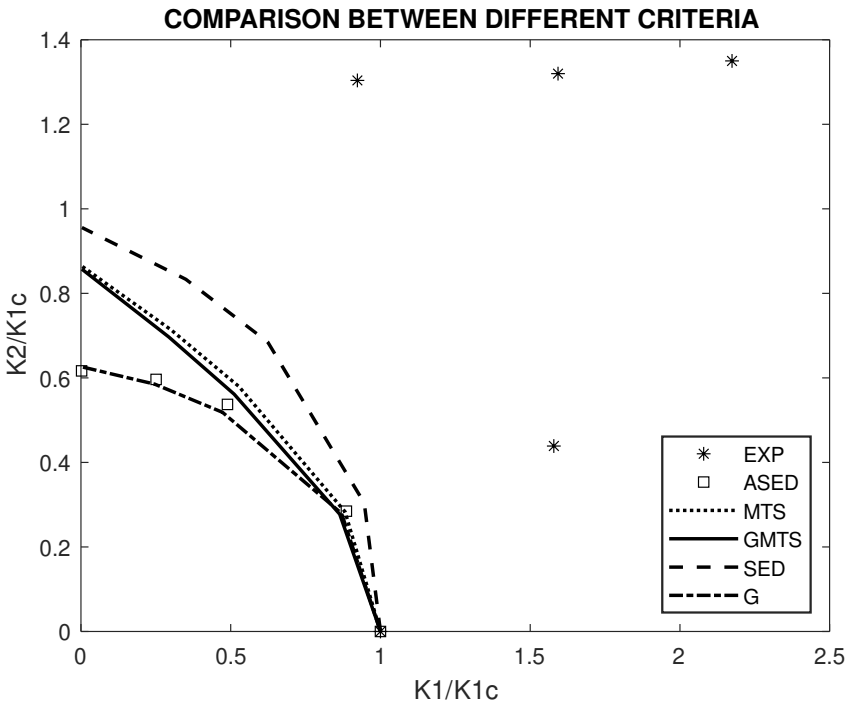

Figure 4.25: Zirconia 4000: normalized stress intensity factors with the experimental values

Chapter 5

Recommendations and conclusion

The ASED criterion and the other theoretical criteria were applied to a large number of materials of different classes.
The first thing possible to conclude is that in the majority of the cases the ASED criterion predictions are coherent with the experimental results. The ASED criterion is based on the assumptions that the fracture toughness K_{Ic} is a given property. This is the reason why the predictions of the pure mode I failure load are convincing, while the discrepancy increases approaching mode II . When the discrepancy between mode I failure loads is huge, there is probably a mistake in the definition of the fracture toughness. This is what happens in section 3.2.3 where the second type of PMMA is tested. Indeed, the toughness is not universally a material property: it depends on the temperature, the material strength, and the thickness of the specimen. But sometimes other relations are found, for example with the test's speed. These are cases in which to apply the ASED criterion could be difficult. Otherwise, if a big discrepancy for mode I failure load is observed, it could be a matter of loading configuration.
For what concerns the normalized stress intensity factors, the ASED curve is in general far from the experimental one compared to the other theoretical criteria. The MTS, GMTS, SED, and G criteria are ancient and their validity is indisputable. The interest of this work was to see how they work with several materials in order to classify their performances for each class. In general, it is possible to conclude that the best for rock and polymers is the GMTS criterion while the SED is the best one for steels and ceramics. The G criterion is always the closest to the ASED for what concerns the normalized stress intensity factors. This is probably because they are both energetic criteria.
The plots regarding the initiation angles of the crack show considerably good accordance between all the criteria, and also with the experimental results, when available. This is interesting. To obtain the plot with the normalized stress intensity factors, the predictions of the toughness are needed. These plots show a relevant scatter zone. This means that the discrepancy between the criteria is not negligible. On the contrary, in the initiation

angle's plots, the scatter zone is tiny. It seems that the mixed-mode coefficient has a higher influence on the angle θ_0 and even using different criteria, the results can not vary largely. θ_0 seems strongly dependent on the loading configuration and poorly dependent on the material, the intensity of the load, or the stress intensity factors.

In general, even if the work gave a good result, some observations can be done.
It was particularly difficult to deal with experimental tests carried out by other researchers. There are several reasons: the main reason is that the ASED and the other criteria are highly dependent on the material properties. It is always better to characterize the material *in loco*, with proper tests on proper samples of the material. There are materials for which the properties depend on variables as the microstructure, the processes, the environment of the test, and so on. It is better to provide these characteristics without looking for them in the literature, that is always a hazard. Besides, as already said, the definition of the fracture toughness is extremely important to achieve good results.
The other aspect that needs to be focused on is related to the specimen shape and the loading configuration. The AFPB test was used for all the materials. With this configuration, it is easy to obtain mixed-mode fracture but it is strongly dependent on the loading distances. It is really important to choose in a proper way the distances concerning the specimen's dimensions, this was already be seen with some materials, sections 3.1.5, 3.1.6. And the specimens used are small. The average thickness is included between 5 or 10 mm. It is difficult to be precise in these conditions, but precision is fundamental to obtain the right stress intensity factors.
To conclude the work it would be interesting to practice a method to deal with ductile materials. Even if in the field of this work all the materials were considered brittle, the influence of the plasticity was seen in different situations. The plasticity around the crack tip affected the predictions of the criteria, but also the plasticity in the point of application of the loads was a problem: when the loads involved are too intense, it is possible to spot plastic deformation also in correspondence with the boundary conditions. Otherwise, with a high load, a brittle material can show cracks, and this is a problem as well because the specimen can fail at unexpected points.
Speaking about ductility, it would be really interesting to apply the EMC, Equivalent Material Concept, to the steels at room temperature or other ductile materials, as some polymers. This was not possible because of the dimensions of the specimens. At room temperature, the toughness increases, and this affects the radius of the control volume. If a huge control volume is required, the specimen should be big enough to host the crack and the volume.

Bibliography

[1] B. Atztori. *Appunti di Costruzione di Macchine*. pp.152-158. Padova: Libreria Internazionale Cortina Padova, 2000.

[2] Y Murakami. *1987. Stress Intensity Factors Handbook, Vol. 1,* pp. 16-18.

[3] Paolo Lazzarin and R Zambardi. 'A finite-volume-energy based approach to predict the static and fatigue behavior of components with sharp V-shaped notches'. In: *International journal of fracture* 112.3 (2001), pp. 275–298.

[4] Seyed Mohammad Javad Razavi, Mohammad Reza Mohammad Aliha and Filippo Berto. 'Application of an average strain energy density criterion to obtain the mixed mode fracture load of granite rock tested with the cracked asymmetric four-point bend specimens'. In: *Theoretical and Applied Fracture Mechanics* 97 (2018), pp. 419–425.

[5] Seyed Mohammad Javad Razavi, MR Ayatollahi and F Berto. 'A synthesis of geometry effect on brittle fracture'. In: *Engineering Fracture Mechanics* 187 (2018), pp. 94–102.

[6] Fazil Erdogan and GC Sih. 'On the crack extension in plates under plane loading and transverse shear'. In: (1963).

[7] DJ Smith, MR Ayatollahi and MJ Pavier. 'The role of T-stress in brittle fracture for linear elastic materials under mixed-mode loading'. In: *Fatigue & Fracture of Engineering Materials & Structures* 24.2 (2001), pp. 137–150.

[8] MR Ayatollahi, MJ Pavier and DJ Smith. 'Determination of T-stress from finite element analysis for mode I and mixed mode I/II loading'. In: *International journal of fracture* 91.3 (1998), pp. 283–298.

[9] MRM Aliha et al. 'Geometry and size effects on fracture trajectory in a limestone rock under mixed mode loading'. In: *Engineering Fracture Mechanics* 77.11 (2010), pp. 2200–2212.

[10] MR Ayatollahi and MRM Aliha. 'Mixed mode fracture in soda lime glass analyzed by using the generalized MTS criterion'. In: *International Journal of Solids and Structures* 46.2 (2009), pp. 311–321.

[11] C Wang, ZM Zhu and HJ Liu. 'On the I–II mixed mode fracture of granite using four-point bend specimen'. In: *Fatigue & Fracture of Engineering Materials & Structures* 39.10 (2016), pp. 1193–1203.

[12] George C Sih. 'Strain-energy-density factor applied to mixed mode crack problems'. In: *International Journal of fracture* 10.3 (1974), pp. 305–321.

[13] RJ Nuismer. 'An energy release rate criterion for mixed mode fracture'. In: *International journal of fracture* 11.2 (1975), pp. 245–250.

[14] MA Hussain, SL Pu and J Underwood. 'Strain energy release rate for a crack under combined mode I and mode II'. In: *Fracture analysis: Proceedings of the 1973 national symposium on fracture mechanics, part II*. ASTM International. 1974.

[15] MA Lifeng and Alexander M Korsunsky. 'On the use of vector J-integral in crack growth criteria for brittle solids'. In: *International journal of fracture* 133.4 (2005), pp. L39–L46.

[16] Sidney Mindess, Frederick V Lawrence and Clyde E Kesler. 'The J-integral as a fracture criterion for fiber reinforced concrete'. In: *Cement and Concrete Research* 7.6 (1977), pp. 731–742.

[17] MR Ayatollahi, S Shadlou and MM Shokrieh. 'Mixed mode brittle fracture in epoxy/multi-walled carbon nanotube nanocomposites'. In: *Engineering Fracture Mechanics* 78.14 (2011), pp. 2620–2632.

[18] Hamid Reza Majidi et al. 'Energy-based ductile failure predictions in cracked friction-stir welded joints'. In: *Engineering Failure Analysis* 102 (2019), pp. 327–337.

[19] Majid Reza Ayatollahi and Mohammad Reza Mohammad Aliha. 'Fracture analysis of some ceramics under mixed mode loading'. In: *Journal of the American Ceramic Society* 94.2 (2011), pp. 561–569.

[20] DK Shetty, AR Rosenfield and WH Duckworth. 'Mixed-mode fracture of ceramics in diametral compression'. In: *Journal of the American Ceramic Society* 69.6 (1986), pp. 437–443.

[21] MRM Aliha, MR Ayatollahi and B Kharazi. 'Numerical and experimental investigations of mixed mode fracture in granite using four-point-bend specimen'. In: *Damage and fracture mechanics*. Springer, 2009, pp. 275–283.

[22] MRM Aliha, SS Mousavi and SMN Ghoreishi. 'Fracture load prediction under mixed mode I+ II using a stress based method for brittle materials tested with the asymmetric four-point bend specimen'. In: *Theoretical and Applied Fracture Mechanics* 103 (2019), p. 102249.

[23] Anthony R Ingraffea et al. 'Mixed-mode fracture initiation in Indiana limestone and Westerly granite'. In: *The 22nd US Symposium on Rock Mechanics (USRMS)*. American Rock Mechanics Association. 1981.

[24] Warren W Krech, Frank A Henderson and Kenneth E Hjelmstad. *A standard rock suite for rapid excavation research*. Vol. 7865. US Bureau of Mines, 1974.

[25] TM Maccagno and JF Knott. 'The fracture behaviour of PMMA in mixed modes I and II'. In: *Engineering fracture mechanics* 34.1 (1989), pp. 65–86.

[26] Paolo Lazzarin and F Berto. 'Some expressions for the strain energy in a finite volume surrounding the root of blunt V-notches'. In: *International Journal of fracture* 135.1-4 (2005), pp. 161–185.

[27] F Berto and P Lazzarin. 'Recent developments in brittle and quasi-brittle failure assessment of engineering materials by means of local approaches'. In: *Materials Science and Engineering: R: Reports* 75 (2014), pp. 1–48.

[28] FJ Gómez, M Elices and J Planas. 'The cohesive crack concept: application to PMMA at- 60° C'. In: *Engineering fracture mechanics* 72.8 (2005), pp. 1268–1285.

[29] MR Ayatollahi and AR Torabi. 'Investigation of mixed mode brittle fracture in rounded-tip V-notched components'. In: *Engineering Fracture Mechanics* 77.16 (2010), pp. 3087–3104.

[30] D Bhattacharjee and JF Knott. 'Effect of mixed mode I and II loading on the fracture surface of polymethyl methacrylate (PMMA)'. In: *International journal of fracture* 72.4 (1995), pp. 359–381.

[31] Dragos Alexandru Apostol et al. 'Particularities of the Asymmetric Four-Point Bending Testing of Polyurethane Foams'. In: *UPB Scientific Bulletin, Series D* 78.2 (2016), pp. 57–66.

[32] Liviu Marsavina et al. 'Refinements on fracture toughness of PUR foams'. In: *Engineering Fracture Mechanics* 129 (2014), pp. 54–66.

[33] S Suresh et al. 'Mixed-mode fracture toughness of ceramic materials'. In: *Journal of the American Ceramic Society* 73.5 (1990), pp. 1257–1267.

[34] Ming Li and Mototsugu Sakai. 'Mixed-mode fracture of ceramics in asymmetric four-point bending: effect of crack-face grain interlocking/bridging'. In: *Journal of the American Ceramic Society* 79.10 (1996), pp. 2718–2726.

[35] Veena Tikare and Sung R Choi. 'Combined Mode I–Mode II Fracture of 12-mol%-Ceria-Doped Tetragonal Zirconia Polycrystalline Ceramic'. In: *Journal of the American Ceramic Society* 80.6 (1997), pp. 1624–1626.

[36] TM Maccagno and JF Knott. 'The low temperature brittle fracture behaviour of steel in mixed modes I and II'. In: *Engineering fracture mechanics* 38.2-3 (1991), pp. 111–128.

[37] Ali Reza Torabi. 'Estimation of tensile load-bearing capacity of ductile metallic materials weakened by a V-notch: The equivalent material concept'. In: *Materials Science and Engineering: A* 536 (2012), pp. 249–255.

[38] AR Torabi, MH Kalantari and MRM Aliha. 'Fracture analysis of dissimilar Al-Al friction stir welded joints under tensile/shear loading'. In: *Fatigue & Fracture of Engineering Materials & Structures* 41.9 (2018), pp. 2040–2053.

[39] D Bhattacharjee and JF Knott. 'Ductile fracture in HY100 steel under mixed mode I/mode II loading'. In: *Acta metallurgica et materialia* 42.5 (1994), pp. 1747–1754.

[40] Sunghak Lee et al. 'Dynamic fracture initiation behavior of an HY-100 steel'. In: *Metallurgical Transactions A* 24.4 (1993), p. 901.